Scanning Microscopy

Volume 1990
Number 4 *Fundamental Electron and Ion Beam Interactions with Solids for Microscopy, Microanalysis, and Microlithography*

Article 20

1990

# Physical Sputtering of Metallic Systems by Charged-Particle Impact

Nghi Q. Lam
*Argonne National Laboratory, Illinois*

**Scanning Microscopy Supplement 4, 1990 (Pages 311-352)** 0892-953X/90$3.00+.00
Scanning Microscopy International, Chicago (AMF O'Hare), IL 60666 USA

# PHYSICAL SPUTTERING OF METALLIC SYSTEMS BY CHARGED-PARTICLE IMPACT

Nghi Q. Lam

Materials Science Division
Argonne National Laboratory, Argonne, Illinois 60439
Phone (708)972-4953
Fax (708)972-4798

## Abstract

The present paper provides a brief overview of our current understanding of physical sputtering by charged-particle impact, with the emphasis on sputtering of metals and alloys under bombardment with particles that produce knock-on collisions. Fundamental aspects of ion-solid interactions, and recent developments in the study of sputtering of elemental targets and preferential sputtering in multicomponent materials are reviewed. We concentrate only on a few specific topics of sputter emission, including the various properties of the sputtered flux and depth of origin, and on connections between sputtering and other radiation-induced and -enhanced phenomena that modify the near-surface composition of the target. The synergistic effects of these diverse processes in changing the composition of the integrated sputtered-atom flux is described in simple physical terms, using selected examples of recent important progress.

**Keywords:** Sputtering, preferential sputtering, ion-solid interactions, sputter depth of origin, displacement cascades, displacement mixing, Gibbsian segregation, radiation-enhanced diffusion, radiation-induced segregation, surface modifications, bombardment-induced composition changes.

## INTRODUCTION

The interaction of an energetic particle beam with a solid gives rise to various phenomena and processes. Right at the solid surface, backscattering of some incident particles, emission of electrons and photons, and sputtering (i.e. ejection of target atoms) take place. Below the surface, to a depth depending mainly on the particle energy and particle-target mass combination, the slowing-down particles transfer their momentum and energy to the target atoms, displacing them from their equilibrium positions. Complex displacement cascades and point defects - vacancies and interstitials - are thus produced in concurrence with the accumulation of implanted particles, which, in turn, can induce other forms of damage within the solid microstructure. Generally, all these processes are interrelated, and often, several must be taken into account for the understanding of the other. Ion backscattering and release of electrons and photons from the target surface have provided different modes for surface and near-surface characterization of materials (see, e.g., Czanderna 1975, Thomas and Cachard 1978). Sputtering, on the other hand, has been used as a means for thin film deposition, surface cleaning, ion etching, microsectioning, and routinely combined with surface analysis techniques for depth-profiling multicomponent materials (Wehner 1975). Bombardment-induced compositional changes and phase transformations in subsurface regions may have either detrimental or beneficial effects, depending on applications. The effects are detrimental and must be minimized during surface analyses (Hofmann 1980a, Lam 1988a), but become beneficial and should be optimized if particle beams are used for surface modifications (Poate et al. 1983, Williams and Poate 1984). An introduction to the sputtering phenomenon and surface compositional modification processes during sputtering of multicomponent materials is presented in this paper; reviews of the other phenomena can be found in this volume.

Atom sputtering from a solid surface during particle bombardment was first discovered more than a century ago (see, e.g., Sigmund 1981 for a historical survey). However, most of the present understanding of the phenomenon has been achieved during the last 30 years. Particularly, the past

## LIST OF SYMBOLS

$a$ = Lindhard's screening radius for the Thomas-Fermi interaction between atoms.
$a_{BM}$ = Born-Mayer screening radius (0.0219 nm).
$a_L$ = Lattice constant.
$a_o$ = Bohr radius (0.0529 nm).
$C$ = Heat capacity per unit volume.
$C_k$ = Concentration (atomic fraction) of k-atoms.
$C_v, C_i$ = Concentrations of vacancies and interstitials.
$C_k^{(n)}$ = Concentration of k-atoms in the nth atomic layer.
$C_k^b$ = Bulk concentration of the component k in the alloy.
$C_m$ = Cross section depending on the power exponent m.
$C_o$ = Cross section for m = 0 ($\pi a_{BM}\lambda_o/2$)
$d_{kj}$ = Diffusivity coefficient for the atom k via the defect j.
$D_k$ = Total diffusion coefficient of the k-atom.
$D_k^j$ = Partial diffusion coefficient of k-atoms via j-defects.
$D^{dm}$ = Displacement-induced interdiffusion coefficient.
$e$ = Electronic charge.
$E$ = Energy of the incident ion.
$E_e$ = Energy of the ejected atom.
$E_d$ = Threshold displacement energy.
$E_{th}$ = Threshold energy for sputtering.
$E_o$ = Initial energy input in a spherical spike.
$F_D(E,\theta,x)$ = Depth distribution of the energy deposited in a random target by an incident ion of energy E at an angle $\theta$ with respect to the surface normal.
$F_D(E,\theta,0)$ = Surface deposited energy.
$f_{(uvw)}$ = Interatomic spacing measured along the [uvw] direction.
$g(r)$ = Radial pair-distribution function.
$\hbar$ = Rationalized Planck constant ($h/2\pi$).
$J_k$ = Flux of the k-species.
$J_k^j$ = Partial flux of k-atoms via j-defects.
$k_B$ = Boltzmann constant.
$K$ = Defect-production rate (displacements per atom per second, dpa/s).
$M_1$ = Mass of the incident ion.
$M_2$ = Mass of the target atom.
$M_k$ = Mass of the component k in the alloy.
$N$ = Number density of target atoms.
$P_k^{(n)}$ = Effective component sputtering yield of k-atoms from the nth layer.
$r$ = Radial distance from the spike center.
$R$ = Average path length.
$R_p$ = Projected ion range.
$s_n(\varepsilon)$ = Reduced nuclear stopping cross section.
$S_k$ = Component sputtering coefficient of the alloying element k.
$S_e(E)$ = Electronic stopping cross section.
$S_n(E)$ = Nuclear stopping cross section.
$t$ = Time.
$t_{max}$ = Time within which heat in the spike is lost to the surroundings.
$T$ = Transferred energy (or recoil energy).
$T_a$ = Ambient target temperature.
$T_m$ = Absolute melting point.
$T_s$ = Average spike temperature (averaged over the spike lifetime).
$T_o$ = Initial temperature rise in the core of the spike.
$U$ = Surface binding energy of the pure metal.
$U_A$ = Surface binding energy of the A-component in an alloy AB.
$U_{AA}, U_{AB}$ = Nearest-neighbor A-A and A-B bond strengths in an alloy AB.
$v$ = Ion velocity.
$x$ = Depth from the bombarded surface.
$x_s$ = Depth of a spherical spike from the surface.
$x_o$ = Mean depth of origin of the sputtered atoms.
$Y$ ($\equiv S$) = Sputtering yield of the pure metal.
$Y_k$ = Partial sputtering yield of the element k in the alloy.
$Y_{th}(T_o,T_a)$ = Thermal sputtering yield from a spike of initial temperature $T_o$ in a target maintained at ambient temperature $T_a$.
$Y_{app}(T_a)$ = Apparent evaporation yield in the late stage.
$Z_1$ = Atomic number of the incident ion.
$Z_2$ = Atomic number of the target atom.
$Z_j$ = Atomic number of the component j in the alloy.
$Z_s$ = Mean surface coordination number.
$Y_{th}^c(T_a)$ = Thermal evaporation yield in the late stage, assuming cylindrical spikes.
$Y_{th}^s(T_a)$ = Thermal evaporation yield in the late stage, assuming spherical spikes.
$\alpha$ = Numerical factor depending on $\theta$, E and $M_2/M_1$.
$\beta_k^{(n)}$ = Sputter fraction of k-atoms from the nth layer.
$\gamma$ = $4M_1M_2/(M_1 + M_2)^2$.
$\delta$ = Thickness of the surface layer removed by sputtering.
$\dot{\delta}$ = Sputtering rate.
$\varepsilon$ = Lindhard's dimensionless energy.
$\eta$ = Factor proportional to the number of atoms changing sites per Frenkel pair generated.
$\theta$ = Angle of incidence (with respect to the surface normal).
$\theta_e$ = Angle of emission (with respect to the surface normal).

$\theta(T_a)$ = Evaporation rate at ambient temperature $T_a$.
$\kappa$ = Thermal diffusivity.
$\lambda$ = Nearest-neighbor distance.
$\lambda_m$ = Dimensionless function of the power exponent m.
$\mu$ = Function of $M_2/M_1$ used in $(\cos\theta)^{-\mu}$ to describe the dependence of the sputtering yield on angle of incidence.
$\nu_k$ = Jump frequency of k-atoms.
$\xi$ = Mean atomic spacing.
$\xi_e$ = Function of the atomic number $Z_1$ (of the order of $Z_1^{1/6}$).
$\rho_o$ = Initial radius of the cylindrical spike.
$\rho_{max}$ = Maximum spike radius for evaporation.
$\sigma$ = Total cross section for ion-target atom collisions.
$\phi$ = Ion flux (ions/cm$^2$s).
$\chi$ = Fitting parameter used in $\cos^{\chi}\theta_e$ to describe the angular distribution of sputtered atoms.
$\Psi_{(uvw)}$ = Efficiency parameter for sputtering from the (uvw) surface.
$\Gamma_{(uvw)}$ = Nonchanneled fraction of the incident beam upon entering the (uvw) surface.
$\Omega$ = Average atomic volume in the alloy.
$\Omega_e$ = Solid angle of ejection.
$\Omega_s$ = Average atomic volume in the first few surface layers.
$\Delta G_s$ = Gibbs free energy of segregation (or adsorption).
$\Delta H_m$ = Heat of mixing.
$\Delta T_{eff}$ = Effective temperature rise in the target.

---

two decades have seen a significant growth of the sputtering field. Advanced theories of energy loss of heavy particles in matter, mainly through the work of Lindhard et al. (1963a,b), and the comprehensive theory of sputtering by Sigmund (1969a) have much stimulated this growth. A considerable amount of systematic research on ion sputtering, both experimental and theoretical, has been undertaken since 1969. The impact of sputtering on research and technology has been remarkable; one can find its applications in many areas of surface physics and chemistry, plasma physics, materials science, and thin film and microelectronic technologies. During the recent years, advances in electronics, ultrahigh vacuum technology and laser techniques have initiated a new class of more sophisticated sputtering experiments. In addition, the availability of high-speed computers has made an increasing number of time-consuming atomistic simulations and phenomenological modelings possible. All these new efforts have been directed toward a basic understanding of the underlying mechanisms and processes as well as of many subfields of sputtering, including dynamics and structure of displacement cascades, depth of origin of sputtered atoms, charge and excitation states of sputtered particles, sputtering of molecules and clusters, electronic excitation-induced sputtering, chemical sputtering, sputtering of alloys and compounds, and sputtering of insulators.

Sputtering occurs when atoms that are displaced in the near-surface region receive sufficient energy to escape from the surface. This type of sputtering is called physical (or knock-on) sputtering, as opposed to chemical sputtering which invokes a chemical reaction (e.g., formation of an unstable compound at the surface) induced by the bombarding particles. The sputtering yield, Y, defined as the average number of target atoms ejected per incident particle, depends on a combination of projectile-target variables, including the particle energy E, the atomic numbers and masses of the projectile and the target, $Z_1$, $M_1$ and $Z_2$ and $M_2$, respectively, the structure of the target surface and the experimental geometry (Sigmund 1969a, 1981). Generally, sputtering yields may range from $10^{-3}$ to ~$10^2$ atoms/ion, but typical values are between 1 and 10. For experimental information on sputtering yields from elemental targets, the reader may find the excellent survey by Andersen and Bay (1981) very useful.

The above definition of sputtering yield is, however, only valid for sputtering of monatomic targets at low fluence. For high-fluence situations where the chemical composition of the target is progressively altered by the accumulation of implanted particles or for sputtering of multicomponent materials, one needs to define the partial sputtering yields for different alloy components. The partial yield, $Y_k$, of the component k is simply the average number of k-atoms removed per incident ion. On the basis of mass and surface binding effects, sputtering is expected to be preferential in most multicomponent materials (Sigmund 1981, 1987a). The mass effect results from the fact that the energy transfers to atoms of unequal masses are different, and the surface binding effect arises because the various alloy components do not have the same surface binding energies and, hence, different energies are required to eject them from the surface. The resulting preferential loss of certain components by sputtering leads to compositional changes, whose spatial extent depends on various diffusional processes. A number of reviews on preferential sputtering of alloys and compounds have appeared in recent years (Andersen 1980, 1984, Betz 1980, Kelly 1980, Betz and Wehner 1983, Lam and Wiedersich 1987, Shimizu 1987).

In addition to preferential sputtering, a number of other processes can also affect the composition and microstructure in the near-surface region of multicomponent targets during exposure to particle beams. These processes, as depicted in Fig. 1, include displacement mixing, radiation-enhanced diffusion, radiation-induced segregation, and Gibbsian segregation (or Gibbsian adsorption) (Andersen 1980, 1984, Lam and Wiedersich 1981, 1987, Lam 1988b, Wiedersich 1984). Each of these processes has been investigated previously, and a good understanding of them already exists. However, in most cases, several of the processes occur simultaneously, and, therefore, compositional changes in alloys and compounds are usually complex. With phenomenological modeling and systematic experimental

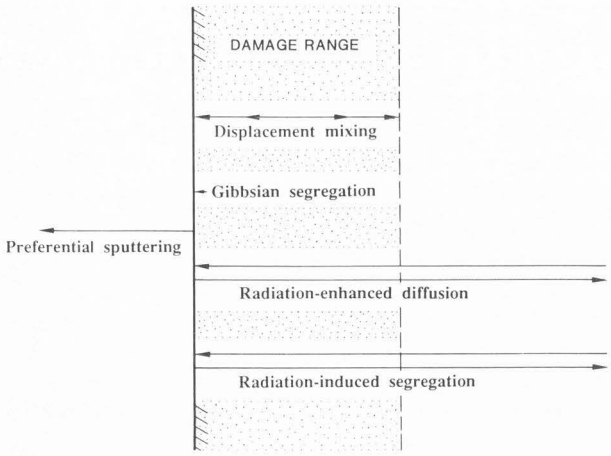


Fig. 1: Basic processes affecting the surface and subsurface compositions of a multicomponent target during ion bombardment.

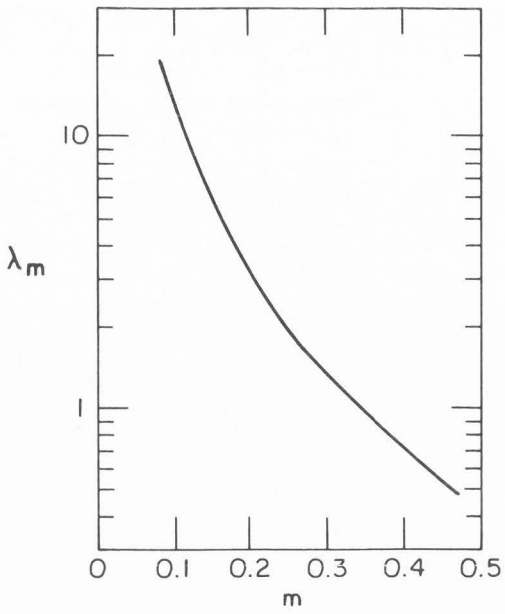


Fig. 2: Numerical constant $\lambda_m$ versus power exponent m. The actual curve is not universal, but somewhat dependent on the potential (here Born-Mayer potential). After Vicanek et al. (1989).

measurements, considerable progress has been made in recent years in identifying the relative contributions from the different processes under various irradiation conditions and understanding their synergistic effects (see, e.g., Lam and Wiedersich 1987 and references therein). The one exception to this statement may, however, be concerned with preferential sputtering. Although sputtering of multicomponent matertials is *a priori* preferential, the experimental information about "true" component sputtering yields, i.e., the partial sputtering yields per unit surface concentrations of the alloy components (Betz and Wehner 1983), is still extremely limited, owing to problems associated with their measurements, namely the low ion-fluence requirement and the complex interplay of various processes in changing the alloy surface composition.

The present paper is not intended to be a comprehensive review of the broad field of sputtering. Within the given limits, we concentrate only on a few specific topics of sputter emission and on connections between sputtering and other radiation-induced and -enhanced processes in the target materials. The main emphasis will be on knock-on sputtering of metallic systems where excitation and/or ionization processes are unimportant for atom ejection and defect production. Topics like electronic sputtering, chemical sputtering, charge and excitation states of sputtered atoms, and sputtering-induced surface topography changes will not be discussed.

## BASIC CONCEPTS

Some knowledge of various aspects of atomic-collision physics, radiation damage and surface science, such as nuclear and electronic stopping of particles in matter, energy deposition, range theory, cascade and defect production, surface binding forces, surface segregation and surface topography, is required for the understanding of sputtering. However, since several extensive reviews on sputtering and these sputtering-related topics have already appeared in recent years, as can be found in volumes edited by Varga et al. (1980), Behrisch (1981, 1983), Remillieux et al. (1982), Betz et al. (1987), Gruen et al. (1987) and Fujimoto (1988), only some basic concepts and newer developments necessary for the discussion in this overview are selected here. The reader seeking further details is referred to the many papers in these volumes and to the primary sources quoted therein.

### Slowing-down of Charged Particles in a Solid

When an energetic particle penetrates a target, its kinetic energy is dissipated via elastic (nuclear collisions) and inelastic (electronic excitation) processes. According to Lindhard et al. (1963a,b), the differential energy loss or stopping power of an infinitesimal thickness dx of the target can be written as a sum of nuclear (n) and electronic (e) stopping powers:

$$\begin{aligned} dE/dx &= (dE/dx)_n + (dE/dx)_e \\ &= - N[S_n(E) + S_e(E)], \end{aligned} \tag{1}$$

where N is the number density of atoms in the medium, and $S_n(E)$ and $S_e(E)$ are the so-called nuclear and electronic stopping cross sections, respectively.

The nuclear stopping cross section is defined as:

$$S_n(E) = \int_0^{T_{max}} T \, d\sigma(E,T), \tag{2}$$

where $d\sigma$ is the interaction cross section, T the transferred energy (or recoil energy) and $T_{max}$ the maximum value of T achieved in a head-on collision,

$$T_{max} = \gamma E. \tag{3}$$

with $\gamma = 4M_1M_2/(M_1+M_2)^2$. The cross section can be approximated by the expression (Lindhard et al. 1963a,b, Sigmund and Sanders 1967):

$$d\sigma(E,T) \simeq C_m E^{-m} T^{-(1+m)} dT; \quad 0 \lesssim T \lesssim \gamma E \tag{4}$$

with

$$C_m = \frac{\pi}{2} \lambda_m a^2 \left(\frac{M_1}{M_2}\right)^m \left(\frac{2Z_1Z_2e^2}{a}\right)^{2m}, \tag{5}$$

$\lambda_m$ being a dimensionless function of the parameter m ($0 \lesssim m \leq 1$). Numerical values of $\lambda_m$ are shown in Fig. 2 (Vicanek et al. 1989).

This power cross section, eq. (4), is valid in the energy regime where the screening of the Coulomb interaction is important, i.e. for $\varepsilon \lesssim 1$ (Lindhard et al. 1968, Winterbon et al. 1970), with $\varepsilon$ being the dimensionless energy defined as:

$$\varepsilon = \frac{M_2 E}{M_1 + M_2} \cdot \frac{a}{Z_1Z_2 e^2}, \tag{6}$$

$$a \simeq 0.885\, a_o \left(Z_1^{2/3} + Z_2^{2/3}\right)^{-1/2}; \quad a_o = 0.0529 \text{ nm}.$$

Integration of eq. (2) yields (Sigmund and Sanders 1967):

$$S_n(E) = \frac{1}{1-m} C_m \gamma^{1-m} E^{1-2m}. \tag{7}$$

The nuclear stopping cross section $S_n(E)$ increases approximately linearly with E at very low energies ($m \simeq 0$), reaches a plateau at intermediate energies, e.g. ~10 - 100 keV ($m \simeq 1/2$) and then decreases at higher energies ($1/2 < m \lesssim 1$) (Fig. 3). In addition, $S_n(E)$ increases with increasing atomic numbers $Z_1$ and $Z_2$. Lindhard et al. (1968) have expressed $S_n(E)$ in a reduced form:

$$S_n(E) = \frac{\pi a^2 \gamma}{(\varepsilon/E)} s_n(\varepsilon) \tag{8}$$

where $s_n(\varepsilon)$ is the reduced nuclear stopping cross section. Numerical values of $s_n(\varepsilon)$ have been tabulated by Lindhard et al. (1968) for Thomas-Fermi interaction. For $\varepsilon \geq 10^{-3}$, $s_n(\varepsilon)$ can also be calculated analytically using the following expression derived recently by Matsunami et al. (1980):

$$s_n(\varepsilon) = \frac{3.441\, \varepsilon^{1/2} \log(\varepsilon + 2.718)}{1 + 6.355\, \varepsilon^{1/2} + \varepsilon(-1.708 + 6.882\, \varepsilon^{1/2})}, \tag{9a}$$

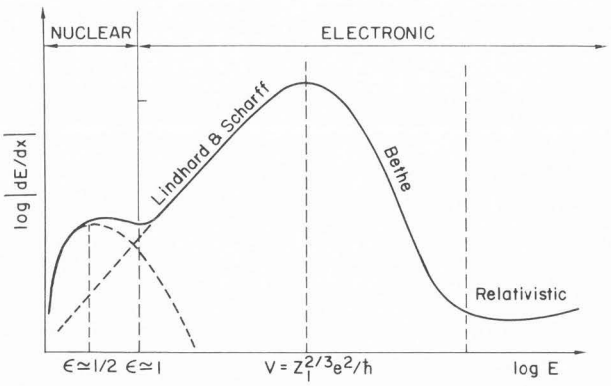


Fig. 3: Schematic description of the stopping power of an ion as a function of energy. After Sigmund (1981).

which approximates the data of Lindhard et al. (1968) to within a few percent.

The Thomas-Fermi screening function, however, overestimates the stopping cross section at small energies ($\varepsilon << 1$, $m \simeq 0$) (Andersen et al. 1975, Loftager et al. 1979). Wilson et al. (1977) found that improvement can be made if a Molière-like screening function is used to describe the nuclear stopping in the low-energy region. Based on calculations performed for a representative case, Kr bombardment of C, these authors suggested a simple approximation for $s_n(\varepsilon)$:

$$s_n(\varepsilon) = 0.5 \ln(1 + \varepsilon)/(\varepsilon + 0.10718\, \varepsilon^{0.37544}). \tag{9b}$$

This analytical expression (called the Kr-C function) yielded good agreement between range calculation and experiment. Refinements of the Wilson et al.'s procedure have been made recently by Biersack and Ziegler (1982) and Ziegler et al. (1985).

At high energies ($\varepsilon >> 1$), energy loss to electronic excitations dominates the slowing-down of the ion (Fig. 3). This loss, however, does not give rise to appreciable scattering of the projectile because of the small electronic mass. In the energy range in which most sputtering experiments have been performed, i.e., for ion velocities $v \lesssim Z_1^{2/3} e^2/\hbar$ the electronic stopping cross section can be approximated by (Lindhard et al. 1963b):

$$S_e(E) = 8\pi e^2 a_o \xi_e \frac{Z_1Z_2}{Z} \frac{v}{e^2/\hbar} = KE^{1/2} \tag{10}$$

where $Z = \left(Z_1^{2/3} + Z_2^{2/3}\right)^{3/2}$, and $\xi_e$ is a function of the atomic number $Z_1$ and of the order of $Z_1^{1/6}$ (Lindhard et al. 1963b). Equation (10) provides a useful means to make correction for electronic stopping contribution in knock-on sputtering (Sigmund 1981).

To treat the sharing of energy between the different atom species in a multicomponent target, Andersen and Sigmund (1974) have introduced a generalized power cross

section of the form:

$$d\sigma_{ij}(E_i,T_i) = C_{ij,m_i} E_i^{-m_i} T_i^{-(1+m_i)} dT; \quad 0 \leq T_i \leq \gamma_{ij} E_i \qquad (11)$$

where $E_i$ is the energy of an i-atom colliding with a stationary j-atom, $T_i$ is the recoil energy of the j-atom, its maximum value being $\gamma_{ij}E_i$,

$$\gamma_{ij} = \frac{4 M_i M_j}{(M_i + M_j)^2}, \qquad (12)$$

and

$$C_{ij,m_i} = \begin{cases} \frac{\pi}{2} \lambda_{m_i} a_{ij}^2 \left(\frac{M_i}{M_j}\right)^{m_i} \left(\frac{2Z_iZ_je^2}{a_{ij}}\right)^{2m_i} & , \; m_i \gtrsim 1/4 \qquad (13a) \\ \frac{\pi}{2} \lambda_{m_i} a'^2_{ij} \left(\frac{M_i}{M_j}\right)^{m_i} (2A'_{ij})^{2m_i} & , \; m_i \lesssim 1/4 \qquad (13b) \end{cases}$$

with

$$a_{ij} = 0.885 \, a_o \left(Z_i^{2/3} + Z_j^{2/3}\right)^{-1/2}$$

and

$$a'_{ij} \simeq 0.0219 \text{ nm}; \quad A'_{ij} \simeq 52 \, (Z_i Z_j)^{3/4} \text{ eV}.$$

Equation (13a) is used when the Thomas-Fermi scattering is essential, whereas eq. (13b) is taken for exponential interactions. Furthermore, since it is the cross sections at low particle energy E that are needed when estimating the recoil density (i.e., the average number of j-atoms recoiling per energy interval (E, dE) in a collision cascade initiated by an i-atom with initial energy $E_i$; Sigmund 1969a) and the slowing-down density (i.e. the average number of j-atoms moving per energy interval (E, dE) during bombardment with a flux of i-atoms of energy $E_i$; Sigmund 1969b), eq. (13b) is mostly used in radiation damage and sputtering calculations. However, for light ions, even in the low-energy regime, the Thomas-Fermi coefficients can be appropriate, and eq. (13a) is applied (Andersen and Sigmund 1974).

The nuclear stopping cross section of an i-atom colliding with a j-atom is thus:

$$S_{n,ij}(E_i) = \frac{1}{1 - m_i} C_{ij,m_i} \gamma^{1-m_i} E^{1-2m_i}. \qquad (14)$$

In a homogeneous medium containing $N_j = C_jN$ atoms of type j per unit volume (N being the atom density and $C_j$ atom fraction of j-atoms, $\Sigma C_j = 1$), the nuclear stopping power of a moving i-atom is given by (Sigmund 1987a):

$$(dE/dx)_{n,i} = - N \sum_j C_j S_{n,ij} \equiv - N S_{n,i} \qquad (15)$$

**Displacement Cascades and Defect Production**

The nuclear stopping process generates displacement (or collision) cascades, in which a large number of target atoms are set in motion (recoil atoms). Displacement cascades that intersect the surface give rise to sputtering, and those created in the bulk provide a mechanism for defect production and contribute to the overall population of defects. The characterization of displacement cascades is therefore of importance for the understanding of many processes induced by irradiation.

Although the original concept of a displacement cascade was introduced almost forty years ago (Brinkman 1954) and although energetic cascades have been considered as the origin of a variety of experimental observations over the years (see, e.g., Seitz and Koehler 1956, Davies 1983, 1984), the detailed characterization of displacement cascades has been a long-standing problem in the field of radiation damage (Averback et al. 1988). It has been difficult to develop a comprehensive, analytical theory of cascade dynamics covering both short- and long-time regimes, due to the complex, nonlinear and many-body nature of cascades. The traditional approaches to the cascade problem have been to treat the initial "collisional" (or "displacement spike") phase ($< 10^{-13}$ s) separately from the subsequent, "cooling" or ("thermal spike") phase ($> 10^{-13}$ s). For example, theories based on binary collision approximation (Beeler 1966, Robinson and Torrens 1974) and linearized Boltzmann transport equations (Sigmund 1969a, 1981, Winterbon et al. 1970, Andersen and Sigmund 1974) have provided much insight into fundamental atomic-displacement mechanisms, but cannot adequately treat the evolution of the cascade beyond the "collisional" phase. On the other hand, the "thermal spike" regime was treated by applying classical heat-transport equation and chemical rate theory, assuming that quasi-local equilibrium is rapidly approached(Vineyard 1976, Kelly 1977, Sanders 1980, Johnson and Evatt 1980, Sigmund and Claussen 1981, Sigmund and Szymonski 1984). The only attempt to make the connection between thermal-spike theory and collision-cascade theory was undertaken by Sigmund (1974). Using power-law approximations to the Thomas-Fermi potential, he has estimated the effective deposited energy density within the individual cascade, the cascade lifetime as well as the quenching rate (under the assumption of local equilibrium). Both the deposited energy density and the cascade quenching rate were found to be strongly dependent on E, $M_1$ and $M_2$. These cascade parameters may be roughly evaluated with the aid of a convenient set of graphs provided by Sigmund (1974). Recently, the availability of super-computers has made systematic, time-consuming molecular-dynamics simulations of energetic displacement cascades possible (Guinan and Kinney 1981, King and Benedek 1983, Diaz de la Rubia et al. 1987, Averback et al. 1988), a more quantitative understanding of the entire cascade evolution is beginning to emerge.

In most metals, the threshold displacement energy, $E_d$,

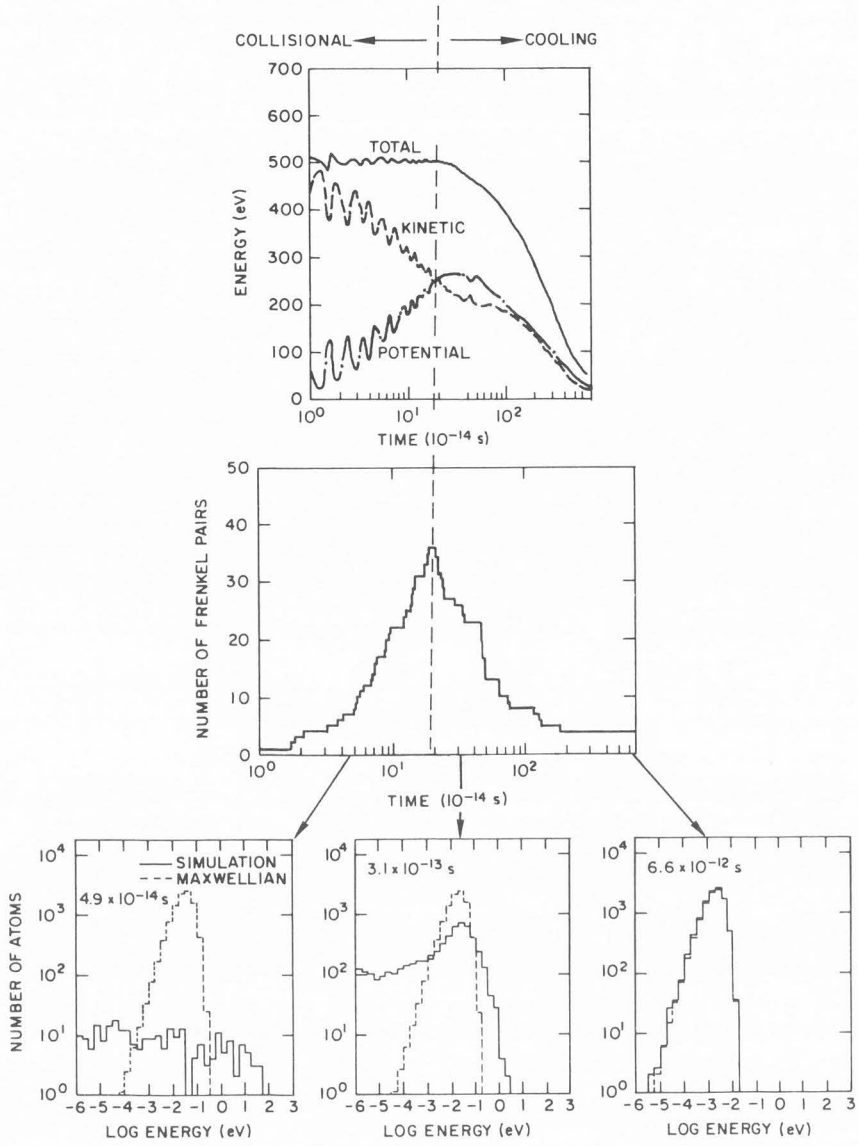


Fig. 4: Time evolution of the total, kinetic and potential energy (top), the number of Frenkel pairs (middle), and the kinetic energy distributions (bottom) for a 500-eV cascade event in a Cu lattice simulated by the Gibson-II potential. After King and Benedek (1983).

i.e., the minimum recoil energy required to create a stable Frenkel pair, is between 15 and 40 eV (Jung 1983). Thus, unless the primary recoil energy is small (e.g., a few times the displacement energy), which produces isolated Frenkel pairs, primary recoil events of hundreds of eV in energy can result in the production of several defects in close proximity to each other (King and Benedek 1983). As the primary recoil event becomes more energetic, a few keV, the number of atoms set in motion within in the cascade volume increases, and a disordered zone is formed in the central core of the cascade, surrounded by interstitial atoms. This disordered state can last several picoseconds (Diaz de la Rubia et al. 1987). Binary-collision simulations have revealed that, for sufficiently high incident-particle energies, the distance between energetic primary recoils (of energy above some keV) is large, and each primary recoil can generate its own subcascade (Beeler and Beeler 1976). Subcascades have, indeed, been observed experimentally, first by Merkle et al. (1963).

Recent molecular-dynamics simulations (King and Benedek 1983, Diaz de la Rubia et al. 1987, 1989a,b) have elucidated many important aspects of the dynamics and structure of displacement cascades. To summarize these aspects, we consider two primary recoil events, first at relatively low energy (500 eV) and then at higher energy (5 keV).

Figure 4 shows the time evolution of a 500-eV event in Cu simulated by the Gibson-II interatomic potential (King and Benedek 1983). The separation between the collisional phase and the cooling phase can be seen clearly. During the collisional phase, binary collisions dominate the dynamics, most of the energy of the lattice is kinetic as the energy of the

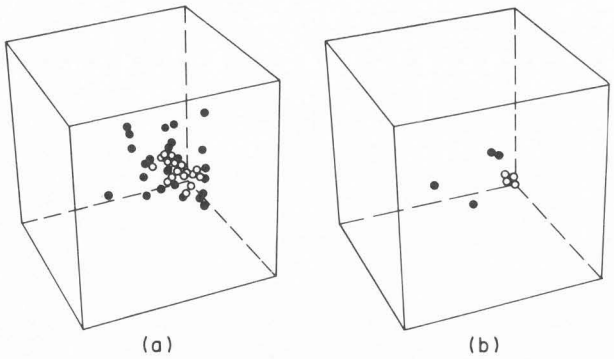


Fig. 5: Snapshots of Frenkel-pair distributions at the end of the collisional phase (a) and at the end of a 500-eV cascade event (b). The open circles represent vacant sites and the filled circles denote dumbbell interstitials. After King and Benedek (1983).

primary knock-on atom is shared among the lattice atoms, the kinetic energy spectrum is far from a thermal-equilibrium Maxwellian distribution, and Frenkel pairs are created. The instantaneous number of these defects and the potential energy increase roughly linearly in log time. At the end of the collisional phase, ~ $2x10^{-13}$ s, the kinetic and potential energies become equipartitioned, all atom kinetic energies have fallen below 5 eV, and the instantaneous number of Frenkel pairs attains a maximum. Moving into the cooling phase, > $2x10^{-13}$ s, the total energy of the cascade begins to drop and the number of Frenkel pairs begins to decrease as a result of extensive athermal rearrangement and mutual recombination of defects. At the end of the cooling phase, after ~ $7x10^{-12}$ s, only a few stable Frenkel pairs remain in the lattice, and the spectrum of atom kinetic energies is almost identical to a Maxwellian distribution corresponding to the temperature of the unirradiated system.

The defect distributions at the end of the collisional phase and of the cooling phase are shown in Figs. 5a and b, respectively. The open circles indicate vacant sites and the filled circles represent dumbbell interstitials. At the end of the collisional phase, a vacancy-rich zone is formed at the cascade center, surrounded by a halo of interstitials. However, by the end of the cascade event, only four stable Frenkel pairs remain. This general picture of a cascade was predicted in the 1950's by Brinkman (1954) and Seeger (1958) and observed in more recent binary-collision simulations (Benedek 1981, Heinisch 1981) as well as in field-ion-microscopy (Current et al. 1983) and transmission-electron-microscopy (Kiritani 1987, English and Jenkins 1987, Jäger and Merkle 1988) experiments.

The average numbers of Frenkel pairs at the end of each phase, calculated as a function of recoil energy, are plotted in Fig. 6a (King and Benedek 1983). The damage function, $\nu(T)$, (i.e., the average number of Frenkel pairs created by a recoil of energy T) increases sharply when $T \simeq E_d \simeq 30$ eV. At the the end of the collisional phase, $\nu(T)$ attains a plateau at ~1 Frenkel pair for $E_d \lesssim T \lesssim 2E_d$ and then increases

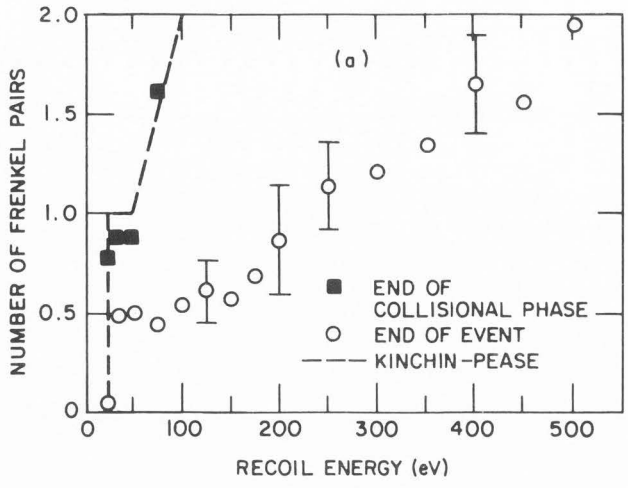


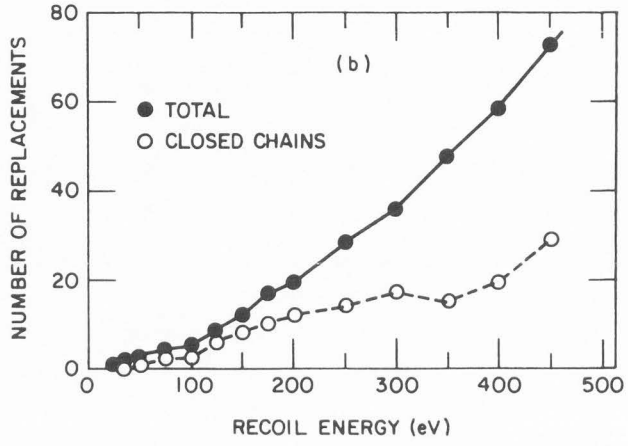


Fig. 6: Average number of Frenkel pairs at the end of the collisional phase and at the end of the events (a) and total number of replacements at the end of the events and the number of replacements in closed chains (b) as a function of recoil energy. The Kinchin-Pease damage function shown in (a) was calculated with $E_d = 25$ eV. After King and Benedek (1983).

monotonically, in good agreement with the Kinchin-Pease damage function (Kinchin and Pease 1955). The "true" damage function $\nu(T)$ obtained at the end of the cooling phase is significantly lower; it exhibits a plateau at ~ 0.5 Frenkel pair over a recoil-energy range ~ 30 - 50 eV, followed by a slow increase at higher recoil energy, reaching a value $\nu(T) = 2$ at 500 eV. The sharp step and plateau in $\nu(T)$ are consistent with experimental observations by King et al. (1983) and Merkle et al. (1983). The reason for the marked reduction of the defect-production efficiency is the strong athermal defect recombination during the cooling phase. The calculated effective recombination radius shows a slight dependence on the recoil energy, increasing roughly linearly from ~ $2.5a_L$ at ~ 30 eV to ~ $4a_L$ at 500 eV ($a_L$ being the lattice constant, 0.3608 nm).

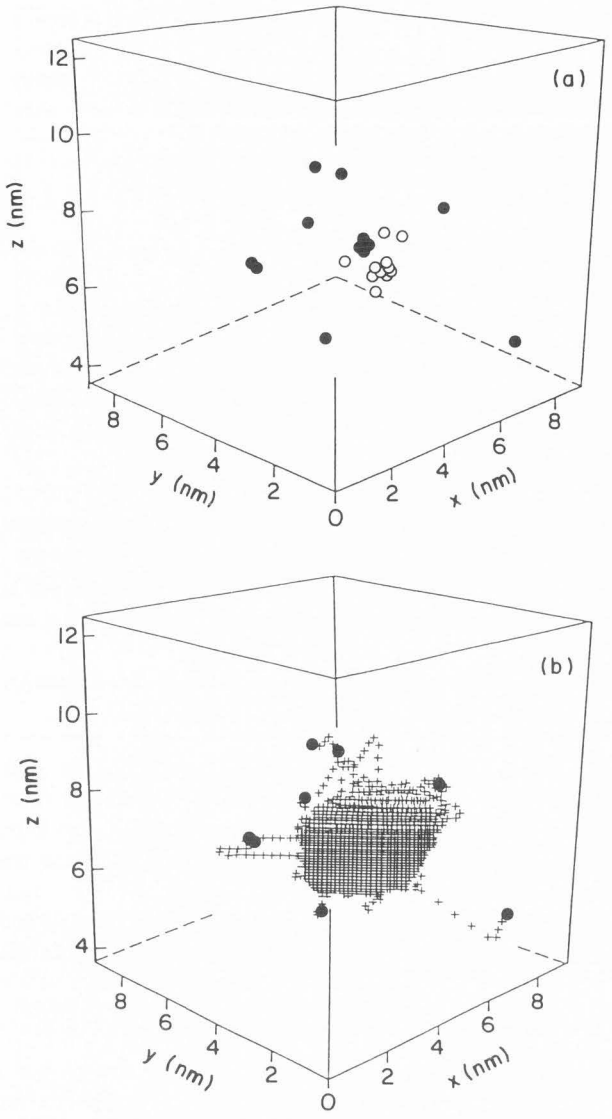


Fig. 7: (a) Spatial distribution of vacancies (open circles) and interstitials (filled circles) at the end of a 5-keV cascade event in Cu. (b) Final locations of interstitials (filled circles) and all the sites on which replacements occurred (crosses) during the time evolution of the cascade. After Diaz de la Rubia (1987).

Most of the displacements occur via sequences of near-neighbor atom replacements, producing a vacancy at the origin of the chain and an interstitial at the end. The results of simulations by King and Benedek (1983) indicate that long, linear replacement chains are rare, and that the frequently-observed chains consist of several straight segments along different close-packed atomic rows; many of them (~ 60 %) close upon themselves with no net defect production. As a result, the number of atoms changing lattice sites is considerably larger than the number of Frenkel pairs created in a displacement event. The total number of replacements counted during the lifetime of the cascade as well as the number of those replacements occurring in closed chains are plotted as a function of recoil energy in Fig. 6b. Almost half of the total number of replacements result from closed chains. Thus, although closed chains do not produce Frenkel pairs, they may cause significant atomic mixing in alloys. By comparing Figs. 6a and 6b, one finds that the number of site replacements per displacement (i.e. per Frenkel pair) is ~ 35; this is an important quantity in the calculation of displacement mixing (Lam and Wiedersich 1987).

Spatial distributions of defects in more energetic displacement cascades have been examined in details recently, using binary-collision (Benedek 1981, Heinisch 1981, 1983) and molecular-dynamics (Guinan and Kinney 1981, Diaz de la Rubia et al. 1987, 1989a,b) simulations. Some important features of these cascades are summarized in the following. Figures 7a and b, for example, show the final positions of interstitials and vacancies remaining at the end of the cooling phase as well as the lattice sites on which atomic replacements have occurred in a 5-keV cascade event in Cu (Diaz de la Rubia et al. 1987). The general picture of the cascade, i.e., a central vacancy-rich zone surrounded by a cloud of interstitials, is observed. The density of replacements in the core region is very high, indicating the many-body character of the thermal spike. A "snapshot" of the atomic configuration within a cross sectional slab of thickness 0.5 $a_L$ near the center of the cascade at t = $1.1 \times 10^{-12}$ s is shown in Fig. 8a. The central zone is considerably disordered. A comparison of the calculated radial pair-distribution function, g(r), with that obtained previously by Foiles (1985) for liquid Cu (Fig. 8b) suggests that local melting indeed occurs (Diaz de la Rubia et al. 1987). The melted region first grows to a maximum size of ~ 2.5 nm in radius, then shrinks as a result of recrystallization occurring at its periphery, and finally disappears at t=$8 \times 10^{-12}$ s (Averback et al. 1988). The average temperature in the central region (r < 1 nm) reaches ~ 5000 K near the end of the collisional phase, t = $2.5 \times 10^{-13}$ s, and decreases rapidly to the melting point, $T_m$, at t = $3.47 \times 10^{-13}$ s, in the middle of the cooling phase. The initial cooling rate in the cascade center is thus ~ $10^{15}$ K/s. At $t \gtrsim 1.4 \times 10^{-12}$ s, the temperature at $r \simeq 2$ nm from the center falls below $T_m$ (Averback et al 1988, Diaz de la Rubia 1989) corresponds to that of the liquid droplet shown in Fig. 8a. In addition, when the core temperature is significantly above $T_m$, expansion in the hot core gives rise to a substantial reduction in atomic density in the cascade center and a high-density ridge outside. As the core temperature falls off, the compressed shell surrounding the core relaxes, and the local density returns to its equilibrium value. The same behavior of core melting was also observed in simulations of Ni (Diaz de la Rubia 1989a,b).

Extensive atomic mixing takes place as a consequence of this local melting. According to Diaz de la Rubia et al. (1987), in contrast to the case of low-energy cascades discussed above, in 5-keV displacement cascades most atomic mixing takes place in the region of the melt (not associated with Frenkel pair production) and during the cooling phase; only a small fraction of mixing occurs in the collisional phase.

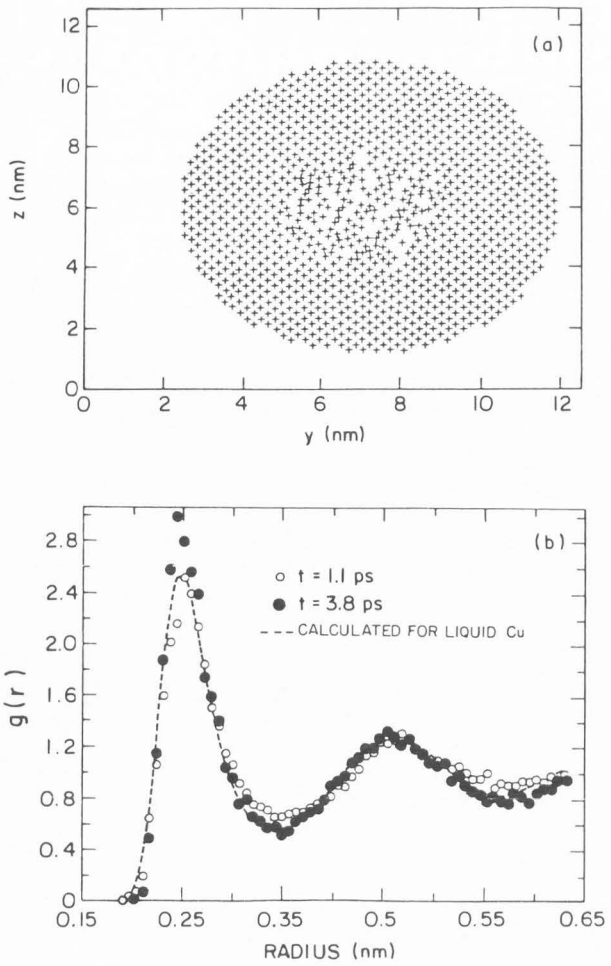


Fig. 8: (a) Projection of a (100) cross sectional slab of thickness $0.5a_L$ near the center of a 5-keV cascade at $t = 1.1 \times 10^{-12}$ s. (b) Radial pair distribution functions of the disordered zone at $t = 1.1 \times 10^{-12}$ and $3.8 \times 10^{-12}$ s. The pair distribution function calculated for liquid Cu by Foiles (1985) is included for comparison. After Diaz de la Rubia (1987).

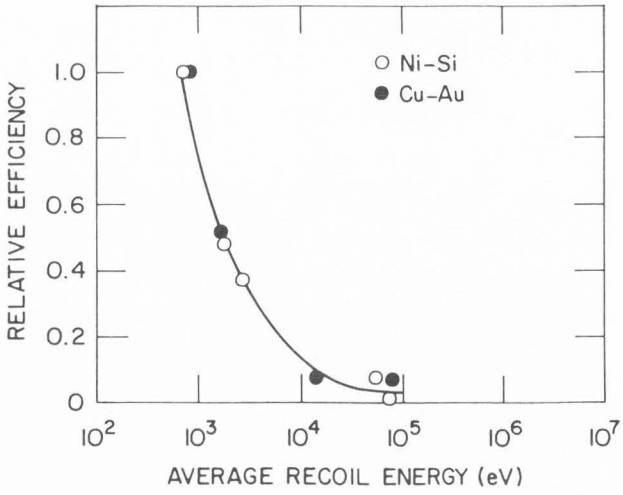


Fig. 9: Relative efficiency (normalized to that of 1-MeV protons) for producing long-range migrating defects (i.e., defects which are free to induce compositional changes at elevated temperatures via radiation-enhanced diffusion and radiation-induced segregation) in Ni-Si and Cu-Au alloys as a function of the calculated, weighted-average recoil energy. Due to Rehn and Okamoto (1987).

Local melting in the cascade center also has important effect on defect production. The vast majority of defects are annihilated in the melted region, only those interstitials that escape this region via low-index replacement sequences survive mutual recombination. Consequently, the defect-production efficiency is quite low, ~ 0.2, relative to the modified Kinchin-Pease relation (Sigmund 1969b,c). This value is in good agreement with experimental observations in Ni-Si and Cu-Au alloys, shown in Fig. 9 (Rehn et al. 1984, Rehn and Okamoto 1987). The most rapid decrease in defect-production efficiency is found to occur over recoil energies up to ~ 5 keV.

In more energetic cascade events, perhaps ~ 10 - 20 keV, the central vacancy-rich regions collapse into vacancy dislocation loops. This has been observed experimentally in a number of metals and alloys (English and Jenkins 1987). In certain materials, however, e.g. Fe, cascades must overlap to a significant extent before collapse occurs (Robertson et al. 1984). At low temperature, where point defects and small defect clusters are immobile, their densities increase with ion dose. Cascade regions begin to overlap, new defects are created in close proximity of existing defects, and, consequently, spontaneous recombination of interstitials and vacancies occurs with increasing frequency. A steady state is achieved when essentially each new defect is formed within the recombination volume of an existing defect. A highly-dense defect structure thus develops in the bombarded material. As the temperature increases, the thermal jump frequencies of point defects become large. The defect moves around in the lattice and can sample a number of potential annihilation sites before a new defect of the opposite type is created within its recombination volume. Thus, losses of mobile vacancies and interstitials also occur by formation of immobile defect clusters and by annihilation at extended sinks such as dislocations, grain boundaries and external surfaces. At sufficiently high temperatures, $\gtrsim 0.6T_m$, defect clusters quickly decompose, and high thermal vacancy concentrations effectively promote annealing processes. As a result, little or no microstructural changes occur during bombardment.

**Phenomenological Description of Sputtering**

Clouds of higher-order low-energy recoil atoms generated in displacement cascades contribute to the sputtering process. However, only those atoms that move toward the surface with sufficient energy to overcome the surface binding forces are sputtered. These sputtered atoms have small ranges and must therefore be located initially within a few atomic layers below the surface (Sigmund 1969a). Thus, phenomenologically, sputtering can be described on the basis of a

simple concept (Wiedersich 1983, Lam and Wiedersich 1987, Rehn and Lam 1987). We define the total number of k-atoms ejected from the target surface per incident ion (i.e., the partial yield of the component k), $Y_k$, as follows:

$$Y_k = \sum_{n=1}^{\infty} P_k^{(n)} C_k^{(n)} , \tag{16}$$

where $P_k^{(n)}$ and $C_k^{(n)}$ are the effective component yield of k-atoms (Betz and Wehner 1983) and the atomic fraction of k-atoms in the nth layer, respectively. The factor $P_k^{(n)}$ is approximately composition-independent and contains all the physical variables that govern the individual sputtering events (primary effects). It is thus related to the sputtering cross section for the k-atoms in the nth layer. The concentrations $C_k^{(n)}$, on the other hand, are perturbed by secondary effects arising from Gibbsian segregation, and radiation-induced and -enhanced processes. Thus, the distinction between the primary and secondary effects, introduced by Sigmund (1981), is made clear in eq. (16).

Writing $P_k^{(n)}$ in the form

$$P_k^{(n)} = \beta_k^{(n)} S_k, \tag{17}$$

eq. (16) reads:

$$Y_k = \sum_{n=1}^{\infty} \beta_k^{(n)} S_k C_k^{(n)} . \tag{18}$$

Here, $\beta_k^{(n)}$ is the sputter fraction of k-atoms from the nth layer (or the contribution of the nth layer to the sputtered-atom flux), $\sum_n \beta_k^{(n)} \equiv 1$, and $S_k$ may be called the k-component sputtering coefficient, i.e., yield per unit concentration of the k-atoms. There may be matrix effects on $S_k$. However, to a first approximation, neglecting these effects, $S_k$ may be taken as the sputtering yield of the pure element k. Furthermore, since the sputtered atoms originate predominantly from the two uppermost atomic layers (Dumke et al. 1983, Lam et al. 1985a,b, Kelly and Oliva 1986a, Lam and Wiedersich 1987, Lam and Hoff 1988, Hoff and Lam 1988, Burnett et al. 1988, Hubbard et al. 1989a, b), eq. (18) can be reduced to:

$$Y_k = S_k \sum_{n=1}^{\infty} \beta_k^{(n)} C_k^{(n)} \simeq S_k \left[ \beta_k^{(1)} C_k^{(1)} + \beta_k^{(2)} C_k^{(2)} \right] , \tag{19}$$

During bombardment with a flux of particles $\phi$ (particles/cm$^2$·s), the target surface is eroded at a velocity or sputtering rate:

$$\dot{\delta} \equiv d\delta/dt = \Omega_s \phi \sum_k S_k \left[ \beta_k^{(1)} C_k^{(1)} + \beta_k^{(2)} C_k^{(2)} \right] , \tag{20}$$

where $\delta$ is the thickness of the surface layer removed by sputtering and $\Omega_s$ is the average atomic volume in the first two atom layers.

## SPUTTERING OF ELEMENTAL TARGETS

For elemental targets, $C_k^{(n)} \equiv 1$, eq. (19) simply becomes:

$$Y = S \sum_{n=1}^{\infty} \beta^{(n)} \equiv S .$$

The sputtering yield Y depends on the energy deposition density in displacement cascades; therefore, in order to estimate Y the cascade regime in which sputtering occurs must be defined. There are three regimes: near-threshold (or few-knockon), linear-cascade, and spike (or nonlinear-cascade) (Andersen 1980, Sigmund 1981). The first regime operates when the energy transferred from the incident particle to target atoms is only enough to produce one or two knockons. This is the case of sputtering with low-energy and/or light ions (e.g., $H^+$, $D^+$ and $He^+$ at $E \lesssim 10$ keV). Sputtering in this regime cannot be well described by the conventional solution of the Boltzmann transport equation (Sigmund 1969a). It is this limitation that separates the near-threshold regime from the linear-cascade regime. The second regime, linear-cascade, is considered when collisions between the impinging particle and target atoms give rise to displacement cascades, but only a small fraction of atoms within the cascade volume are set in motion. Here, the cascade can be visualized as a series of binary collisions between a moving and a stationary atom. The collisional phase of these cascades can be well described by transport equations. Sputtering in the linear-cascade regime was theoretically treated in most detail by Sigmund (1969a) using linearized Boltzmann equation. For bombardment with high-energy, heavy ions or with molecular ions, the density of recoil atoms within the cascade is so high that encounters between moving atoms become frequent events, the linearity assumption is no longer satisfied, and the third regime, spike, becomes important.

It is obvious here that we have adopted the conventional picture suggested by Sigmund (1981), in which sputtering is regarded as a cascade process, with thermal and electronic-excitation effects being variants. Kelly (1984a,b), however, has emphasized a different description of the sputtering event, in which the time scale plays a role. The concept of temporal separation of cascade and spike effects has originated in earlier work of Thompson and Nelson (1962), and the importance of the time scale in sputtering has also been discussed by Sigmund (1977).

### Sputtering Yields

**Linear-cascade regime.** The major tool used to understand sputtering and to calculate the sputtering yield Y is the linear-cascade theory developed by Sigmund (1969a). This theory predicts a linear dependence of Y on the energy deposited in elastic collision events at the surface of a random target, $F_D(E,\theta,0)$:

$$Y(E) = \frac{x_0}{\pi^2 U} F_D(E,\theta,0) . \tag{21}$$

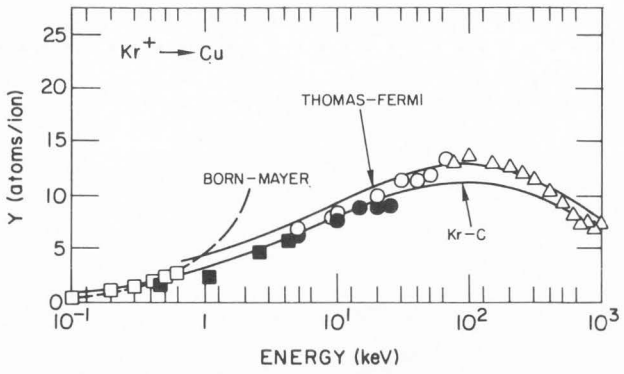


Fig. 10: Energy dependence of the sputtering yield of Cu under $Kr^+$ ion bombardment at normal incidence. Theoretical curves are calculated by eq. (23), using Born-Mayer, Thomas-Fermi and Kr-C interaction potentials, with $\lambda_o = 24$ and U = 3.51 eV. For references to experimental data, see Sigmund (1969a). After Sigmund (1987b).

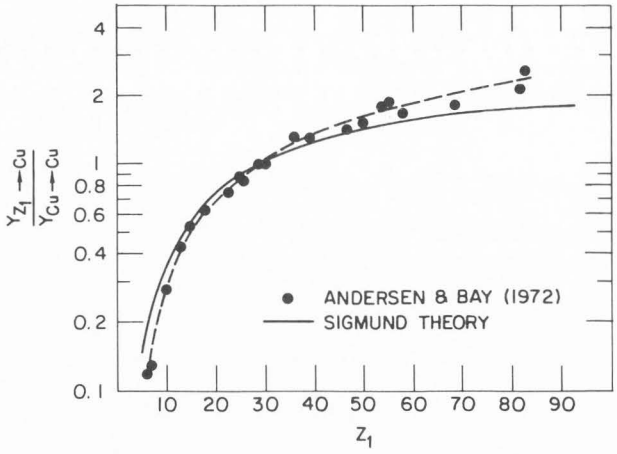


Fig. 11: Sputtering yields of Cu bombarded with 21 different ions at 45 keV normalized to Cu self-sputtering. The solid curve is given by eq. (23). After Andersen and Bay (1972).

Here, U is the surface binding energy, taken to be the sublimation energy, and $x_o = 3/4NC_o$ is the effective depth of origin of the sputtered atoms, with $C_o = \pi\lambda_o a_{BM}^2/2$ [corresponding to $C_m$ in eq. (5) with m = 0 and $a \equiv a_{BM}$ = 0.0219 nm (a Born-Mayer constant)]. Using the conventional value $\lambda_o \simeq 24$ and, hence, $C_o \simeq 0.0181$ nm$^2$, Sigmund (1969a) obtained $x_o \simeq 0.5$ nm. The surface deposited energy $F_D(E,\theta,0)$ can be obtained from the depth distribution of the energy deposited in nuclear collisions in the solid, $F_D(E,\theta,x)$, by an incident particle of energy E aligned at an angle $\theta$ with respect to the surface normal (x-direction). With (Sigmund 1977).

$$F_D(E,\theta,0) = \alpha N S_n(E) \tag{22}$$

one has

$$Y(E) = \left(\frac{6}{4\pi^3 a_{BM}^2 \lambda_o}\right)\frac{\alpha S_n(E)}{U}$$

$$= \frac{1.01}{\lambda_o U}\alpha S_n(E), \tag{23}$$

a well-known Sigmund expression for the sputtering yield from a planar surface. Here, $\alpha$ is a numerical factor depending on $\theta$, E and $M_2/M_1$. Within the accuracy of the power cross sections, for perpendicular incidence and purely elastic collisions, $\alpha$ can be expressed as a function of $M_2/M_1$ only. Numerical values of $\alpha$ have been plotted by Sigmund (1969a) for $M_2/M_1 \leq 10$. For $M_2/M_1 \leq 0.5$, $\alpha$ is nearly constant, ~ 0.2. However, it rises sharply with increasing $M_2/M_1$ above 0.5. Within the range of $0.5 < M_2/M_1 \leq 10$, $\alpha$ can be approximated by (Chen 1984):

$$\alpha = 0.3(M_2/M_1)^{2/3}. \tag{24}$$

Equation (23) is quoted in the form involving the constant $\lambda_o$ because, as shown recently by Vicanek et al. (1989), a more accurate evaluation of $\lambda_o$ can significantly improve the estimates of the sputtering yield and the sputter depth of origin.

It is worth mentioning that the proportionality of the yield Y(E) to the nuclear stopping cross section $S_n(E)$ was first derived by Brandt and Laubert (1967), who also conceptualized sputtering as being governed by kinetic energy imparted to surface atoms by displacement cascades. Their simple theory provided a rough estimate for the sputtering yield of a random target.

The dependence of Y on energy and atomic numbers is contained in $S_n(E)$, while its mass dependence is reflected in both $S_n(E)$ and $\alpha$. The simple, analytical nature of eq. (23) has made the Sigmund theory widely applied to interpret experimental observations. In general, the agreement between theoretical predictions and experiment is fairly good for most monatomic materials sputtered in the linear-cascade regime (Sigmund 1969a, Andersen and Bay 1981).

Figures 10 and 11, for example, compare theory and experiment for the E- and $Z_1$-dependence of Y for Cu, respectively. The reasonableness of eq. (23) is evident. As seen in Fig. 10 (Sigmund 1969a, 1987a), the theoretical curve calculated with $\lambda_o = 24$ and $S_n(E)$ derived for Thomas-Fermi interaction [eq. (8), Lindhard's $s_n(\varepsilon)$] is in excellent agreement with experiment at $E \gtrsim 30$ keV, but is systematically higher at low energies because, as discussed above, the Thomas-Fermi function overestimates the stopping power in this energy regime. Using $S_n(E)$ calculated with the Kr-C potential of Wilson et al. (1977) [eqs. (8) and (9b)], the agreement is very good at both low and high energies. The discrepancy between theory and experiment is, however, noticeable in the region near the maximum where the yields are larger than 10 atoms/ion. This discrepancy is suggestive of important spike

or nonlinear effects, which are not included in the linear-cascade theory. The yields calculated with the Born-Mayer potential are also shown. The measured $Z_1$-dependence for sputtering of Cu (Andersen and Bay 1972) is in very good agreement with predictions of eq. (23) for relatively low $Z_1$, below ~ 50 (Fig. 11). For larger $Z_1$, however, the experimental measurements of the normalized yield are markedly larger than the theoretical values. This deviation was also attributed to nonlinear effects. Andersen and Bay (1973) measured the $Z_1$-dependence for sputtering of Si and Ag, and showed that the nonlinear effects are nonexistent for Si, but quite pronounced for Ag.

In addition to early refinements and corrections (Sigmund 1981), a number of modifications to the basic theory have been suggested over the past few years. They concerned (i) non-negligible effect of electronic energy loss of moving target atoms (Biersack and Eckstein 1984, Jakas and Harrison 1984, 1985), (ii) adjustment of the cross section for low-energy collisions, $C_0$, based on the identification of $x_0$ with $1/NC_0$ (instead of $3/4NC_0$) (Falcone 1986, Falcone et al. 1987), (iii) effect of the surface of a semi-infinite medium on the recoil ejection process (Falcone et al. 1987), and (iv) different identification of the surface binding energy (Kelly 1987b, Oliva et al. 1987).

The sputtering theory of Sigmund (1969a) also describes the dependence of the sputtering yield on angle of incidence $\theta$ of the beam. For not-too-oblique incidence:

$$\frac{Y(E,\theta)}{Y(E,0)} = (\cos\theta)^{-\mu} \qquad (25)$$

where $\mu$ is a function of $M_2/M_1$. For $M_2/M_1 \gtrsim 5$, $\mu \simeq 1$, i.e., the dependence is roughly $1/\cos\theta$. For $M_2/M_1 \lesssim 3$, $\mu \simeq 5/3$, independent of the mass ratio (Sigmund 1969a). The sputtering yield rises with increasing $\theta$, according to eq. (25), because there is a higher probability to generate displacement cascades in the vicinity of the surface. For high values of $\theta$ (near 90°), however, the incident beam simply bounces off the surface, much less energy is deposited, and the yield decreases rapidly. The maximum in the sputtering yield occurs at an angle $60 \lesssim \theta \lesssim 80°$. This general behavior has been observed experimentally (Sigmund 1969a, Oechsner 1975, Andersen and Bay 1981). The agreement between Sigmund's prediction of $(\cos\theta)^{-1}$-dependence and experiment is reasonably good for heavy-ion bombardment in the medium-energy regime. At low energies, the linear-cascade theory cannot explain the angular influence on the sputtering yield (Oechsner 1975, Roth 1980).

**Near-threshold regime.** In the near-threshold regime (i.e., bombardment with low-energy and/or light ions), sputtering is generally characterized by very low sputtering yields, rapid decrease of the yield at low energies, and similarity in the shapes of the sputtering curves (yield vs energy). For further details, see extensive reviews by Roth (1980) and Andersen and Bay (1981). Early theoretical studies, performed in the 1970's (Weissman and Sigmund 1973, Guseva and Martinenko 1976, Smith 1978) were unable to quantitatively describe light-ion sputtering. Facing the lack of a suitable theory at that time and the need of light-ion sputtering data in fusion research, Bohdansky et al. (1980) developed an empirical formula for the sputtering yield, based on simple scaling laws suggested by Bay et al. (1977). The sputtering yield was characterized by a normalized function which depends only on the surface binding energy and the masses of the ion and target. The surface binding energy entered the empirical expression through the definition of the threshold energy for sputtering (Behrisch et al. 1979, Bohdansky et al. 1980):

$$E_{th} = \begin{cases} U/\gamma(1-\gamma) & \text{for } M_1/M_2 \le 0.3 \\ 8U(M_1/M_2)^{2/5} & \text{for } M_1/M_2 > 0.3 \end{cases} \qquad (26)$$

The empirical formula of Bohdansky et al. (1980) enabled to estimate the sputtering yield with reasonable confidence for most elemental targets bombarded with light ions at normal incidence up to a few keV.

Matsunami et al. (1980) found that the E-dependence of the sputtering yields for a large number of ion-target combinations could be described with the linear-cascade theory, if one multiplied the Sigmund expression, eq. (23), by an empirical factor $[1 - (E_{th}/E)^{1/2}]$ to account for the threshold effect. A correction factor of the relative order of $(E_{th}/E)^{1/2}$ for the yield in the low-energy region was first suggested by Sigmund (1977).

Littmark and Fedder (1982) showed that the sputtering yields for light ions on heavy targets could be estimated if one assumed that sputtering was due to reflected ions, i.e., only the primary recoils were responsible for sputtering. However, computer simulations by Biersack and Eckstein (1984) indicated that the contribution of secondary recoils to sputtering increased with the primary energy, surpassing the contribution from primary recoils at $E \simeq 1$ keV for $He^+$ ions.

More recently, Bohdansky (1984) demonstrated that, by modifying Sigmund's description of backward sputtering in the approximation of linear-cascade theory, a universal relation for the sputtering yield could be derived for monatomic solids at normal ion incidence. Two modifications were made to extend the applicability of the Sigmund formula, eq. (23), to low projectile energies. The first modification concerned the evaluation of the "effective" deposited energy because, at low energies, a considerable number of primary recoils do not receive sufficient energy to overcome the surface barrier. And the second modification was related to the energy distribution of recoiling target atoms, which was approximated with an $E_e^{-2}$-dependence ($E_e$ being the ejection energy), for both heavy and light ions. In addition, it is known that the Sigmund formula is not valid for light ions because, via the dependence of $\alpha$ on $M_2/M_1$, the deposited energy is overestimated. A crude correction for this overestimation was to divide $\alpha S_n(E)$ by $R/R_p$ (i.e., the ratio of the average path length to the projected range). This ratio represents the average number of surface crossings of the

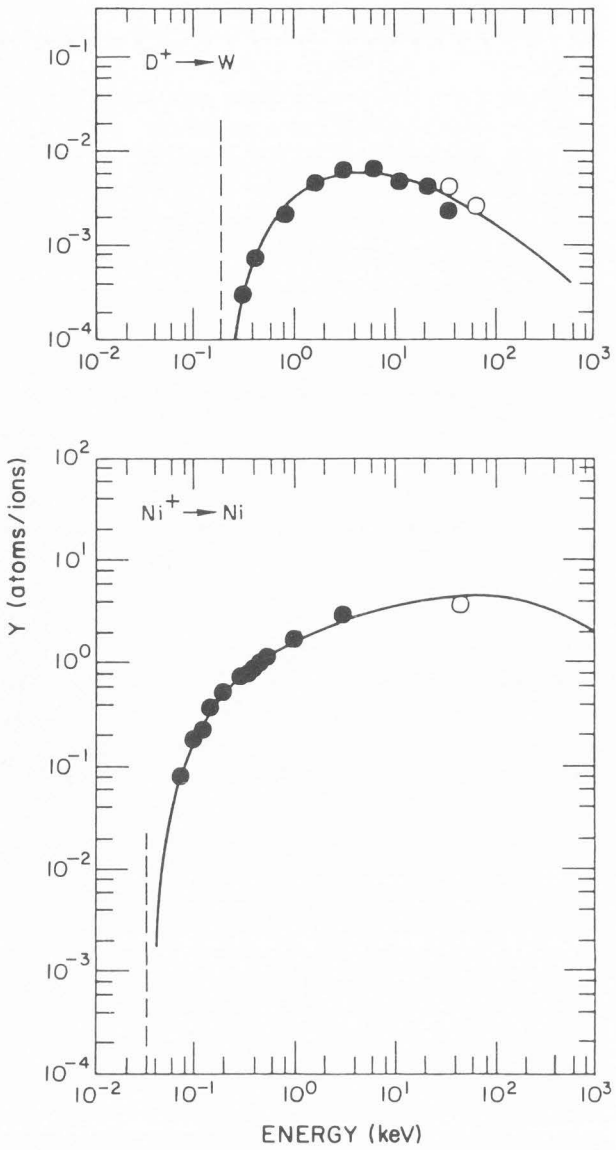


Fig. 12: Comparison of the Bohdansky expression [eq. (27), solid curve] with experimental data for $D^+$ sputtering of W (top) and self-sputtering of Ni (bottom). The threshold energies are indicated by the vertical, dashed lines. After Bohdansky (1984).

primaries and, to a first approximation, can be calculated analytically (Lindhard et al. 1963b). With these modifications, Bohdansky (1984) proposed the following empirical expression for the sputtering yield:

$$Y(E) = \frac{0.042}{U} (R_p/R)\alpha S_n(E) [1 - (E_{th}/E)^{2/3}][1 - (E_{th}/E)]^2. \quad (27)$$

This formula is applicable to sputtering with heavy and light ions, both within and above the threshold regime. It is practically identical to the Sigmund expression, eq. (23) with $\lambda_o = 24$, for bombardment with heavy ions ($R_p \simeq R$) at energies far above threshold ($E >> E_{th}$).

A typical comparison of the Bohdansky relation with experimental data is presented in Figs. 12a and b for light- and heavy-ion sputtering, respectively. The agreement here is very good. The same agreement was also obtained for over 100 other ion-target combinations (Bohdansky 1984).

Sputtering in the near-threshold regime has also been investigated, more systematically in recent years (Andersen 1987), by computer simulations, using either molecular dynamics (see, e.g., Harrison 1983) or binary collision codes, especially Monte-Carlo program TRIM (Biersack 1987). In general, with a proper choice of interatomic potentials, one can obtain good agreement between simulation results and experiment. For example, using the Kr-C potential, eq. (9b), and taking the heat of sublimation as the surface binding energy in their TRIM simulations of sputtering of Ni under various bombardment conditions, Biersack and Eckstein (1984) have achieved excellent agreement with experimental data up into the linear-cascade regime.

**Spike regime.** In the spike regime (i.e., bombardment with high-energy, heavy atomic ions or with energetic molecular ions), the Sigmund formula, eq. (23), underestimates the sputtering yield (Sigmund 1969a, 1981). Sputtering in this regime is characterized by excessively high yields over a broad energy range around the maximum (Sigmund 1981, Andersen and Bay 1981, Thompson 1981), pronounced low-energy peaks in the energy spectra due to evaporation from local regions around the point of ion impact (Chapman et al. 1972, Szymonski and DeVries 1977, Ahmad et al. 1980), yield enhancement factor significantly larger than 2 for heavy diatomic-ion bombardment (Andersen and Bay 1973, 1974, 1975, Johar and Thompson 1979, Oliva-Florio et al. 1979, Thompson 1981, Thompson and Johar 1981, Hofer et al. 1983), and formation of surface craters (Merkle and Jäger 1981, Pramanik and Seidman 1983).

Several theoretical models have been developed to describe sputtering in the spike regime: some assumed shockwave propagation (Yamamura and Kitazoe 1978, Carter 1979, 1980, Karashima 1982), some considered crater formation (Merkle 1977, Johar and Thompson 1979, Merkle and Jäger 1981, Roosendaal et al. 1982), but the majority of them were based on the thermal conduction and evaporation from collision-induced spikes (Thompson and Nelson 1962, Sigmund 1974, 1977, Vineyard 1976, Kelly 1977, 1979, Sanders 1980, Johnson and Evatt 1980, Sigmund and Claussen 1981, Claussen 1982, Szymonski 1982, 1984, Sigmund and Szymonski 1984, Urbassek and Sigmund 1984). Recent evaluation of the various models by Sigmund (1987b) suggests that the physical model invoking evaporation from high-temperature spikes is apparently better than the rest, although it has not yet been developed into a quantitative theory. Therefore, our discussion in this section will be based on this thermal-spike model.

Kelly (1977, 1979) and Johnson and Evatt (1980) used the equilibrium vapor pressure to determine the thermal sputtering yield (i.e., the number of evaporated atoms per

incident ion) during the decay of the spike. Sigmund and coworkers (Sigmund and Claussen 1981, Claussen 1982, Urbassek and Sigmund 1984, Sigmund and Szymonski 1984) and Szymonski (1984), on the other hand, considered the sputtered-atom flux at constant volume, using an ideal-gas description of the evaporation process. Whereas Kelly (1984a,c) pictured a sputtering event as a succession of four operational processes: prompt collisional ($10^{-15} \leq t \leq 10^{-14}$ s), slow collisional ($10^{-14} \leq t \leq 10^{-13}$ to $10^{-12}$ s), prompt thermal ($10^{-13}$ to $10^{-12} \leq t \leq 10^{-11}$ to $10^{-10}$ s), and slow thermal ($t >> 10^{-11}$ to $10^{-10}$ s, to treat sputtering in the spike regime, Sigmund and Szymonski (1984) subdivided the event into three stages that are well separated in time: linear cascade (over $10^{-13}$ s), elastic-collision spike ($10^{-13} \lesssim t \lesssim 10^{-11}$ s), and late state ($t >> 10^{-11}$ s). In the linear-cascade stage (corresponding roughly to the initial stage of the collisional phase shown in Fig. 4), the ion slows down, sharing its energy with a number of primary recoils. Then, smaller portions of the kinetic energy are transferred to higher-order recoil atoms, some of which may be ejected from the surface. This sequence of events can be described by the linear-cascade theory of sputtering (Sigmund 1969a, 1981). In the elastic-collision-spike stage (corresponding to the cooling phase shown in Fig. 4), energy has been shared among many atoms within a limited volume, and the resulting spike attains a very high temperature, typically from several thousand to ~ $10^4$ K. This high initial density of kinetic energy is a necessary condition for the observation of large sputtering enhancements in this stage. In the final stage (late state), evaporation of atoms occurs at a characteristic temperature close to the ambient target temperature, which must be approaching the melting point in order for the process to be significant. This low-temperature component, relative to the spike stage, is associated with the long-time behavior of the decaying spike, i.e., noticeable evaporation is achieved only if the late stage lasts over a large timescale, over which spikes overlap. As a result this continuous erosion effect bears little relation to the individual sputtering event; it is rather a macroscopic evaporation arising from the cumulative effect of several bombarding ions. In the following, we will briefly review some important theoretical evaluations of ion-induced evaporation, proceeding from the high-temperature (elastic-collision spike) regime to the low-temperature (late state) regime.

The simple cylindrical spike model of Sigmund and Claussen (1981) was the first to provide qualitative predictions of thermal sputtering from elastic-collision spikes. This model assumes a straight ion track surrounded by a cylindrical spike and neglects heat loss by evaporation as well as the effect of ambient target temperature. With reasonable input regarding primary energy deposition (constant deposition rate), initial temperature distribution, heat conductivity, and planar surface binding as in linear-cascade theory, Sigmund and Claussen (1981) obtained for the thermal sputtering yield:

$$Y_{th}(T_o,0) = 0.036 \frac{\lambda_o a_{BM}^2 F_D^2}{U^2} g(U/k_B T_o) , \qquad (28)$$

where $T_o$ is the initial temperature rise in the core of the spike, $F_D$ is the deposited energy per unit track length, related to $T_o$ by

$$k_B T_o = F_D/2\pi N\langle\rho_o^2\rangle \qquad (29)$$

with $\langle\rho_o^2\rangle^{1/2}$ being the initial radius of the cylindrical spike, and $g(U/k_BT_o)$ is an exponential-like function.

Several important features of thermal sputtering were derived from the Sigmund-Claussen model:

(i) Adding eqs. (23) and (28) together gives the total sputtering yield $Y_{total}$. A comparison of $Y_{total}$ with the linear yield Y, eq. (23), indicates that substantial thermal sputtering can only occur for $Y \gtrsim 10$.

(ii) The thermal sputtering yield $Y_{th}$ increases more rapidly than $F_D^2$ because of the monotonic increase of $g(U/k_BT_o)$ with increasing $F_D$ (or $T_o$) in eq. (28).

(iii) It follows from (ii) that, for bombardment with an n-atomic molecule, $Y_{th}$ increases faster than $n^2$.

(iv) The relative importance of thermal sputtering increases with increasing ratio of deposited energy to surface binding energy.

In general, these predictions have been found to be in good qualitative accord with experimental observations. (see, e.g., Thompson 1981, Sigmund 1987b, Schou 1989, and references therein).

Additional evaluations of thermal sputtering have been performed following this model. Claussen (1982) treated sputtering from a spherical spike and concluded that the cylindrical spike model provides a more adequate description of the measured yields. Urbassek and Sigmund (1984) found that the neglect of energy loss through evaporation in the Sigmund-Claussen model was justified for metals and many other solids with $U \gtrsim 1$ eV. In a subsequent work, Sigmund and Szymonski (1984) modified the earlier cylindrical model by including the effect of ambient target temperature, $T_a$. They proposed the following expression for the yield:

$$Y_{th}(T_o,T_a) = 0.024 \frac{\lambda_o a_{BM}^2 F_D^2}{U^2} (1 + T_a/T_o)^4 g[U/k_B(T_o + T_a)]. \qquad (30)$$

For not-too-high spike temperatures (i.e., $U >> k_BT_o$), the exponential-like function g is reduced to

$$g\,[U/k_B(T_o + T_a)] = 2\exp[-U/k_B(T_a + T_a)]. \qquad (31)$$

Equation (30) is practically identical to the result obtained by Sigmund and Claussen (1981) in the limit of $T_a = 0$. Comparing eq. (30) with eq. (28),

$$\frac{Y_{th}(T_o,T_a)}{Y_{th}(T_o,0)} = \left(1 + \frac{T_a}{T_o}\right)^4 \exp\left(\frac{U}{k_B T_o} \cdot \frac{T_a}{T_o + T_a}\right) \qquad (32)$$

Sigmund and Szymonski (1984) suggested that the higher the spike temperature, $T_o$, the less pronounced the yield variation is with target temperature $T_a$. Under typical spike conditions, the high-temperature component of the yield is only very

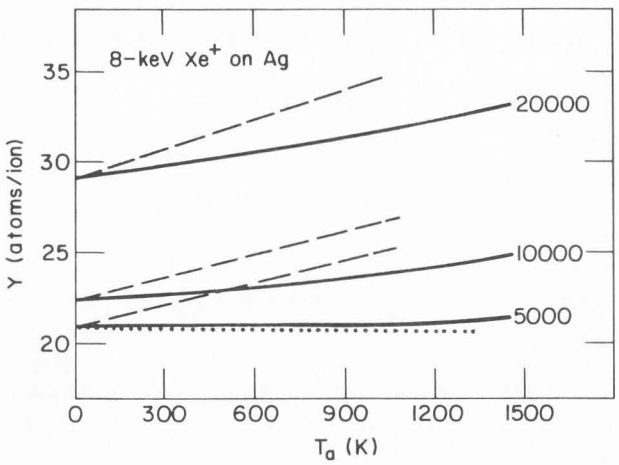


Fig. 13: Sputtering yields of Ag under 8-keV $Xe^+$ ion bombardment at normal incidence. The dotted line indicates the linear-cascade contribution [eq. (23)]. The solid lines represent the sums of linear-cascade and high-temperature spike contributions [eq. (23) + eq. (30)] calculated for various initial spike temperatures $T_o$ (indicated on curves). The dashed lines show the experimental data of Besocke et al. (1982), scaled from differential yields and normalized at $T_a = 0$. After Sigmund and Szymonski (1984).

weakly dependent on ambient temperature. Thus, all the qualitative predictions of yield enhancements that the Sigmund-Claussen model has provided can also be made here for the high-temperature regime.

Sample calculations by Sigmund and Szymonski (1984) for the case of 8-keV $Xe^+$ bombardment of Ag, which was investigated experimentally by Besocke et al. (1982), indicated that (i) at perpendicular incidence, the total yield $Y_{total}$ is dominated by the linear-cascade component, eq. (23), and (ii) there is no dramatic variations of $Y_{total}$ with $T_a$. The results are illustrated and compared with experimental data in Fig. 13. Good qualitative agreement between theory and experiment was obtained.

Equation (32) also shows that the $T_a$-dependence of $Y_{th}$ is an exponential function of U. Thus, it is expected to observe a more pronounced yield variation with $T_a$ for Au [U = 3.80 eV (Gschneidner 1964)] than for Ag (U = 2.96 eV). Sigmund and Szymonski (1984) found that $Y_{th}(T_o,T_a)/Y_{th}(T_o,0)$ increases linearly by a factor 3 over the temperature interval 0 - 1500 K. The variation of $Y_{total}$ with $T_a$ is less pronounced, depending on the relative significance of the $T_a$-independent linear-cascade component.

In a treatment of "prompt thermal" sputtering (which, based on the time scale, is similar to sputtering in the elastic-spike stage), Kelly (1977, 1979) considered the initial temperature distribution in the cascade volume as being equivalent to a three-dimensional Gaussian distribution of deposited energy with parameters known from the linear-cascade theory. He derived a general expression for the sputtering yield containing a double integral that was difficult to evaluate from first principles. Partial evaluation, however, led to the following criterion for thermal sputtering:

$$\text{Vapor pressure } p(T_{surface}) \geq 10^{2\pm1} \text{ atm.}$$

This would suggest that thermal sputtering can be neglected in most metals.

As the initial high-energy input is dissipated rapidly, the spike temperature approaches the ambient target temperature. In this late stage, the evaporation yield can be estimated by (Sigmund and Szymonski 1984):

$$Y_{th}^{c}(T_a) = \frac{F_D}{C}\frac{d\theta(T_a)}{dT_a}\, t_{max}\,, \tag{33a}$$

where C is the heat capacity per unit volume, $\theta(T_a)$ is the evaporation rate (number of atoms evaporated per unit time and area), given by a function of the type $\theta(T_a) = A\exp(-B/T_a)$, and $t_{max}$ is the time within which heat is lost to the surroundings by radiation or conduction. At $t_{max}$, the maximum spike radius for evaporation is $\rho_{max} = \infty$.

In view of this large size of the evaporating area, a spherical spike centered at some depth $x_s$ with initial energy $E_o$ may provide a better description of the late stage. For $x_s << (2\kappa t)^{1/2}$, with $\kappa$ being the thermal diffusivity, Sigmund and Szymonski (1984) found:

$$Y_{th}^{s}(T_a) = \frac{2E_o}{C}\left(\frac{t_{max}}{\pi\kappa}\right)^{1/2}\frac{d\theta(T_a)}{dT_a} \tag{33b}$$

The ambient-temperature yields, eqs. (33a) and (33b), depend on the macroscopic evaporate rate $\theta(T_a)$, and, unlike the high-temperature yield from elastic-collision spikes, are a linear function of the deposited energy $F_D$ or $E_o$.

Equations (33a) and (33b) are only valid in the limit of small ion flux because they refer to the late stage of a single spike. However, to a first approximation, the cumulative effect of many spikes can be estimated in the continuum limit. During bombardment with an ion flux $\phi$, the beam-induced evaporation rate is:

$$\theta(T_a + \Delta T_{eff}) = \phi Y_{th}(T_a), \tag{34}$$

which is equivalent to the effect of temperature rise:

$$\Delta T_{eff}^{s} = \phi\,\frac{2E_o}{C}\left(\frac{t_{max}}{\pi\kappa}\right)^{1/2} \tag{35}$$

for hemi-spherical spikes. The apparent evaporation yield is then:

$$Y_{app}(T_a) = \frac{1}{\phi}\left[\theta(T_a + \Delta T_{eff}) - \theta(T_a)\right], \tag{36}$$

which depends on ion flux. For high $\phi$, eq. (36) may no longer be valid because $\Delta T_{eff}$ may become so large than the linear approximation for $\theta(T_a + \Delta T_{eff})$ breaks down.

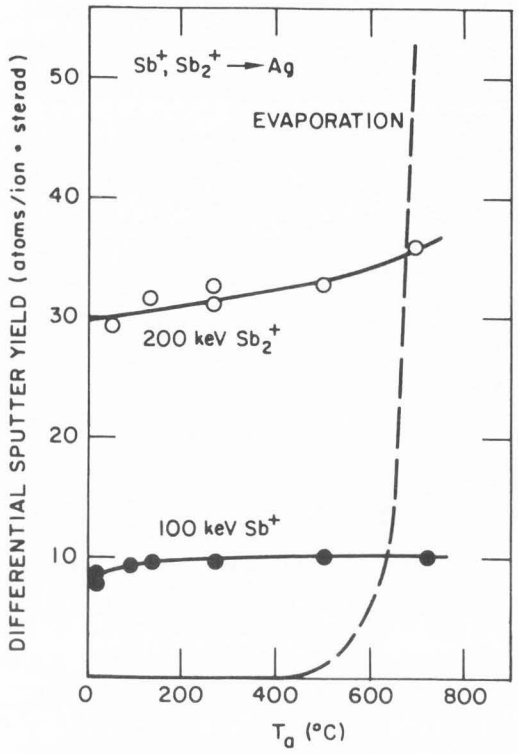


Fig. 14: Sputtering yields of polycrystalline Ag versus the target temperature due to the impact of 100-keV $Sb^+$ and 200-keV $Sb_2^+$ ions. The angles of incidence and ejection were $\theta = 45^\circ$ and $\theta_e = 0^\circ$, respectively. Also shown is the evaporation component (dashed curve) measured with the same detector and settings as for the sputtering. After Hofer et al. (1983).

Model calculations by Sigmund and Szymonski (1984) for beam-induced evaporation of Ag under 45-keV ion bombardment suggested that, with standard values for the thermal conductivity and capacity, any discernable evaporation effect from the low-temperature stage must occur in the long time regime ($t > 10^{-9}$ s) where spikes overlap and give rise to a uniform target temperature increase. For ion fluxes $\phi \lesssim 6.25 \times 10^{15}$ ions/cm$^2$·s (i.e. $\lesssim 10^3$ μA/cm$^2$), pronounced variations of the erosion rate with target temperature are expected only for $T_a \geq$ 1100 K. However, even at these fluxes, it is difficult to separate the beam-induced evaporation from equilibrium evaporation; so very precise measurements are required in order to detect the small difference. Besocke et al. (1982) and Hofer et al. (1983) did not observe any pronounced influence of target temperature on the sputtering yields of Ag under heavy-ion bombardment at temperatures up to ~1050 K (Fig. 14). No temperature effect was also reported for 15-keV $Ar^+$ sputtering of Ca and Cr (Husinsky et al. 1985). The theoretical results are thus in agreement with these observations.

The early, controversial measurements of the temperature dependence of the sputtering yield by Nelson (1965) for 45-keV $Xe^+$ on various metals showed an exponential increase of $Y_{total}$ with temperature above ~ 0.7 $T_m$, which he attributed to thermal spike contributions. These experimental data clearly contradict the more recent observations mentioned above and are not supported by the Sigmund-Szymonski model. An explanation for Nelson's puzzling results has first come from the careful study by Besocke et al. (1982) and Hofer et al. (1983) on sputtering of Ag. They found that the anomalously-large sputtering at $T \geq 900$ K persisted even if the ion beam was turned off, indicating that the drastic variation of $Y_{total}$ with temperature did not prove anything on thermal spikes, but only reflected the effect of significant, continuous thermal evaporation from the target surface.

**Angular Distribution and Energy Spectrum of Sputtered Atoms**

The angular distribution and energy spectrum of sputtered particles are contained in the differential sputtering yield (Thompson 1968, Sigmund 1981),

$$\frac{d^2Y}{dE_e\, d\Omega_e} \propto \frac{E_e}{(E_e + U)^3} \cos\theta_e \,, \qquad (37)$$

for atoms emerging with energy ($E_e$, $dE_e$) and angle ($\theta_e$, $d\Omega_e$) against the surface normal. This relation implies a planar surface barrier and m = 0. Furthermore, it was derived for a random target, and thus the anisotropic particle ejection, as observed in ion bombarded single crystals (Wehner 1956, Anderson and Wehner 1960, Roosendaal 1981, Hofer 1986 and references therein), was not accounted for.

According to eq. (37), the ejection of sputtered atoms obeys a simple cosine law. Experimentally, however, the simple cosine distribution is rarely observed, because it can be affected by many factors, including ion energy, depth of origin, impurities, and surface conditions (Sigmund 1981, 1987b). The dependence of the angular distribution of sputtered particles on ion energy and ion type has been systematically simulated recently by Biersack and Eckstein (1984). Their results are shown in Figs. 15a and b for Ni under normal incidence of $Ne^+$ ions at different energies, and of various types of ions at 1 keV, respectively. As seen in Fig. 15a, at very low ion energy (close to the threshold), the distribution is under-cosine (or heart-shaped (Andersen 1988)), i.e., less atoms ejected in the direction normal to the target surface, because of anisotropic collision cascades. With increasing energy, the distribution changes to cosine (around 300 eV), and then to over-cosine (at E > 300 eV). No further change in the distributions is found between 5 and 100 keV. Furthermore, the angular distribution is virtually independent of ion type and binding energy (Fig. 15b). These deviations from the ideal (isotropic) cosine distribution have been observed experimentally (e.g., Wehner and Rosenberg 1960, Patterson and Tomlin 1962, Rödelsperger and Scharmann 1976, Hofer et al. 1978, Bay et al. 1980, Andersen et al.

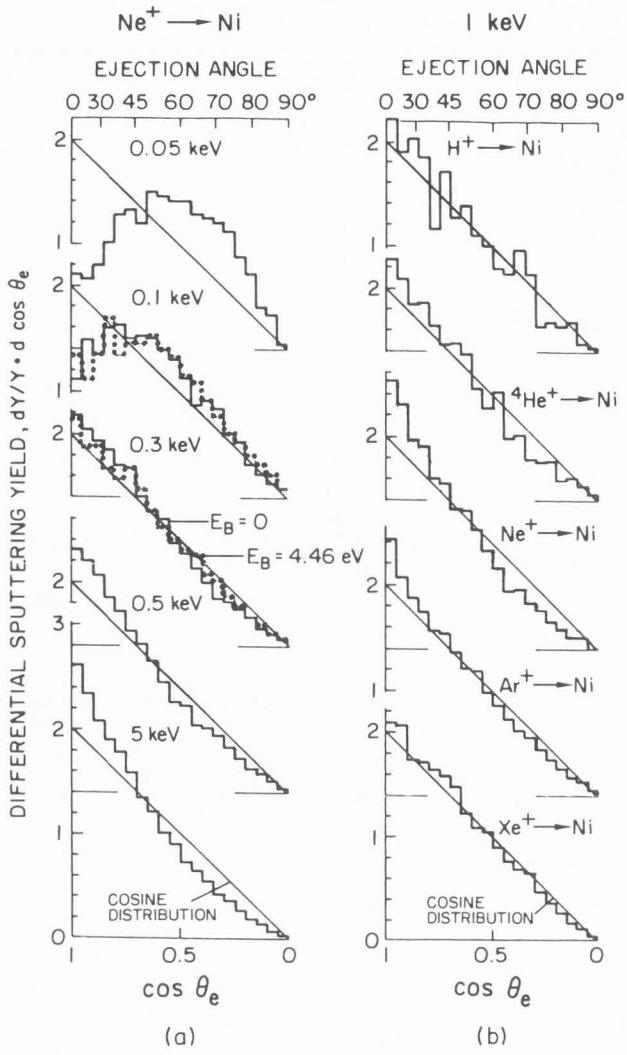


Fig. 15: Differential sputtering yields of Ni as a function of the cosine of the polar emission angle of the sputtered particles, calculated for normal incidence of $Ni^+$ ions at different energies (a) and of various ions at 1 keV (b), using the Monte Carlo program TRIM.SP. A cosine distribution (straight line) is included for easy comparison. The angular distribution is virtually the same for a bulk binding energy $E_B = 0$ as for $E_B = U = 4.46$ eV. After Biersack and Eckstein (1984).

1982, 1985). In general, the measured distributions can be analyzed using a cosine law of the form $\cos^{\chi}\theta_e$, where $\chi$ is a fitting parameter. Usually, as derived from fitting of experimental data, the value of $\chi$ varies between 1.0 and 2.0, depending on ion energy (Andersen et al. 1985). Two possible explanations for the over-cosine distributions have been proposed (see, e.g., Sigmund 1981, Andersen et al. 1985), based on surface-induced anisotropy of the recoil flux below the surface and/or anisotropic surface scattering of the recoil flux passing through the surface. Concerning the latter effect, Robinson (1969) suggested that an atom leaving the surface at an oblique angle experiences a net deflection toward the surface normal because of an asymmetric distribution of scattering centers. A rough estimation showed that this effect could be quite significant, causing an increase of $\chi$ from 1.0 to 1.55 (Sigmund 1987a). In addition, Sigmund et al. (1982) have pointed out that the polar angular distributions can be quite different for atoms sputtered from the first and second atomic layers. Since the angle of ejection is correlated with the depth of origin of sputtered atoms, i.e., grazing ejection prefers shallow depths, the angular distribution for first-layer ejected atoms is broad, whereas the distribution of atoms sputtered from the second layer is sharper, i.e. directed strongly towards the surface normal. This suggestion is supported by the results of molecular dynamics simulations for Cu (Shapiro et al. 1985) and experimental measurements on binary alloys (Andersen et al. 1982, 1984a,b, Dumke et al. 1983, Ichimura et al. 1984, Tombrello 1987, Hubbard et al. 1989a).

Equation (37) also shows that for a fixed ejection angle $\theta_e$, the energy spectrum of the sputtered particles exhibits a maximum at $E_e = U/2$ and falls off in proportion to $E_e^{-2}$ at high ejection energies. This behavior is borne out well experimentally. In fact, energy spectra of this type were first measured on Au by Thompson (1968) and on Cu by Farmery and Thompson (1968). Subsequently, the same behavior has been observed on other metals (Hucks et al. 1978, Weller and Tombrello 1978, Pedrys et al. 1981, Bay et al. 1980, Husinsky et al. 1984, Dembowski et al. 1987) as well as on insulators (Haring et al. 1984, Schou 1987, Chrisey et al. 1988). An example is given in Fig. 16 for the energy spectra of neutral atoms sputtered from Cu, V and Nb target under 2-keV $Ar^+$ bombardment (Dembowski et al. 1987). The individual spectrum has a maximum at an energy close to one-half of the sublimation energy ($U_{Cu} = 3.51$ eV, $U_V = 5.32$ eV and $U_{Nb} = 7.58$ eV, Gschneidner 1964), and the distribution tail shows a characteristic asymptotic $E_e^{-2}$-behavior.

In the spike regime, the peak of the energy spectrum of sputtered particles has been observed to occur at an energy substantially lower than 0.5U (Chapman et al. 1972, Szymonski and DeVries 1977, Ahmad et al. 1980) owing to contribution from elastic-spike effects, in qualitative agreement with the theoretical descriptions of Sigmund and Claussen (1981), and Sigmund and Szymonski (1984). The asymptotic behavior of the spectrum is still $E_e^{-2}$, which is characteristic for particles sputtered by momentum transfer during the collisional, linear-cascade phase (Ahmad et al. 1980, Szymonski 1982, Kelly 1984a).

**Depth of Origin of Sputtered Particles**

The sputter depth of origin has received great attention recently. The current interest in the determination of this depth has been motivated by the critical dependence of monolayer resolution of surface-sensitive analytical techniques and sputtering properties of multicomponent materials on the origin of sputtered atoms. Several theoretical efforts (Sigmund 1969a, Falcone and Sigmund 1981, Falcone 1986, Kelly and Oliva 1986a, Falcone et al. 1987, Sigmund et al.

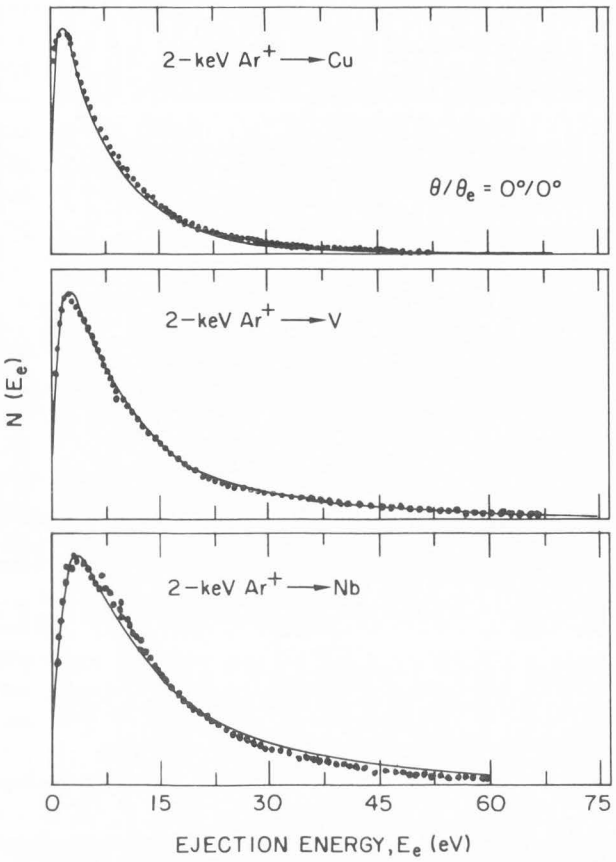


Fig. 16: Normalized energy spectra of neutral Cu, V and Nb atoms ejected perpendicular to the surface during 2-keV $Ar^+$ ion bombardment at normal incidence. The thin solid line represents the $E_e(E_e + U)^{-3}$-dependence. After Dembowski et al. (1987).

1989, Vicanek et al. 1989) have been devoted to evaluate the depth of origin of sputtered particles, $x_o$, which depends mainly on target parameters. This depth must be distinguished from the saturation depth, which is a minimum target thickness for which the sputtering yield attains its infinite-thickness value (Sigmund 1969a, Sigmund et al. 1989). The latter depth depends on both bombardment and target variables. For elemental targets, the depth of origin of sputtered atoms is only of theoretical interest; it is used in the derivation of the sputtering yield, but does not enter quantitatively into experiments. It is, however, an important quantity to be characterized in sputtering experiments on segregating alloys and layered compounds. In fact, thus far, all experimental measurements of $x_o$ have been made on alloy systems (Dumke et al. 1983, Morita et al. 1983, 1984, Krauss et al. 1984, Pellin et al. 1985, Lam et al. 1985 a, b, Lam and Hoff 1988, Hoff and Lam 1988, Burnett et al. 1988, Hubbard et al. 1989a,b).

As discussed in previous section, the energy spectrum of sputtered atoms exhibits a maximum at energies of a few eV (~ 0.5U). This means that most of sputtered atoms originate from a rather shallow depth. The $E_e^{-2}$-tail on the spectrum at higher energies may be associated with the emergence of high-energy recoils from greater depths. On the basis of linear-cascade theory, the mean depth of origin was estimated to be $x_o \simeq 0.5$ nm (Sigmund 1969a). In addition, Falcone and Sigmund (1981) showed that the distribution of the depth of origin of sputtered atoms in the low-fluence limit could be described by an exponential function, with $x_o \simeq 0.5$ nm being the characteristic depth. This estimate was fairly consistent with those derived from Monte Carlo simulations indicating a mean depth of origin of $x_o \simeq 0.7$ nm and a tail into larger depths (Ishitani and Shimizu 1975, Biersack and Eckstein 1984). It was, however, in disagreement with the results of binary collision simulations (Robinson 1983, Rosen et al. 1983) and molecular dynamics simulations (Harrison 1983, Shapiro et al. 1985) showing that virtually all atoms were ejected from the top two surface layers, i.e., from a depth less than half the thickness expected from the linear-cascade theory.

Recently, it has been suggested that the depth of origin of sputtered atoms is determined by the elastic collisional mean free path of an atom moving towards the surface, i.e., $x_o$ is the average depth at which a recoiling atom makes its last collision before passing through the surface (Falcone 1986). Since the energies of sputtered atoms are quite low, $x_o$ should be of the order of one mean atomic spacing, $\xi$. Kelly and Oliva (1986a) performed a detailed analysis of experimental and simulation data, and proposed a characteristic depth of sputtering of $x_o = (0.8 \pm 0.1)\xi$, which is roughly a factor of 3 smaller than the value obtained by Sigmund (1969a). Taking this difference into account together with a correction for semi-infinite geometry of the sputtered medium (i.e. the recoils participating in sputtering move only towards the surface in straight lines without further collisions), Falcone et al. (1987) suggested an effective increase, by a factor of ~ 3, in the value of the cross section $C_o$.

The incoherent picture of the sputter depth provided by the different approaches has motivated Sigmund and coworkers to reconsider the issue recently. Firstly, a "round robin" computer simulation of ejection probability in sputtering was undertaken in order to make a direct comparison of the predictions of different codes (Sigmund et al. 1989). Six molecular dynamics codes, four binary-collision lattice simulation codes and eight Monte Carlo codes were applied to simulate the ejection of a low-energy Cu recoil ($5 \leq E \leq 50$ eV) from a certain depth interval ($0 \leq x \leq 0.45$ nm) within a Cu target. Although large differences were found between the results of the various codes, partly caused by different cutoff radii and treatment of electronic stopping, a fairly clear picture was obtained for the depth range and the angular range for low-energy ejection. All molecular dynamics and binary collision simulations clearly indicate that, for a crystalline Cu target, atoms are sputtered largely from the outermost two layers. The Monte Carlo simulations show deeper tails. It should be pointed out, however, that the depth distributions evaluated in these simulation efforts are not depth

distributions of sputtered atoms, because no averaging was made over the energy spectrum of recoil atoms and their distribution in source depth.

And, secondly, a detailed theoretical analysis was carried out for the actual depth of origin of sputtered atoms, applying several schemes of solving the linear Boltzmann equation as well as Monte Carlo simulation (Vicanek et al. 1989). The results indicate that $x_0$ is determined primarily by the stopping of the recoil atoms on their way to the surface. Comparison between simulation results and those obtained by straight-line approximation of particle trajectories showed that there was practically no effect of angular scattering of the recoil atoms on the distributions in depth of origin and emission angle. These distributions do not depend significantly on whether the scattering medium is an infinite medium with a reference plane or a halfspace. The mean sputter depth was found to be $x_0 = (0.639 \text{ to } 0.800)/NC_0$, which is a large value, similar to the previous estimate, $x_0 = 3/4NC_0$ (Sigmund 1969a). However, Vicanek et al. (1989) showed that $x_0$ can be brought into close agreement with results from more realistic models (i.e., $x_0$ must be reduced by at least a factor of 2) if one improves the estimate of the constants that determine the approximation of the standard power cross section to Born-Mayer scattering. In fact, the m = 0 power law was shown to underestimate the cross section toward lower values of the Lindhard energy-angle variable $t^{1/2} = \varepsilon \sin\theta/2$. For Cu, for example, the scaled stopping cross section (Sigmund 1969a) is about a factor of 2 too low within the typical energy range for sputtered atoms, $\varepsilon = 10^{-4} - 10^{-3}$ (Vicanek et al. 1989). Correcting for this underestimation of $C_0$ decreases $x_0$ by the same factor; the new value is thus closer to the estimate by Kelly and coworkers (Kelly and Oliva 1986a, Falcone et al. 1987, Oliva et al. 1987) and is in agreement with the results of molecular dynamics and binary collision simulations.

It is worth mentioning some experimental measurements of the depth of origin here, even though they were made on alloys. Dumke et al. (1983) found that, during 15-keV and 25-keV $Ar^+$ bombardment of a liquid Ga-In eutectic alloy, 85% and 70% of the sputtered species originate from the first atom layer, respectively. This sensitivity of the sputter fraction to the ion energy is in contradiction with the prediction of the linear-cascade theory. Repeating Dumke's experiment using $Ar^+$ ions at various energies, Hubbard et al. (1989a,b) recently found that ~ 87% of the sputtered-atom flux comes from the first layer and that this sputter fraction is indeed independent of projectile energy within the range of 25 - 250 keV investigated. Only at very low energy, 3 keV, was the contribution of the top layer to the sputtered flux observed to increase to 94%. This increase in the first-layer contribution has also been observed in several computer simulations (Harrison 1983, Robinson 1983, Biersack 1987). Investigations of the temperature dependence of steady-state surface composition have led to the conclusion that ~ 65% of the sputtered atoms come from the outermost layer in 3-keV $Ne^+$ bombarded Ni-Cu (Lam et al. 1985b), ~ 50-65% in Ni-Au (Lam et al. 1985a), ~ 55% in Ni-Ge (Hoff and Lam 1988), ~ 70% in Ni-Pd (Tang and Lam 1989), and ~ 95-100% in Ni-Si alloys (Lam and Hoff 1988). Measurements of Burnett et al. (1988) indicated that ~ 66% of the sputtered-atom flux is from the first layer in the Cu-Ru system.

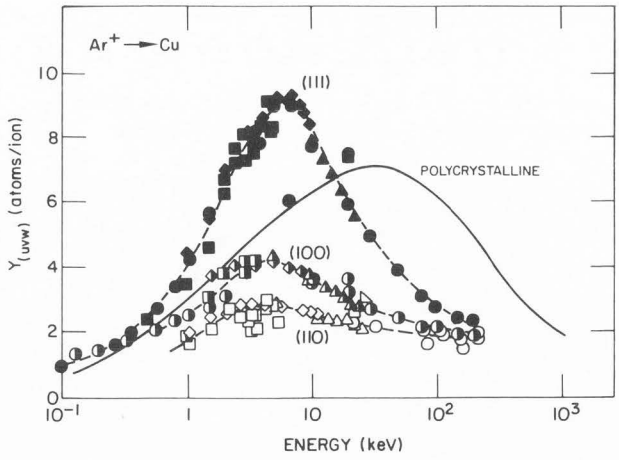


Fig. 17: Energy dependence of the sputtering yields for $Ar^+$ ions on the (100), (110) and (111) surfaces of Cu. Also shown are the sputtering yields of polycrystalline Cu. After Roosendaal (1981).

**Crystallographic Dependence of the Sputtering Yield**

All the sputtering theories discussed above were developed for random targets. It has long been known, however, that the sputtering process in crystalline materials is strongly influenced by the crystallographic orientation of the surface relative to the incident beam direction. Numerous investigations of sputtering of single crystals have been carried out, mostly in the 1950's and 1960's. Extensive reviews of theoretical aspects (Robinson 1981) and experimental measurements (Roosendaal 1981) of monocrystal sputtering have been published.

Several general features of the crystallographically-dependent single-crystal sputtering yield, $Y_{(uvw)}$, have been established (Roosendaal 1981). Some important aspects of the energy dependence of $Y_{(uvw)}$ from a (uvw) surface are summarized here. For normal ion incidence on FCC targets, it was found that $Y_{(111)} > Y_{(100)} > Y_{(110)}$. Similarly, the energy $E^{max}_{(uvw)}$, at which the $Y_{(uvw)}$ curve exhibits a maximum, also showed the inequality $E^{max}_{(111)} > E^{max}_{(100)} > E^{max}_{(110)}$. An example is shown in Fig. 17 for $Ar^+$ ions on a Cu single crystal (Roosendaal 1981). The common observation is: the larger the interatomic spacing $f_{(uvw)}$ measured along the [uvw] direction, the higher the $Y_{(uvw)}$ and the $E^{max}_{(uvw)}$. Moreover, $Y_{(111)}$ was found to be larger than the value of Y obtained from a polycrystalline target under the same incidence conditions at low energies, but became smaller than Y at high energies. The energy at which $Y_{(111)} = Y$ depends on the ion-target combination. For BCC, HCP and diamond-type lattices, the same general rule seems to apply (Roosendaal 1981).

The crystallographic variation of $Y_{(uvw)}$ at energies above a few keV can be understood with the theoretical model of Onderdelinden (1966, 1968), which includes the effect of channeling on sputtering. Assuming that only nonchanneled incoming particles contribute to the sputtering process, Onderdelinden (1966, 1968) obtained the following expression relating the single-crystal yield $Y_{(uvw)}$ to the polycrystalline yield Y:

$$Y_{(uvw)}(E) = \Psi_{(uvw)}\, \Gamma_{(uvw)}(E)\, Y(E), \qquad (38)$$

where $\Psi_{(uvw)}$ is an "efficiency" parameter, which is always larger than unity, and $\Gamma_{(uvw)}(E)$ is the nonchanneled fraction of the incident beam upon entering the crystal surface, which can be estimated using the channeling theory of Lindhard (1965). $\Gamma_{(uvw)}(E)$ is a function of $f_{(uvw)}$ and the critical angle for channeling along the [uvw] direction. Equation (38) predicts that the yield $Y_{(uvw)}$ shows a minimum whenever the incident beam coincides with a channeling direction.

For incident ions of energy above a few keV on low-index planes, the Onderdelinden model provides a good qualitative interpretation of the dependence of $Y_{(uvw)}$ on the lattice spacing $f_{(uvw)}$ and incident energy. However, for planes with higher indices, the model fails to make correct predictions for this dependence. On the other hand, for ion energies below a few keV, the application of the channeling theory is not justified, and the Onderdelinden model breaks down. At very low energies (below ~ 500 eV), $Y_{(uvw)}$ is mainly determined by the surface binding energy $U_{(uvw)}$.

Recently, interest in sputtering of monocrystalline materials seems to be renewed again, as reflected by the increasing number of computer simulations of sputtering, which often involve crystalline lattices (Shulga 1983, 1984, 1985, Harrison 1983, Harrison et al. 1987, Shapiro et al. 1985, 1988, Shapiro and Tombrello 1987, Hautala and Likonen 1988). New computational efforts have been directed toward a basic understanding of the directional effects on atom ejection, ejection mechanisms and patterns as well as sputter depth of origin.

**Sputtering of Clusters**

The presence of polyatomic species or clusters in the sputtered flux from a bombarded surface was first observed three decades ago (Honig 1958, Krohn 1962). Experimental data have now been accumulated for cluster emission from a wide variety of target materials covering metals, semiconductors, alloys, compounds, frozen gases, and organic substances. A review of the subject can be found in recent articles by Oechsner (1985), Hofer (1980,1986), Urbassek (1987), de Vries (1987), and Gnaser and Hofer (1989).

The sputtered clusters can be either neutral or positively or negatively charged, and their abundance in the sputtered flux can be quite large. For instance, results obtained from Cu, Ag and Ge showed that the fraction of neutral diatomic clusters was approximately 20% (Gnaser and Hofer 1989). Similar to atomic ejection, emission of clusters from single crystals can also be anisotropic. Measurements carried out with charged clusters on BCC (Staudenmaier 1972, 1973) and recently with neutral clusters on FCC (Hofer and Gnaser 1987) single crystals have shown enhanced emission of di- and triatomic clusters along close packed directions. Moreover, since the probability for clusters to dissociate increases with their kinetic energy, the energy spectrum of sputtered clusters is expected to drop faster than the $E_e^{-2}$-dependence for single atoms at high energies (Staudenmaier 1972, de Vries 1987).

Several concepts have been proposed for cluster sputtering; however, no basic mechanism has been universally accepted (Urbassek 1987, de Vries 1987). The two most important models are the direct-emission and recombination models. The former, which is conceptually the simplest, suggests that collective ejection of the whole cluster from the surface occurs if the cluster binding energy is large, relative to the surface binding energy of the cluster. This model has been treated in some detail recently by Urbassek (1987). The latter model describes the formation of clusters above the target surface by statistical association of independently-ejected atoms (Oechsner and Gerhard 1974, Können et al. 1974, 1975, Harrison and Delaplain 1976, Garrison et al. 1978, Winograd et al. 1979). This implies that the individual atoms involved must be ejected from nearest or next-nearest neighbor sites. Combining this separation restriction with the shallow sputter depth of origin suggests that the atoms which are to be bound into a cluster above the surface originate from a very small volume. In addition, the atoms involved must be emitted within a maximum time interval of $\sim 10^{-14}$ s (Staudenmaier 1973), which is quite small compared with the duration of the collisional phase ($\sim 10^{-13}$ s) of a displacement cascade. These requirements indeed make the difference between the two models less obvious.

A number of features connected with well-known ejection processes for atoms, such as linear-collision cascades, thermal spikes and evaporation have also been found for molecules (de Vries 1987). However, experimental evidence indicates that the types of molecules that are sputtered are mainly determined by chemical bond strengths and chemical reactions in the surface region of the solid.

## SPUTTERING OF MULTICOMPONENT MATERIALS

In this section, we concentrate only on metallic systems in which the effects of electronic excitation and/or ionization on atom ejection and defect formation can be neglected. For a review of sputtering of insulators and oxides, the reader is referred to recent articles written by Kelly (1981, 1984b, 1987a), Townsend (1983), and Betz and Husinski (1988).

**"True" Preferential Sputtering (Primary Effects)**

By definition, the primary effects include the physics of the individual sputtering events (Sigmund 1981). We thus consider here preferential sputtering of a homogeneous target, in the limit of low fluence where bombardment-induced local

composition changes are insignificant. Equations (16) and (19) phenomenologically define the partial sputtering yield of the element k in an alloy:

$$Y_k = \sum_{n=1}^{\infty} P_k^{(n)} C_k^{(n)} \simeq S_k \sum_{n=1}^{2} \beta_k^{(n)} C_k^{(n)} .$$

"True" preferential sputtering is said to occur whenever $P_k^{(n)} \neq P_j^{(n)}$ in any layer, i.e., whenever $\beta_k^{(n)} \neq \beta_j^{(n)}$ and/or $S_k \neq S_j$. Since there is no information, neither experimental nor theoretical, about the relative sputter fractions, $\beta_k^{(n)}$ versus $\beta_j^{(n)}$, we will limit our discussion of "true" preferential sputtering to the effect of $S_k \neq S_j$ (assuming $\beta_k^{(n)} = \beta_j^{(n)} = 1$).

For sputtering of a random alloy in the linear-cascade regime, the sputtering coefficient ratio of two components k, j is given by (Andersen and Sigmund 1974, Sigmund 1981, 1987a):

$$\frac{S_k}{S_j} = \frac{C_k}{C_j} \left(\frac{M_j}{M_k}\right)^{2m} \left(\frac{U_j}{U_k}\right)^{1-2m} \qquad (39)$$

where C, M and U denote the atom concentration, mass and surface binding energy, respectively. The inverse proportionality of S to M and U shown in eq. (39) predicts that the lightest component and/or the component with the lowest binding energy should be sputtered preferentially. The relative importance of the mass and surface-binding effects depends on the magnitude of m. However, since m is usually small, $m \simeq 0.1$ (Vicanek et al. 1989), the effect of a difference in surface binding energies is more important than that caused by different masses.

The stronger deflection of a lighter atom leaving the surface toward the surface normal is also a possible cause of preferential sputtering in isotopic systems (Sigmund 1987a,b). Since, for a planar surface barrier, the sputtering yield increases with increasingly normal ejection, preferential ejection of the lighter isotope will occur.

Preferential sputtering of the lighter element is most pronounced during light-ion bombardment at energies near the sputter threshold (Taglauer and Heiland 1978, Varga and Taglauer 1981, Taglauer 1982, Baretzky et al. 1987). For the particular case of $Ta_2O_5$ bombarded with 1.5 - 2.0 keV $He^+$ ions at room temperature, for example, the preferential ejection of oxygen atoms led to significant oxygen depletion at the surface. The measured buildup time to steady state, steady-state sputtering yield and concentration depth profiles could be compared quantitatively with standard binary-collision theory, based entirely on mass effects (Baretzky et al. 1987). It is important, however, to point out that, for bombardment with heavy ions, preferential sputtering of the heavy component would occur near threshold (Sigmund 1988).

For sputtering in the spike regime, Sigmund (1981) made the same predictions for the effects of different masses and binding energies on sputtering preference; however, the dependence of $S_k/S_j$ on $U_k$ and $U_j$ was expressed in a Boltzmann exponential form involving the spike temperature $T_o$.

Experimental measurements of "true" preferential sputtering are generally difficult, because very low fluences are required in order to avoid secondary effects. The theoretically simple case of preferential sputtering in isotopic systems has been investigated using SIMS (Okano et al. 1985, Gnaser and Hutcheon 1988). However, the interpretation of experimental data was not unambiguous, because of the mass dependence of the ionization probability (Shimizu and Hart 1982, Slodzian 1983, Schwartz 1986). "Computer" experiments with both molecular dynamics and Monte Carlo techniques have been useful in testing the theoretical predictions for the mass effects at low ion fluence. Simulational results showed either stronger (Haff 1977, Shapiro et al. 1988) or weaker (Watson and Haff 1980, Haff et al. 1981) mass dependence of preferential sputtering than that given by eq. (39). In the latter studies, the calculations were performed under the assumption of hard-sphere collisions, with an energy-independent hard-sphere radius; therefore, the results are essentially equivalent to those obtained without taking the factor $(M_i/M_j)^{m_i}$ into account in eq. (13a). Consequently, all linear effects were excluded from the beginning, and only quadratic effects were retained (Sigmund 1987b).

The prediction of binding-energy effects on preferential sputtering, on the other hand, can be tested quantitatively only when information on $U_k$ and $U_j$ for the alloys is available. There is, however, strong evidence that the surface binding energies of the alloying elements depend on alloy composition. For example, Szymonski (1980) demonstrated that $U_{Zn}$ in Cu-Zn alloys decreased with increasing Zn concentration towards the pure-Zn value, while $U_{Cu}$ decreased from the elemental value to a substantially smaller one. Oechsner and Bartella (1981) and Schorn et al. (1988) have made similar observations in Ni-W and Cu-Li alloys, respectively. Noticeable matrix effects on the surface binding energy were also found for Cr atoms in different alloys (Husinsky et al. 1987). Moreover, based on "quasi-chemical" thermodynamics, Kelly (1978, 1980) has proposed the following composition dependence of the surface binding energy $U_A$ in a random binary alloy AB:

$$U_A = - Z_S \left[ C_A^{(1)} U_{AA} + C_B^{(1)} U_{AB} \right] , \qquad (40)$$

where $Z_S$ is the mean surface coordination number, and $U_{AA}$ and $U_{AB}$ are the nearest-neighbor A-A and A-B bond strengths, which are related to the heat of atomization and the heat of mixing, respectively. Taken together with eq. (39), eq. (40) suggests that the species which is sputtered preferentially has the weaker bonding.

The effect of preferential sputtering on the near-surface composition of a binary alloy AB is schematically shown in Fig. 18 for the case where $P_A^{(1)} > P_B^{(1)}$ (e.g., $S_A > S_B$ and $\beta_A^{(1)} = \beta_B^{(1)} = 1$). At short sputtering times, since A atoms are

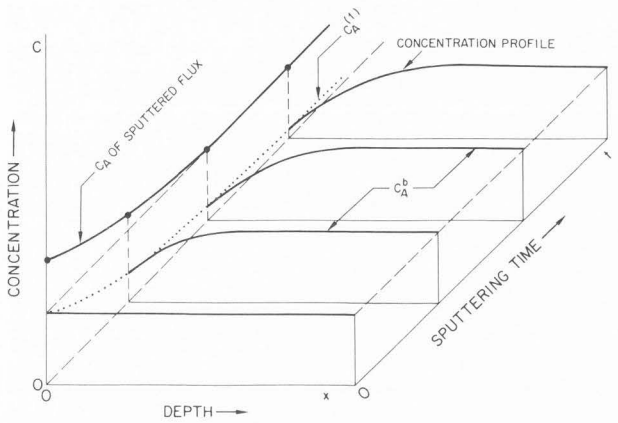


Fig. 18: Schematic description of the effect of genuine preferential sputtering on the time evolution of the sputtered-flux composition and the development of the concentration profile.

sputtered preferentially, the concentration of A atoms in the sputtered-atom flux is larger than that in the bulk. The preferential removal of A atoms leads to a gradual decrease in the surface concentration of the A component, $C_A^{(1)}$, with increasing fluence. After a certain sputtering time, however, a steady state will be reached; at that time, the composition of the sputtered-atom flux becomes identical to the bulk composition, as dictated by the law of matter conservation (Patterson and Shirn 1967, Shimizu et al. 1973):

$$\frac{S_A C_A^{(1)}}{S_B C_B^{(1)}} = \frac{C_A^b}{C_B^b} . \qquad (41)$$

Here, $C_A^b$ and $C_B^b$ denote the concentrations of A and B atoms in the bulk. It is noted that eq. (41) is applicable only for the case where all the sputtered atoms originate from the outermost surface layer. If the second layer also makes significant contributions to the sputtered-atom flux, then the condition for steady state will be:

$$\frac{S_A \sum_{n=1}^{2} \beta_A^{(n)} C_A^{(n)}}{S_B \sum_{n=1}^{2} \beta_B^{(n)} C_B^{(n)}} = \frac{C_A^b}{C_B^b} . \qquad (42)$$

Furthermore, the above steady-state conditions, e.g., eq. (41), for binary alloys can be generalized to multicomponent systems, requiring that any pair of the alloy components obeys the following relationship (Qu 1985, 1986):

$$\frac{S_k C_k^{(1)}}{S_j C_j^{(1)}} = \frac{C_k^b}{C_j^b} . \qquad (43)$$

**Kinetic Processes (Secondary Effects)**

In addition to preferential sputtering, several distinct chemical and physical processes can change the near-surface composition of solids undergoing bombardment (see Fig. 1). These processes include displacement mixing during the defect-production stage, and Gibbsian segregation, radiation-enhanced diffusion and radiation-induced segregation during the defect-migration stage. For the sake of completeness, two additional processes should also be mentioned, namely, ion implantation and nuclear transmutations. However, these latter effects will not be discussed here, because they are highly specific to the type of irradiating particles.

Frequently, under a given set of conditions, more than one of the above processes take place simultaneously, and thus the resulting compositional and microstructural changes are quite complex. To discuss the synergistic effects of these diverse processes on alloy composition modifications, we first briefly characterize them in simple physical terms.

**Gibbsian segregation.** When the alloy is held at an elevated temperature, a thermodynamic driving force gives rise to composition changes at the surface in order for the system to minimize its surface free energy. This thermally-activated segregation phenomenon can be described within the framework of a thermodynamic formalism for interfaces, by the use of the so-called Gibbs Adsorption Equation (Hondros and Seah 1977, Wynblatt and Ku 1979, Guttmann and McLean 1979, Hofmann 1985), and is therefore called Gibbsian segregation or Gibbsian adsorption. At equilibrium, this phenomenon only causes compositional perturbations in the "surface" phase which is confined to the outermost one or two atom layers, a thickness comparable to the sputter depth. Thus, while preferential sputtering tends to pin the alloy surface composition at a value that is different from the bulk value, Gibbsian segregation has a tendency of changing this composition, i.e., enriching or depleting the k-component at the surface, depending on whether the heat of adsorption for this element is negative or positive, respectively (Wynblatt and Ku 1979, Guttmann and McLean 1979).

If the rate of thermally-activated or radiation-enhanced atom exchange between the outermost and underlaying atomic layers is sufficiently fast, the concentration ratio $C_A^{(1)}/C_B^{(1)}$ in, e.g., a binary alloy AB will approach its thermal equilibrium value given by the relationship (Wynblatt and Ku 1979):

$$C_A^{(1)}/C_B^{(1)} = \left(C_A^b/C_B^b\right) \exp(-\Delta G_s/k_B T_a), \qquad (44)$$

where $T_a$ is the absolute temperature of the alloy, and $\Delta G_s$ is the segregation free energy, i.e., the energy change associated with the exchange of a B atom in the "surface phase" with an A atom in the adjacent layer belonging to the "bulk phase". The equilibrium is attained by a net flux of A atoms into the surface layer defined as:

$$\Omega J_A^{Gs} = \left(\nu_A^{b(1)} C_A^b C_B^{(1)} - \nu_A^{(1)b} C_A^{(1)} C_B^b\right) \xi \qquad (45)$$

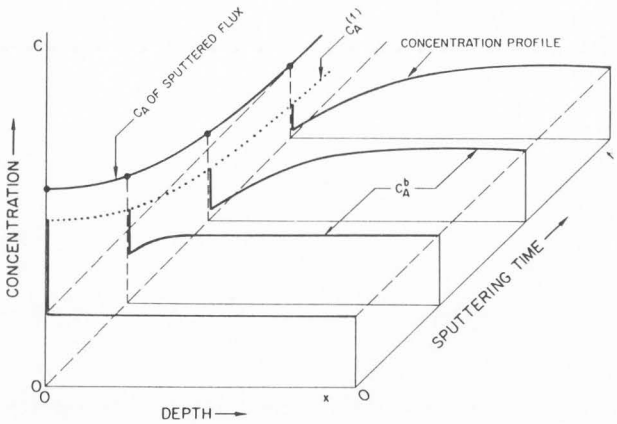


Fig. 19: Schematic description of the simultaneous effects of preferential sputtering and Gibbsian segregation on the time evolution of the sputtered-flux composition and the development of the subsurface altered layer.

where $\nu_A^{b(1)}$ and $\nu_A^{(1)b}$ are the jump frequencies of A atoms from the bulk to the outermost atomic layer and from the outermost layer into the bulk, respectively. These frequencies are related to each other by the following equation:

$$\nu_A^{(1)b} = \nu_A^{b(1)} \exp(\Delta G_s / k_B T_a), \qquad (46)$$

which is derived from the condition of equilibrium, $J_A^{Gs} = 0$. It is clear that, for a surface-segregating element ($\Delta G_s < 0$), the activation energy for a backward surface-to-bulk jump is effectively increased by the adsorption energy, relative to the migration energy in the bulk. In addition, since these atom jump frequencies are proportional to the concentrations and jump frequencies of point defects (Lam and Wiedersich 1987), Gibbsian segregation can be strongly enhanced by irradiation at temperatures where the concentration of thermal vacancies is smaller than those of radiation-induced defects ($T_a \lesssim 0.6T_m$). At very low temperatures, where normal thermally-activated diffusional processes become negligible, the mixing-induced motion of atoms within the cascades may promote Gibbsian segregation. The contribution of this "quasi-thermal" diffusional process can be accounted for by including a temperature-independent term representing the cascade-induced atom jump frequency on the right-hand side of eq. (46).

The synergistic effects of Gibbsian segregation and preferential sputtering on the development of the near-surface concentration profile are schematically illustrated in Fig. 19 for the case where $S_A > S_B$ (with $\beta_A^{(1)} = \beta_B^{(1)} = 1$), and initially $C_A^{(1)} >> C_A^b$. At short bombardment times, enhanced preferential sputtering of the A-component occurs, because the A atoms are not only sputtered preferentially, but also are enriched in the surface layer. Consequently, the A concentration in the sputtered-atom flux is excessively higher than the bulk concentration. As the sputtering continues, the surface concentration of A atoms and, hence, the A concentration in the sputtered flux, gradually decrease toward their steady-state values. Since the alloy system always attempts to evolve toward thermodynamic equilibrium [eq. (44)], the concentration of A atoms in the subsurface region also decreases accordingly. At low temperatures, the region of depletion is spread out mainly by displacement mixing; the thickness of the resulting altered layer should not exceed the damage range. However, at elevated temperatures, where the vacancy mobility is significant, point defects escape from the damage region, and radiation-induced and -enhanced processes lead to large altered layers that extend far into the target.

The complementing or competing effects of Gibbsian segregation and preferential sputtering make it difficult to derive definitive information regarding "true" preferential sputtering from measured surface compositional changes or compositions of the sputtered-atom flux. In fact, a correlation between the component that is observed to be sputtered preferentially during bombardment and the component that segregates to the surface in the same alloy upon heating was established by Kelly (1978, 1980). The connection between surface segregation of a low-surface-binding-energy component and sign of preferential sputtering was also pointed out by Andersen (1979a).

Rehn et al (1979) have interpreted their measurements of excessive Cu depletion in the subsurface region of a Ni-Cu alloy sputtered at elevated temperatures in terms of Gibbsian adsorption-induced preferential removal of Cu by sputtering. The pronounced influence of Gibbsian adsorption on the sputtering profile of oxygen in Nb at elevated temperatures was measured by Hofmann (1980b). He proposed a segregation-induced diffusion model, which enabled the evaluation of the diffusion coefficient for the segregating solute. The angular distributions of sputtered alloy elements are affected by the compositional gradient in the surface region. Measurements of these distributions have provided useful information about Gibbsian segregation during irradiation (Andersen et al. 1982, 1984a,b, Ichimura et al. 1984).

**Displacement mixing.** During a displacement cascade event, spatial relocation of atoms occurs, and point defects are produced. In alloys, this atom relocation process is called displacement mixing, which comprises, in principle, recoil implantation and cascade mixing (Sigmund and Gras-Marti 1981, Littmark and Hofer 1984, Littmark 1985). Recoil implantation takes place when one type of atoms is preferentially transported in the beam direction due to preferential momentum transfer, whereas cascade mixing is a random-walk process resulting from the movement of higher-order recoils.

Recent theoretical treatment by Sigmund (1988) has provided new insight into the mechanisms of recoil implantation in polyatomic targets. Angular scattering of slowing-down recoil atoms is the main factor that determines the direction of their implantation. At low ion energies, angular scattering causes the heavier species to be implanted

preferentially. At high energies, the relative importance of this effect decreases, and preferential implantation of light atoms becomes favored. However, since recoil implantation involves direct ion-atom collisions which are relatively rare events, and since the rapid transfer of energy from recoiling atoms to other atoms gives rise to an efficient randomization of recoil directions, most of the atom relocation events in energetic cascades contribute to isotropic mixing rather than preferential recoil implantation (Littmark and Hofer 1980). Thus, the effect of isotropic mixing is much larger than that of recoil implantation. Various physical models and theoretical treatments of displacement mixing have been discussed in a recent review by Littmark and Hofer (1984). Reviews on experimental measurements of ion beam mixing are also available (Matteson and Nicolet 1983, Mayer and Lau 1983, Averback 1986).

To a first approximation, displacement mixing can be estimated within a diffusion model (Andersen 1979b, Matteson et al. 1981, Lam and Wiedersich 1981). The intermixing flux of k-atoms, $J_k^{dm}$, across a fixed lattice plane is calculated by:

$$\Omega J_k^{dm} = - D^{dm} \nabla C_k, \qquad (47)$$

where $\Omega$ is the average atomic volume in the alloy, and $D^{dm}$ is the displacement-induced interdiffusion coefficient, which can be approximated as $D^{dm} \simeq \lambda^2 \eta K/6$ (Lam and Wiedersich 1981, 1987). Here, $\lambda$ is the nearest-neighbor distance, K is the spatially-dependent defect-production rate (displacements per atom per second, dpa/s) and $\eta$ is a factor proportional to the number of atoms changing sites (i.e. making jumps of length $\lambda$) per Frenkel pair generated (Wiedersich 1986, Lam and Wiedersich 1987).

Values of $\eta$ within the range $10^2$ - $10^3$ have been derived from experimental measurements of ion beam mixing (Kim et al. 1985, Averback 1986) and of disordering rates in ordered alloys (Kirk and Blewitt 1982, Zee et al. 1983) at low temperatures. The product $\eta K$ and, hence, the coefficient $D^{dm}$ are generally temperature independent; thus, displacement mixing can be considered as an athermal process. It is noted that, although replacement collisions and atom relocations in energetic events tend to randomize the alloy system, induced defect migration and recombination that take place during the "cooling" phase ($\gtrsim 10^{-13}$ s) may be influenced by thermodynamic forces. These "quasi-thermal" diffusional processes within the cascades may, in addition to promoting Gibbsian segregation (as discussed above), give rise to observed "chemical" effects in ion beam mixing, where the heat of mixing and/or the chemical affinity can affect the intermixing rate (Cheng et al. 1984, d'Heurle et al. 1985, Averback et al. 1986). These "chemical" effects can be accounted for, to a first approximation, by multiplying $D^{dm}$ by the factor $(1 - 2\Delta H_m/kT_s)$, which reflects the influence of the heat of mixing $\Delta H_m$ on ion mixing under thermal spike conditions (Cheng et al. 1984, Averback 1986):

$$D_A^* = D^{dm}(1 - 2\Delta H_m/k_B T_s). \qquad (48)$$

Here, $T_s$ is the average spike temperature (averaged over the spike lifetime). For $\Delta H_m < 0$, enhanced mixing will occur; however, with $\Delta H_m > 0$, reduced mixing, or even de-mixing, will take place. The role of thermodynamics in bombardment-induced atomic rearrangements in alloys has been discussed by Johnson et al. (1985). Recently, Kelly (1989) pointed out that the thermal-spike description of mixing has two problems: it neglects the importance of point defect motion following each impact, and it sometimes violates the condition that the chemical driving force be greater than ~ $k_B T_a$. He proposed a mixed ballistic-thermodynamic description of ion-beam mixing: each ballistic relocation can be envisaged as being terminated by a chemical step which ranges from a relaxation of the disordered lattice to defect diffusion.

Displacement mixing of alloying elements is the dominant atom-transport mechanism at low temperatures where vacancies are immobile, i.e. below ~ $0.2T_m$. It can spread compositional changes induced in the outermost atom layers to greater depths. It is not, however, an efficient feeding mechanism for preferential sputtering of an alloy component, because the threshold displacement energy is much larger than the surface binding energy, $E_d/U \simeq 5$ - 10 (Andersen 1984).

**Radiation-enhanced diffusion**. At elevated temperatures, between ~ 0.2 and ~ $0.6T_m$ (dependent on damage rate), thermally-activated diffusion processes becomes dominant. In this temperature regime, radiation-induced point defects are mobile, and their concentrations can exceed the thermodynamic-equilibrium values by many orders of magnitude. Since the average diffusion coefficients of the atoms in the alloy are functions of the defect concentrations, $C_v$ and $C_i$,

$$D_A \equiv D_A^v + D_A^i = d_{Av} C_v + d_{Ai} C_i, \qquad (49)$$

atomic diffusion is strongly enhanced by irradiation. Here, $D_A^v$ and $D_A^i$ are the partial diffusion coefficients of A atoms via vacancies and interstitials, and $d_{Av}$ and $d_{Ai}$ are the diffusivity coefficients which contain the kinetic information regarding jump distances, jump frequencies and factors related to preferential association of A-atoms with vacancies and interstitials, respectively (Wiedersich et al. 1979, Wiedersich and Lam 1983).

In the regime where diffusion of defects is limited by their mutual recombination, the radiation-enhanced diffusion coefficient is proportional to the square root of the particle flux (i.e., the defect-production rate), and the slope of the Arrhenius plot corresponds to one-half of the migration energy of vacancies (the slower moving species). On the other hand, in the dominant sink-annihilation regime, the diffusion

coefficient is linearly proportional to the flux and temperature independent for a fixed sink density (Wiedersich 1972, Lam and Rothman 1976).

The enhancement of the defect concentrations by irradiation has been treated theoretically by Damask and Dienes (1963), Wiedersich (1972), Lam et al. (1974), Sizmann (1978), Brailsford and Bullough (1978). The buildup of point-defect diffusion profiles toward steady state in a foil during irradiation was first modeled by Rothman et al. (1973) and discussed in detail by Sizmann (1978). Steady-state defect concentration profiles in a thin film or a semi-infinite solid can be calculated analytically using the expressions derived by Lam et al. (1974). Recent reviews of radiation-enhanced diffusion are available (Adda et al. 1975, Lam and Rothman 1976, Sizmann 1978, Rothman 1983).

At higher temperatures, generally above ~ $0.6T_m$, the concentration of thermal vacancies becomes higher than the concentrations of radiation-generated defects, and thermal diffusion via vacancy mechanism is dominant.

**Radiation-induced segregation**. The same point defects that are responsible for radiation-enhanced diffusion can also induce segregation of the alloying elements, a phenomenon called radiation-induced segregation, a widely-accepted terminology since 1972 (Anthony 1972). In contrast to radiation-enhanced diffusion, which accelerates the approach to an equilibrium compositional distribution, radiation-induced segregation tends to drive the alloy system away from thermodynamic equilibrium, producing local concentration gradients which can, in turn, lead to precipitation of metastable phases. Several extensive reviews of this phenomenon have been published recently (Johnson and Lam 1978, Okamoto and Rehn 1979, Rehn 1982, Wiedersich and Lam 1983, Rehn and Okamoto 1983, Ardell and Janghorban 1983, Martin et al. 1983, Wiedersich 1986).

Radiation-induced segregation results from two combined effects: (i) radiation-induced point-defect fluxes that persist in time, and (ii) preferential coupling of a particular alloy component to these fluxes. During irradiation at elevated temperatures, there are always persistent defect fluxes, which originate from the spatial nonuniformity in defect annihilation and/or defect production. Local elimination of radiation-induced point defects at, e.g., the bombarded surface is a cause for defect fluxes toward the surface. Furthermore, the rates of defect production during ion bombardment depend on the ion penetration depth. Usually, they are relatively small near the surface, but increase rapidly to a maximum before dropping off to zero near the end of range. This defect-production nonuniformity also gives rise to persistent defect fluxes out of the peak-damage zone into the mid-range and beyond-range regions. Almost always, these fluxes are preferentially coupled to certain solute elements, the reason being given in the following. The flow of defects involves a corresponding flow of lattice atoms: an interstitial flux is associated with an atom flux of the same magnitude and in the same direction, whereas a vacancy flux induces a flux of atoms equal in magnitude, but opposite in direction. The total defect fluxes can thus be partitioned into partial fluxes occurring via different alloy components, e.g., A and B atoms in a binary alloy AB:

$$J_i = J_A^i + J_B^i$$

and (50)

$$J_v = -\left(J_A^v + J_B^v\right).$$

If the partitioning of the defect fluxes is exactly in the same proportion as the atomic fractions of the alloy constituents, i.e., $J_A^i/J_B^i = J_A^v/J_B^v = C_A/C_B$, then there is no disproportionate transport of A or B atoms into or out of any local regions, and thus there is no radiation-induced segregation. However, in general, the various alloy components do not participate in the defect flow strictly in proportion to their local concentrations, i.e., $J_A^i/J_B^i \neq C_A/C_B$ and/or $J_A^v/J_B^v \neq C_A/C_B$; for example, interstitials may migrate preferentially via A atoms, and vacancies may preferentially exchange with B atoms. Therefore, a preferential coupling between defect and solute fluxes will ensue, giving rise to radiation-induced segregation.

It is pointed out that radiation-induced segregation only occurs within the temperature range where annihilation of mobile defects at extended sinks is important, i.e., between ~ 0.2 and $0.6T_m$ (Johnson and Lam 1976, 1977, 1978, Wiedersich and Lam 1983). Outside this range, radiation-induced segregation is insignificant, because dominant defect recombination reduces long-range migration of defects at lower temperatures, and effective back-diffusion prevents concentration gradients from building up at higher temperatures.

Radiation-induced segregation and Gibbsian segregation of an alloy component may occur in the same direction, but may also occur in opposite directions. For example, in Ni-Si alloys, Si enrichment at the surface can result from either Gibbsian segregation (Lam and Hoff 1988) or radiation-induced segregation (Lam et al. 1978, Rehn and Okamoto 1983), whereas, in Ni-Cu alloys, Gibbsian segregation causes strong Cu enrichment in the surface layer (Lam et al. 1985b) and radiation-induced segregation gives rise to pronounced surface and subsurface Cu depletion (Wagner et al. 1983). An example is given in Fig. 20 for the Ni-Cu case. Heating the alloy to 550°C without irradiation produced a thin Cu-enriched layer at the surface. On the contrary, heating and bombarding with 3-MeV $Ni^+$ ions at the same temperature caused a significant Cu depletion. It should also be noted that the thickness of the segregated layer resulting from radiation-induced segregation is always at least an order of magnitude larger than the thickness of the Gibbsian-segregated layer. In addition, radiation-induced segregation can be more effective than radiation-enhanced diffusion in changing the alloy composition at large depths in the specimen undergoing sputtering (Rehn et al. 1985).

The synergistic effects of radiation-induced segregation and preferential sputtering on the sputtering rates and near-surface compositional changes were theoretically modeled by Lam et al (1979, 1980) for various alloy systems.

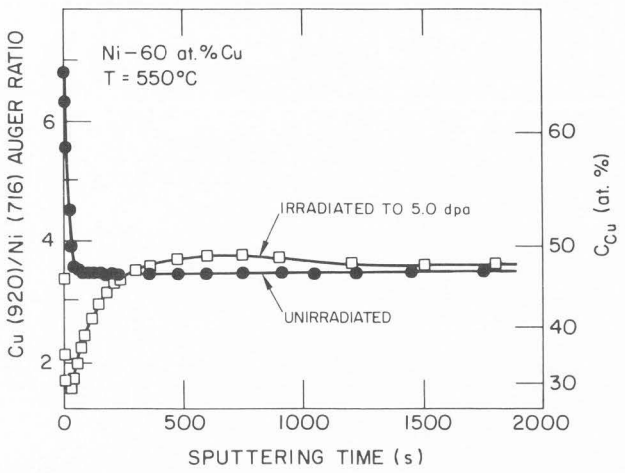


Fig. 20: AES depth profiles of a Ni-60 at.% Cu solid solution after thermal annealing at 550°C without irradiation and after 3-MeV $Ni^+$ ion bombardment to a dose of ~5 dpa at the same temperature (Wagner et al. 1983). Note that, since high-energy Auger transitions (920 eV for Cu and 716 eV for Ni) were used, the Cu concentration indicated on the right-hand ordinate represents an average over several atom layers. As a result, a steady-state Auger ratio representing 48 at.% Cu was obtained for a Ni-60 at.% Cu alloy. This does not necessarily indicate preferential sputtering of Cu. Moreover, the cause of the Cu enrichment at the very surface seen on the "irradiated" curve is not well known. It may have resulted from Gibbsian segregation during the relatively-slow cooling of the specimen to room temperature before the AES analysis.

### Near-surface Composition Changes during Sputtering

During sputtering at elevated temperatures, the interplay among the diverse processes described above in changing the surface and subsurface compositions of multicomponent targets can be quite complex. The early models formulated by Pickering (1976), Haff (1977), Ho (1978), Webb et al. (1978), and Chou and Shafer (1980) considered only the effects of preferential sputtering and radiation-enhanced diffusion. The analytical model of Ho (1978), in particular, has been widely applied to the quantification of depth-profiling techniques. However, measurements of sputtering at elevated temperatures by Rehn et al. (1979) indicated that the compositional alterations and depths of altered layers were substantially larger than could be accounted for by these models. They suggested the important contribution of Gibbsian segregation as an effective mechanism for feeding atoms of a certain alloy component into the surface layer where they are removed by preferential sputtering. Theoretical models of Swartzfager et al. (1981), Itoh and Morita (1984), Kelly (1985), and Kelly and Oliva (1986b) included the simultaneous effects of preferential sputtering, radiation-enhanced diffusion and Gibbsian segregation on the development of the concentration profiles.

The most comprehensive model of bombardment-induced surface composition changes, which includes in addition radiation-induced segregation and displacement mixing, was developed by Lam and Wiedersich (1981, 1982a,b, 1987). The effects of each individual process or of a combination of processes can be systematically studied with this phenomenological model.

The inclusion of the five basic processes in the model introduces a large number of physical parameters into the calculations (Lam and Wiedersich 1981, 1987). First, three parameters are needed to describe the effect of preferential sputtering: the component sputtering coefficients, $S_A$ and $S_B$, and the sputter fraction from the second atom layer, $\beta$ (assuming $\beta_A = \beta_B \equiv \beta$). Second, for displacement mixing, one needs two parameters: the number of replacements per Frenkel pair created, $\eta$, and the defect-production efficiency [the damage rate and distribution can be calculated using the TRIM code (Biersack and Haggmark 1980)]. Third, the characterization of Gibbsian segregation requires two parameters: the enthalpy and entropy of segregation, $\Delta H_a$ and $\Delta S_a$. (These two quantities can be measured experimentally for many alloy systems). And fourth, in order to quantify radiation-enhanced diffusion and radiation-induced segregation, information regarding the diffusivities of vacancies and interstitials via the various alloy components and of defect-solute complexes is necessary. That is, the pre-exponential defect jump frequencies, defect migration energies, and defect-solute binding energies must be provided. In addition, the effective defect formation energies in the alloy and the concentration of radiation-induced sinks are also needed.

Calculations have been carried out to predict the dependence of near-surface compositions on several material and irradiation variables, as well as to fit and interpret experimental data. For example, the time evolution of the concentration profiles calculated for Cu and Si atoms in Ni-40 at.% Cu and Ni-9.5 at.% Si alloys during 3-keV $Ne^+$ sputtering at 500°C is shown in Figs. 21 and 22, respectively. Since both Cu and Si are enriched in the surface atom layer due to Gibbsian segregation (Lam et al. 1985b, Lam and Hoff 1988), $C_{Cu}^{(1)}$ and $C_{Si}^{(1)}$ are initially very high. With increasing bombardment time, they decrease gradually as a result of preferential sputtering, and finally attain steady-state values. The shapes of the Cu and Si concentration profiles and the thicknesses of altered layers are noticeably different, because of different radiation-induced segregation behaviors, i.e., Si atoms segregate toward the surface whereas Cu atoms move away from the surface during irradiation (Rehn and Okamoto 1983). This example demonstrates that detailed information about the synergistic effects of the various processes on compositional changes can be obtained using the Lam-Wiedersich model. The fitting of model calculations to experimental measurements has, in fact, provided useful information regarding the properties of point defects and defect-solute interactions in bombarded alloys (Lam and Hoff 1988, Hoff and Lam 1988, Tang and Lam 1989). Recently,

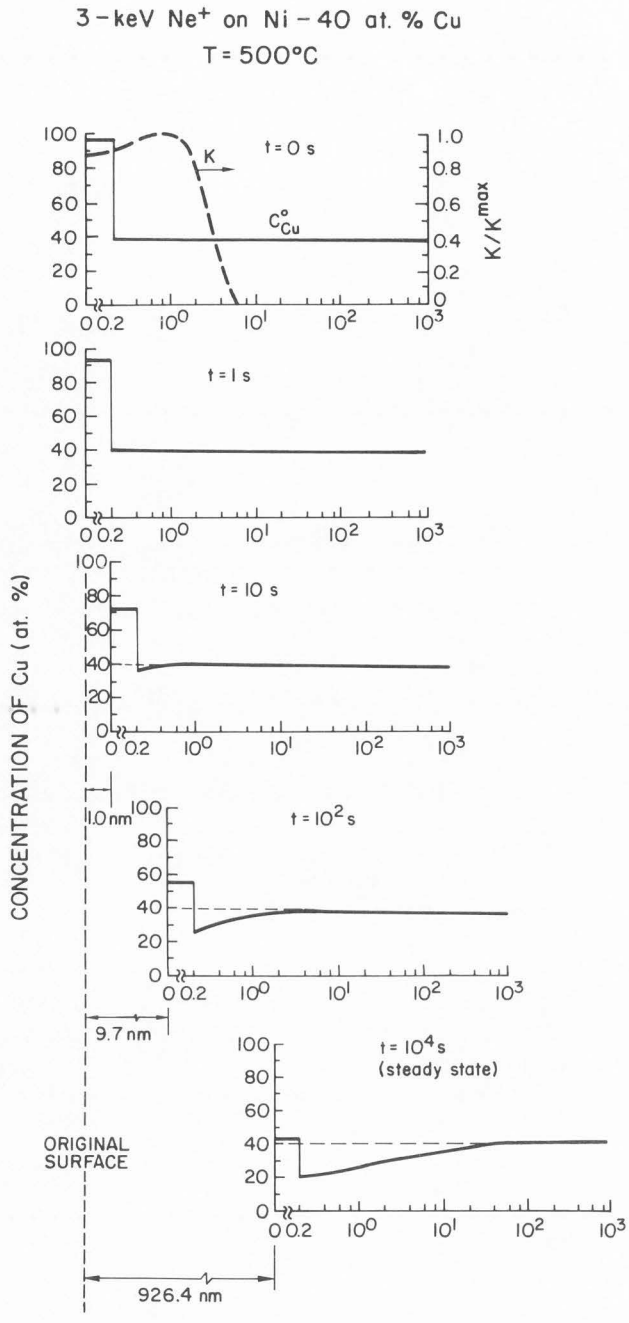


Fig. 21: Calculated time evolution of Cu concentration profile in a Ni-40 at.% Cu alloy during 3-keV $Ne^+$ bombardment at 500°C (Lam and Wiedersich 1987). The spatially-dependent damage rate K is shown by the dashed curve in the top portion, and the thicknesses of sputtered layers are indicated for various times.

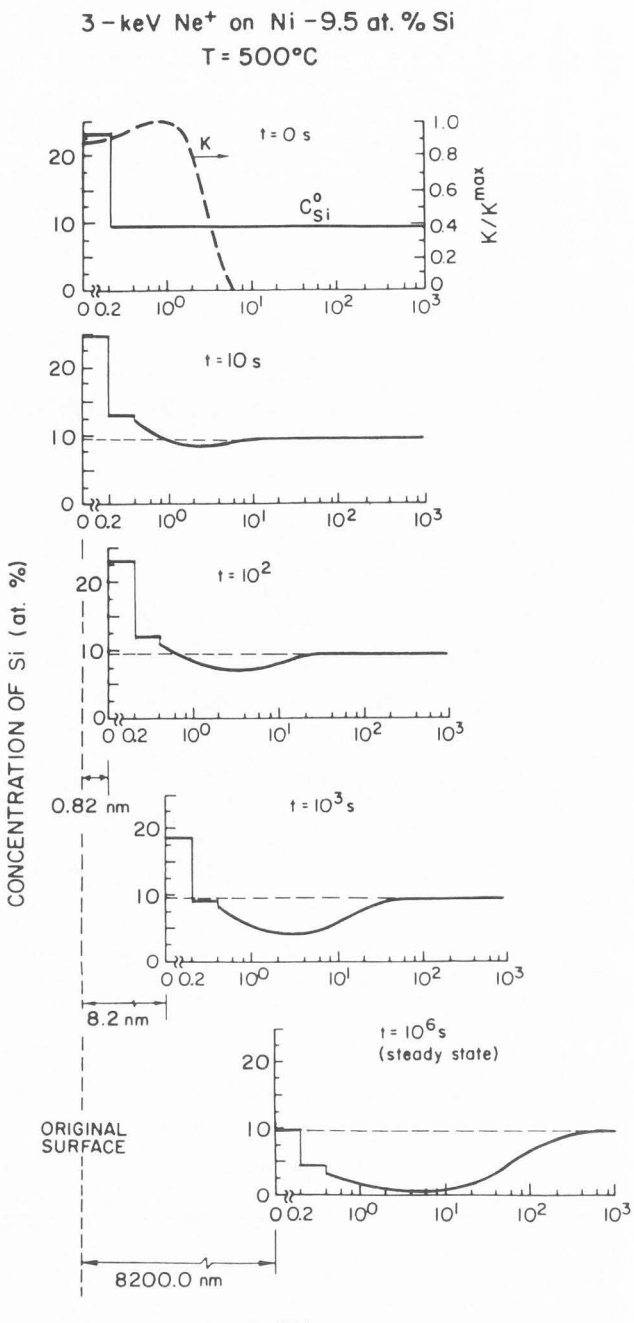


Fig. 22: Calculated time evolution of Si concentration profile in a Ni-9.5 at.% Si alloy sputtered with 3-keV $Ne^+$ ions at 500°C (Lam 1988a). Also shown are the spatially-dependent damage rate K (dashed curve in top portion) and the thicknesses of sputtered layers at various times.

this model has been extended to treat the case of near-surface composition modifications in ternary systems (Yacout et al. 1989).

On the experimental side, the first study of bombardment-induced alterations of the surface composition was undertaken by Shimizu et al. (1975). Their observations of a strong temperature effect on near-surface composition indicated the significance of thermally-activated processes in alloy sputtering. Simultaneous AES measurements of near-

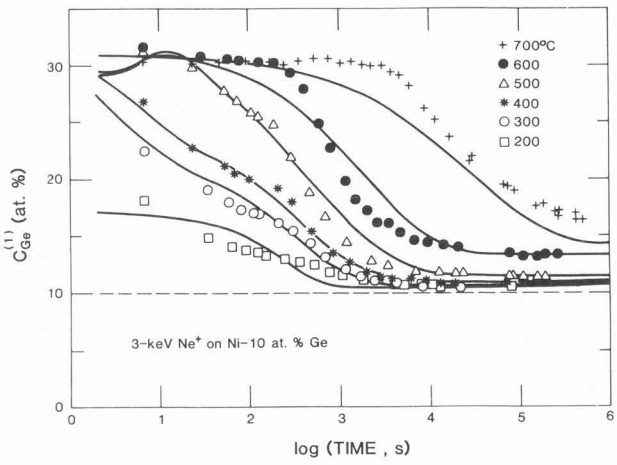


Fig. 23: Time evolution of the Ge surface concentration in a Ni-10 at.% Ge alloy during 3-keV $Ne^+$ sputtering at various temperatures. The various symbols represent the experimental measurements, and the solid curves are calculated using the Lam-Wiedersich model. After Hoff and Lam (1988).

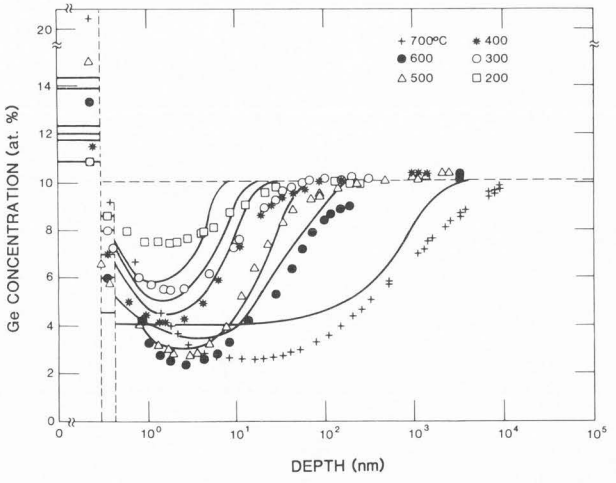


Fig. 24: Steady-state Ge concentration profiles in a Ni-10 at.% Ge alloy after sputtering with 3-keV $Ne^+$ ions at different temperatures. The various symbols are the experimental measurements, and the curves are calculated with the Lam-Wiedersich model. The vertical, dashed lines indicate the boundaries between the first and second, and the second and third atom layers. After Hoff and Lam (1988).

surface compositional changes in Cu-Ni and Ni-Si alloys during 5-keV $Ar^+$ sputtering at elevated temperatures were made by Rehn et al. (1979, 1983). These measurements revealed that Gibbsian segregation and radiation-enhanced diffusion of solute elements played important roles in the formation of the altered layer. The time required to achieve steady state in the near-surface region was found to increase rapidly with increasing temperature. Steady-state concentration profiles, measured after rapid specimen cooling to room temperature, indicated that deviations from the bulk composition occurred up to remarkably large depths in the sputtered specimens. Swartzfager et al. (1981) carried out a similar study on Cu-Ni, Ag-Au and Au-Pd alloys using ISS, which is a surface layer-sensitive technique. The alloys were sputtered with 2-keV $Ne^+$ ions at temperatures between 200 and 500°C, and the compositional changes in the outermost atom layer were probed in situ with the same ions. Similar to AES studies, it was found that the altered-layer thickness increased rapidly with temperature above ~ 400°C. With the aid of the Ho (1978) model, the steady-state concentration profiles were analyzed in order to obtain information about radiation-enhanced diffusion in the bombarded alloy. The diffusion coefficients were found to be between $10^{-16}$ and $10^{-15}$ $cm^2/s$, virtually independent of temperature below ~ 400°C, indicating that in this regime radiation-generated point defects annihilate mainly at extended sinks.

Systematic ISS study of bombardment-induced surface modifications in a number of Ni-based alloys was carried out by Lam et al. (1985a,b), Lam and Hoff (1988), and Hoff and Lam (1988). Both the compositional changes in the outermost atom layer during sputtering and steady-state concentration profiles were measured. Some of their recent results are shown in Figs. 23 and 24, where the evolution of $C_{Ge}$ measured on a Ni-10 at.% Ge alloy during 3-keV $Ne^+$ sputtering at temperatures and during depth-profiling at room temperature, respectively, is plotted (Hoff and Lam 1988). Longer times were required to reach steady state at higher temperatures because of the rapidly-increasing thicknesses of the altered layers. The experimental measurements could be quantitatively fitted by the results of theoretical modeling using the Lam-Wiedersich (1981, 1987) model. The noticeable temperature dependence of $C_{Ge}^{(1)}$ at steady state (Fig. 23) was interpreted in terms of significant contribution of the second atom layer (~ 45%) to the sputtered-atom flux. In fact, as discussed previously, Gibbsian segregation rapidly increases $C_{Ge}^{(1)}$, relative to $C_{Ge}^{(n \geq 2)}$ in deeper layers, as the rate of atom exchange between the outermost and deeper layers increases with temperature. The steady-state condition [eq. (42)] can be met with an increased $C_{Ge}^{(1)}$ if this increase is balanced by a corresponding decrease in $C_{Ge}^{(2)}$ and a sufficiently large sputter fraction from the second layer. Appreciable depletion of surface-segregating elements in the subsurface layers has indeed been observed experimentally in many alloy systems (Rehn et al. 1979, 1983, Swartzfager et al. 1981, Li et al. 1983, Lam et al. 1985a,b, Koshikawa and Goto 1987, Lam and Hoff 1988, Hoff and Lam 1988, Li 1988, 1989).

**Angular Distributions of Sputtered Atoms**

The steep compositional gradient that exists within the sputter depth of origin can significantly influence the angular distributions of the sputtered alloy components (Sigmund et al. 1982). In a binary alloy AB, for example, the more abundant species, e.g., A atoms, at the surface will have a normal $\cos^{\chi}\theta_e$ distribution; however, since the sputtered B atoms must come through the outer A-rich layer, they will have a sharper angular distribution, as schematically shown in

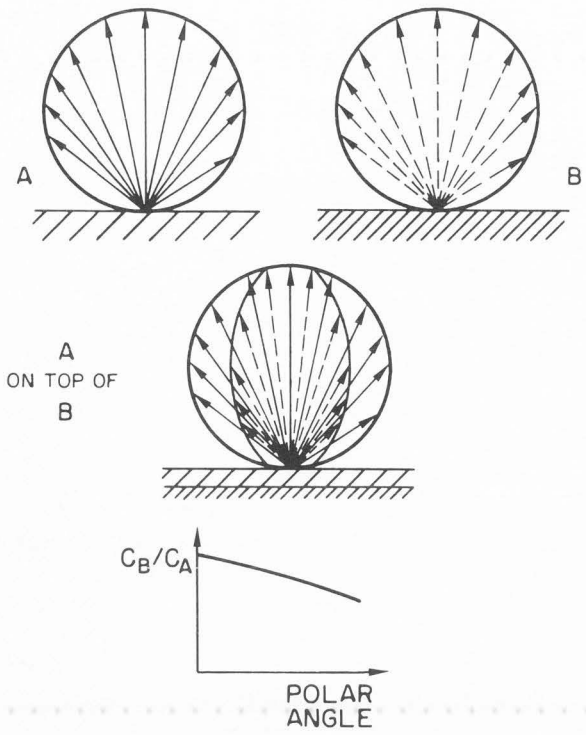


Fig. 25: Schematic description of the effect of a segregated layer on the angular distribution of the sputtered flux. After Andersen (1988).

Fig. 25 (Andersen 1988).

This information was first used by Andersen and coworkers as a means to determine the presence of a segregated layer (Andersen et al. 1982, 1984a) as well as to identify the surface-segregating element (Andersen et al. 1984b). Ichimura et al. (1984) also used the concentration gradient-dependent angular distributions of sputtered atoms to study the effect of surface segregation on sputtering of Cu-Ni, Co-Ni and Fe-Ni alloys.

Dumke et al. (1983) and, subsequently, Hubbard et al. (1989a,b) measured the angular distribution of sputtered atoms from a liquid Ga-In eutectic alloy. In this system, Gibbsian segregation gives rise to an outermost atom layer that is virtually pure In. As predicted, their data for $Ar^+$ sputtering showed that the In atoms sputtered from the first surface layer had a normal $\cos^{\chi}\theta_e$ distribution, with $\chi = 1.8 \pm 0.1$, independent of ion energy. The angular distribution of Ga atoms was significantly sharper, with $\chi = 3.2 \pm 0.2$ in the ion energy range of 15 - 250 keV, and $\chi = 4.9 \pm 0.3$ at 3 keV. The increase in the value of $\chi$ at this low energy was accompanied by an increase in the contribution of the uppermost atomic layer to the sputterd-atom flux, as a result of a decrease in the average energy of higher-order recoil atoms (Hubbard et al. 1989a).

**Sputtering with Relativistic Electrons**

It has long been known that, although bombardment with low-energy ($E \lesssim 1$ keV) electrons cannot cause sputtering in metals, it can induce sputtering in insulators and semiconductors via electronic excitation or ionization (Townsend 1983, Itoh 1987, Betz and Husinsky 1988). At high energies, above ~ 200 keV (depending on the atomic mass of the target), the electrons become capable of transferring enough energy to lattice atoms in direct collisions with nuclei to cause atomic displacements, and, of course, knock-on sputtering in metals. This phenomenon was first observed by Cherns et al. (1976, 1977) ten years ago, in their study of sputtering of gold thin films inside a high-voltage electron microscope. Recently, there have been reports of substantial electron beam sputtering of specimens containing light elements in 100-keV analytical electron microscopes (Thomas 1985).

Considerable progress in the development of medium-voltage (300-400 keV), analytical electron microscopy has been made over the past few years. The motivation behind the introduction of these new microscopes, popularly known as "medium-voltage" microscopes, is their improved spatial resolution and enhanced microanalytical capabilities relative to instruments operated at ~100 keV (Rajan 1987). However, there are a number of limitations related to atomic displacement effects that must be taken into consideration. Atomic displacements can alter the composition in the analyzed volume by displacement mixing, by preferential loss of material through the surface via preferential sputtering, and if the temperature is sufficiently high, by radiation-enhanced diffusion and radiation-induced segregation. Increasing concern about the effects of these processes during microanalysis of thin films in medium-voltage electron microscopes has recently motivated various studies of sputtering (Zaluzec and Mansfield 1987, Bradley and Zaluzec 1988, Bradley 1988) and compositional changes (Régnier et al. 1982, 1983, Régnier and Lam 1983, Zaluzec et al. 1985, Lam and Okamoto 1986, Mansfield et al. 1987) in alloys by electron beam of hundreds of keV in energy.

Radiation-induced compositional redistribution can occur during microanalysis of alloys when two conditions are fulfilled. Firstly, the energy transferred from the incident electrons to the target atoms must be above the threshold displacement energy, $E_d$, in order to displace atoms permanently from their lattice sites. Secondly, the sample temperature must be sufficiently high for point defects to migrate distances of the order of the diameter of the analyzed area during the time required for taking measurement. Observations of beam-induced compositional change during microanalysis of an Al-1.95 at.% Zn alloy using X-ray Energy-Dispersive Spectroscopy (XEDS), have been reported recently (Zaluzec et al. 1985, Mansfield et al. 1987). It was found that the measured Zn/Al $K_\alpha$ intensity ratio was time-independent during 300-keV analysis at room temperature, but decreased with time at 157°C. This decrease in Zn intensity could be attributed to the loss of Zn atoms from the irradiated volume as a result of radiation-induced radial segregation of Zn from the beam center [because Zn is an undersized solute in Al] (Lam and Okamoto 1986) and transient preferential

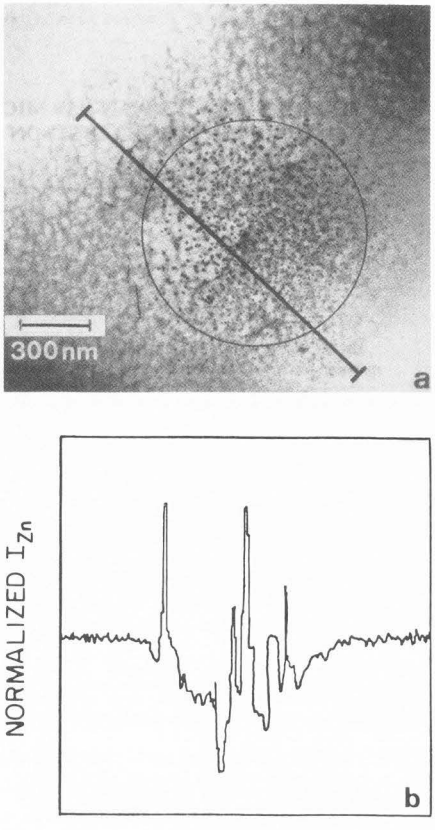


Fig. 26: (a) Micrograph showing an area of an Al-1.95 at.% Zn alloy irradiated at 160°C with a 300-keV focused electron beam for ~ $9x10^3$ s. The beam diameter was 2 μm, as shown by the circle. The small black dots in the beam area are radiation-induced β-phase precipitates. (b) XEDS Zn $K_\alpha$ intensity line scan taken across the irradiated area as indicated in the micrograph. The Zn intensity was normalized to the adjacent spectrum background. The depletion of Zn in the irradiated zone is clearly visible. The compositional spikes in the scan correspond to small Zn-rich β particles. After Mansfield et al. (1987).

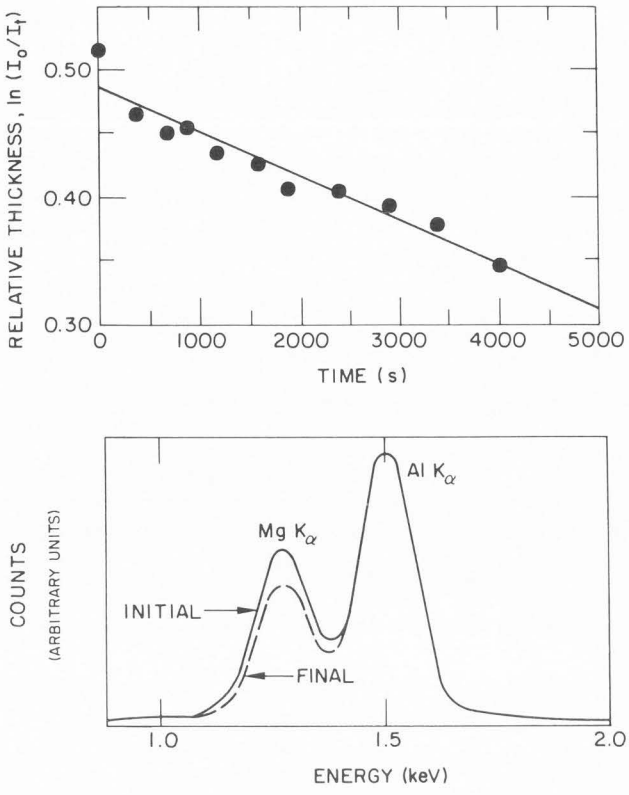


Fig. 27: (a) Measured change in the thickness of an Al-Mg alloy specimen during irradiation with a 120-keV electron beam in a Philips EM420T microscope. The probe diameter was 180 nm. (b) Measured X-ray energy dispersive spectra before and after ~ $4x10^3$ s irradiation. The Al $K_\alpha$ lines have been normalized to the same value for comparison. Change in the relative intensity ratio of Mg to Al $K_\alpha$ lines indicates a preferential loss of Mg by sputtering. After Zaluzec and Mansfield (1987).

sputtering of Zn from the lower surface of the alloy film [because the Zn concentration in the surface atomic layer was estimated to be ~ 20 at.% due to Gibbsian adsorption (Mansfield et al. 1987)]. The depletion of Zn was indeed observed in the irradiated volume after ~ $9x10^3$ s irradiation with a 300-keV focused electron beam at 160°C (Fig. 26). It is noted that 300 keV is above the threshold voltage for Al (~170 keV), but is below the threshold for Zn (~355 keV). Hence, Zn atoms are not displaced by direct electron-Zn collisions; they can only be displaced by secondary collisions with Al atoms which have been set in motion after direct collisions with electrons. The effectiveness of secondary collisions in producing point defects in alloys containing light solutes during sub-threshold irradiations has been investigated systematically by Régnier et al. (1982, 1983) and Régnier and Lam (1983, 1985).

Preferential sputtering of Mg - the lighter element - from polycrystalline Al-Mg thin foil during XEDS microanalysis with a 120-keV electron beam has been reported recently (Zaluzec and Mansfield 1987). The effect is quite noticeable when comparing the XEDS spectra recorded at the beginning and the end of the irradiation (Fig. 27).

## CONCLUSION

This paper has reviewed several fundamental aspects of physical sputtering in metals and multicomponent materials.

Analytical theories of elemental sputtering in various regimes have been summarized. In general, these theories provide good descriptions of the sputtering yield and energy and angular distributions of the sputtered atoms in regimes where thermal spike effects are unimportant. For sputtering in the spike regime, theories describe the right trends and patterns, but only qualitatively. The sputtering yield is

virtually independent of target temperature in all regimes. There was some confusion in the past about whether or not the sputtering yield would increase exponentially as the melting point is approached, due to some sort of thermal spike-induced evaporation process. However, recent measurements indicate that this enhanced sputtering is simply caused by the onset of significant thermal evaporation from the target surface and has nothing to do with thermal spikes. The characteristic depth of sputtering is quite small, similar to the mean atomic spacing. Almost all the sputtered atoms originate from the first two atomic layers. Their angular distributions can be accurately described only if the effect of surface scattering is accounted for. Although sputtering of clusters and molecules has been observed in a wide variety of materials, no basic ejection mechanism has been universally accepted, and this complex process is understood only very qualitatively.

From a theoretical point of view, "true" preferential sputtering can be understood in terms of mass and surface-binding-energy differences among the alloy components. The binding-energy effect is predicted to be more important than that caused by different masses. Preferential sputtering of the lighter element is only pronounced during light-ion bombardment at near-threshold energies. In concurrence with sputtering, many other processes also take place in the target materials. They include displacement mixing, Gibbsian segregation, radiation-enhanced diffusion, and radiation-induced segregation. The relative contributions of these different processes in changing the near-surface composition of an alloy under various bombardment conditions have been identified recently.

In general, the phenomenon of bombardment-induced compositional changes is simplest when only the athermal processes, i.e. preferential sputtering and displacement mixing, are operative. The thickness of the resulting altered layer is approximately equal to the ion range in this case. However, very often at least one of the thermally-activated processes also occurs, complicating the compositional-change picture. It is important to realize that Gibbsian segregation, which can be accelerated by irradiation, is capable of causing substantial change in the near-surface composition of an alloy during sputtering even in the absence of all other processes. Any component which is Gibbsian-segregated in the upmost layer will be preferentially removed by sputtering because more of it is located within the sputter depth. The similar consequences of "true" preferential sputtering and of the combined effects of Gibbsian segregation and nonpreferential sputtering on the near-surface composition make it difficult to identify "true" preferential sputtering.

In most alloys, defect migration-assisted processes become important only at temperatures well above ambient. Gibbsian segregation effectively drives the alloy towards its thermodynamic equilibrium state, in which the outermost atom layer is enriched in one alloy component. Radiation-enhanced diffusion causes the altered layer, which is produced in the near-surface bombarded region by the complex interplay among the various processes, to extend to significantly greater depths at elevated temperatures. Radiation-induced segregation, on the other hand, tends to drive the alloy system away from thermodynamic equilibrium, leading to significant compositional redistribution. It is quite effective in spreading changes of the alloy composition to large depths in the specimen undergoing sputtering. The predictions of current models of bombardment-induced near-surface composition changes are generally in good qualitative agreement with existing observations. For cases where experimental measurements are systematic, the fitting of model calculations to these measurements can provide useful information regarding the properties of point defects and mass transport in alloys.

Preferential sputtering of light elements and radiation-induced compositional changes can occur in thin alloy films during examination with electron beams of hundreds of keV in energy. These effects can have major implications to the accuracy of quantitative microanalysis.

## Acknowledgements

The author has greatly benefited from stimulating discussions with Prof. P. Sigmund and Dr. H. Wiedersich during the preparation of this review. He is indebted to them, as well as to Prof. H. H. Andersen, Dr. W. O. Hofer, and Dr. R. Kelly, for carefully reading the manuscript and making numerous suggestions and critical comments.

Work supported by the U. S. Department of Energy, BES-Materials Sciences, under Contract W-31-109-Eng-38.

## REFERENCES

Adda Y, Beyeler M, Brebec G. (1975). Radiation effects on solid state diffusion, Thin Solid Films **25**, 107-156.

Ahmad S, Farmery BW, Thompson MW. (1980). The effect of ion mass and target temperature on the energy distribution of sputtered atoms, Nucl. Instr. and Meth. **170**, 327-330.

Andersen HH. (1979a). Sputtering of multicomponent metal and semiconductor targets, J. Vac. Sci. Technol. **16**, 770-771.

Andersen HH. (1979b). The depth resolution of sputter profiling, Appl. Phys. **18**, 131-140.

Andersen HH. (1980). Sputtering of multicomponent metals and semiconductors, in: The Physics of Ionized Gases (SPIG 1980), M. Matic (ed), Boris Kidrić Institute of Nuclear Sciences, Beograd, 421-483.

Andersen HH. (1984). Ion bombardment-induced composition changes in alloys and compounds, in: Ion Implantation and Beam Processing, J. S. Williams and J. M. Poate (eds), Academic Press, Sydney, 127-187.

Andersen HH. (1987). Computer simulations of atomic collisions in solids with special emphasis on sputtering, Nucl. Instr. and Meth. **B18**, 321-343.

Andersen HH. (1988). Sputtering from atomic-collision cascades, Nucl. Instr. and Meth. **B33**, 466-473.

Andersen HH, Bay H. (1972). The $Z_1$ dependence of heavy-ion sputtering yield in Cu, Rad. Effects **13**, 67-74.

Andersen HH, Bay H. (1973). Sputtering-yield studies on silicon and silver targets, Rad. Effects **19**, 139-146.

Andersen HH, Bay HL. (1974). Nonlinear effects in heavy-ion sputtering, J. Appl. Phys. **45**, 953-954.

Andersen HH, Bay HL. (1975). Heavy-ion sputtering yields of gold: Further evidence of nonlinear effects, J. Appl. Phys. **46**, 2416-2422.

Andersen HH, Bay HL. (1981). Sputtering yield measurements, in: Sputtering by Particle Bombardment I (Top. Appl. Phys. **47**), R. Behrisch (ed), Springer-Verlag, Berlin, 145-218.

Andersen HH, Bøttiger J, Wolder Jørgensen H. (1975). Ranges of ions with $Z_1 \geq 54$ in Al and $Al_2O_3$, Appl. Phys. Lett. **26**, 678-679.

Andersen HH, Chernysh V, Stenum B, Sørensen T, Whitlow HJ. (1982). Measurements of angular distributions of sputtered material as a new tool for surface-segregation studies: segregation in CuPt alloys, Surface Sci. **123**, 39-46.

Andersen HH, Stenum B, Sørensen T, Whitlow HJ. (1984a). Temperature dependence of the angular distribution of material sputtered from a CuPt alloy, Nucl. Instr. and Meth. **B2**, 623-626.

Andersen HH, Stenum B, Sørensen T, Whitlow HJ. (1984b). Transients in the composition of material sputtered from alloy targets, Nucl. Instr. and Meth. **B2**, 601-605.

Andersen HH, Stenum B, Sørensen T, Whitlow HJ (1985). Angular distribution of particles sputtered from Cu, Pt and Ge targets by keV $Ar^+$ ion bombardment, Nucl. Instr. and Meth. **B6**, 459-465.

Andersen N, Sigmund P. (1974). Energy dissipation by heavy ions in compound targets, Mat. Fys. Medd. Dan Vid. Selsk. **39**, No. 3.

Anderson GS, Wehner GK. (1960). Atom ejection patterns in single-crystal sputtering, J. Appl. Phys. **31**, 2305-2313.

Anthony TR. (1972). Solute segregation and stresses generated around growing voids in metals, in: Radiation-Induced Voids in Metals, J. W. Corbett and L. C. Ianniello (eds), National Technical Information Service, Springfield, Virginia, 630-646.

Ardell AJ, Janghorban K. (1983). Irradiation-induced phase transformations in binary nickel and palladium base alloys, in: Phase Transformations during Irradiation, F. V. Nolfi, Jr. (ed), Applied Science Publishers, London, 291-329.

Averback RS. (1986). Fundamental aspects of ion beam mixing, Nucl. Instr. and Meth. **B15**, 675-687.

Averback RS, Diaz de la Rubia T, Benedek R. (1988). Dynamics and structure of energetic displacement cascades, Nucl. Instr. and Meth. **B33**, 693-700.

Averback RS, Peak D, Thompson LJ. (1986). Ion beam mixing in pure and in immiscible copper bilayer systems, Appl. Phys. **A39**, 59-64.

Baretzky B, Möller W, Taglauer E. (1987). Collisional processes in preferential sputtering of tantalum oxide, Nucl. Instr. and Meth. **B18**, 496-500.

Bay HL, Bohdansky J, Hofer WO, Roth J. (1980). Angular distribution and differential sputtering yields for low-energy light-ion irradiation of polycrystalline nickel and tungsten, Appl. Phys. **21**, 327-333.

Bay HL, Roth J, Bohdansky J. (1977). Light-ion sputtering yields for molybdenum and gold at low energies, J. Appl. Phys. **48**, 4722-4728.

Beeler JR, Jr. (1966). Displacement spikes in cubic metals. I. α-Iron, Copper and Tungsten, Phys. Rev. **150**, 470-487.

Beeler JR, Jr, Beeler MF. (1976). Collision cascades in iron for energies up to 5 MeV, in: Fundamental Aspects of Radiation Damage in Metals, M. T. Robinson and F. W. Young (eds), CONF-751006-P1, National Technical Information Service, Springfield, Virginia, 28-34.

Behrisch R. (1981) ed. Sputtering by Particle Bombardment I (Top. Appl. Phys. **47**), Springer-Verlag, Berlin.

Behrisch R. (1983) ed. Sputtering by Particle Bombardment II (Top. Appl. Phys. **52**), Springer-Verlag, Berlin.

Behrisch R, Maderlechner G, Scherzer BMU, Robinson MT. (1979). The sputtering mechanism for low-energy lights ions, Appl. Phys. **18**, 391-398.

Benedek R. (1981). Spatial characteristics of displacement cascades in metals, J. Appl. Phys. **52**, 5557-5565.

Besocke K, Berger S, Hofer WO, Littmark U. (1982). A search for a thermal spike effect in sputtering. I. Temperature dependence of the yield at low-keV, heavy-ion bombardment, Rad. Effects **66**, 35-41.

Betz G. (1980). Alloy sputtering. Surface Sci. **92**, 283-309.

Betz G, Husinsky W. (1988). Sputtering of insulators, Nucl. Instr. and Meth. **B32**, 331-340.

Betz G, Husinsky W, Varga P, Viehböck F. (1987) eds. Symposium on Sputtering, Nucl. Instr. and Meth. **B18**, 321-678.

Betz G, Wehner GK. (1983). Sputtering of multicomponent materials, in: Sputtering by Particle Bombardment II (Top. Appl. Phys. **52**), R. Behrisch (ed), Springer-Verlag, Berlin, 11-90.

Biersack JP. (1987). Computer simulations of sputtering, Nucl. Instr. and Meth. **B27**, 21-36.

Biersack JP, Eckstein W. (1984). Sputtering studies with the Monte Carlo Program TRIM.SP, Appl. Phys. **A34**, 73-94.

Biersack JP, Haggmark LG. (1980). A Monte Carlo computer program for the transport of energetic ions in amorphous targets, Nucl. Instr. and Meth. **174**, 257-269.

Biersack JP, Ziegler JF. (1982). Refined universal potentials in atomic collisions, Nucl. Instr. and Meth. **194**, 93-100.

Bohdansky J. (1984). A universal relation for the sputtering yield of monatomic solids at normal ion incidence, Nucl. Instr. and Meth. **B2**, 587-591.

Bohdansky J, Roth J, Bay HL. (1980). An analytical formula and important parameters for low-energy ion sputtering, J. Appl. Phys. **51**, 2861-2865.

Bradley CR. (1988). Calculations of atomic sputtering and displacement cross-sections in solid elements by electrons with energies from threshold to 1.5 MV, Argonne National Laboratory Report ANL-88-48, National Technical Information Service, Oak Ridge, Tennessee.

Bradley CR, Zaluzec NJ. (1988). Atomic sputtering in the analytical electron microscope, in: Electron Beam Induced Spectroscopies with High Spatial Resolution, C. Colliex and M. Isaacson (eds), Proc. NSF/CNRS Workshop, Aussois, 466-469.

Brailsford AD, Bullough R. (1978). Void growth and its relation to intrinsic point defect properties, J. Nucl. Mater. **69 & 70**, 434-450.

Brandt W, Laubert R. (1967). Unified sputtering theory, Nucl. Instr. and Meth. **47**, 201-209.

Brinkman JA. (1954). On the nature of radiation damage in metals. J. Appl. Phys. **25**, 961-970.

Burnett JW, Biersack JP, Gruen DM, Jørgensen B, Krauss AR, Pellin MJ, Schweitzer EL, Yates JT, Young CE. (1988). Depth of origin of sputtered atoms: experimental and theoretical study of Cu/Ru(0001), J. Vac. Sci. Technol. **A6**, 2064-2068.

Carter G. (1979). Spike and shock processes in high energy deposition density atomic collision events in solids, Rad. Effects Lett. **43**, 193-199.

Carter, G. (1980). A semi quantitative approach to ion impact induced shock processes in solids, Rad. Effects Lett. **50**, 105-109.

Chapman GE, Farmery BW, Thompson MW, Wilson IA. (1972). The energy distribution of sputtered atoms from gold, Rad. Effects **13**, 121-129.

Chen GL. (unpublished work) Quoted in: Bohdansky J. (1984). A universal relation for the sputtering yield of monatomic solids at normal ion incidence, Nucl. Instr. and Meth. **B2**, 587-591.

Cheng YT, Van Rossum M, Nicolet MA, Johnson WL. (1984). Influence of chemical driving forces in ion mixing of metallic bilayers, Appl. Phys. Lett. **45**, 185-187.

Cherns D, Finnis MW, Mathews MD. (1977). Sputtering of gold foils in a high voltage electron microscope. A comparison of theory and experiment. Philos. Mag. **35**, 693-714.

Cherns D, Minter FJ, Nelson RS. (1976). Sputtering in the high voltage electron microscope, Nucl. Instr. and Meth. **132**, 369-376.

Chou NJ, Shafer MW. (1980). On the phenomenological model of preferred sputtering for SIMS and Auger profiling: A critical analysis, Surface Sci. **92**, 601-616.

Claussen C. (1982). Sputtering from elastic-collision spikes-spherical geometry, Nucl. Instr. and Meth. **194**, 567-571.

Chrisey DB, Boring JW, Johnson RE, Phipps JA. (1988). Molecular ejection from low temperature sulfur by keV ions, Surface Sci. **195**, 594-618.

Current MI, Wei CY, Seidman DN. (1983). Direct observations of the primary state of damage of ion-irradiated tungsten. II. Definitions, analyses and results, Philos. Mag. **A47**, 407-434.

Czanderna AW. (1975) ed. Methods of Surface Analysis (Methods and Phenomena **1**), Elsevier, Amsterdam.

Damask AC, Dienes GJ. (1963). Point Defects in Metals, Gordon and Breach, New York.

Davies JA. (1983). Collision cascades and spike effects, in: Surface Modification and Alloying, J. M. Poate, G. Foti, and D. C. Jacobson (eds), Plenum Press, New York, 189-209.

Davies JA. (1984). High energy density collision cascades and spike effects, in: Ion Implantation and Beam Processing, J. S. Williams and J. M. Poate (eds), Academic Press, Sydney, 81-97.

de Vries AE. (1987). Sputtering of molecules and clusters, Nucl. Instr. and Meth. **B27**, 173-180.

d'Heurle F, Baglin JEE, Clarke GJ. (1985). Correlation between chemistry and the amount of mixing in bilayers submitted to ion bombardment, J. App. Phys. **57**, 1426-1429.

Diaz de la Rubia T. (1989). The Structure and Dynamics of Energetic Displacement Cascades in Cu and Ni. A Molecular Dynamics Computer Simulation Study. PhD Thesis, University of New York, Albany, New York.

Diaz de la Rubia T, Averback RS, Benedek R, King WE. (1987). Role of thermal spike in energetic displacement cascades, Phys. Rev. Lett. **59**, 1930-1933.

Diaz de la Rubia T, Averback RS, Hsieh H, Benedek R, (1989a). Molecular dynamics simulation of displacement cascades in Cu and Ni: Thermal spike behavior, J. Mater. Res. **4**, 579-586.

Diaz de la Rubia T, Smalinskas K, Averback RS, Robertson IM, Hsieh H, Benedek R. (1989b). Mechanisms of cascade collapse, Mat. Res. Soc. Symp. Proc. **138**, 29-34.

Dembowski J, Oechsner H, Yamamura Y, Urbassek M. (1987). Energy distributions of neutral atoms sputtered from Cu, V and Nb under different bombardment and ejection angles, Nucl. Instr. and Meth. **B18**, 464-470.

Dumke MF, Tombrello TA, Weller RA, Housley RM, Cirlin EH. (1983). Sputtering of the Gallium-Indium eutectic alloy in the liquid phase, Surface Sci. **124**, 407-422.

English CA, Jenkins ML. (1987). Insight into cascade processes arising from studies of cascade collapse, Mater. Sci. Forum **15-18**, 1003-1022.

Falcone G. (1986). Ejection process in collisional sputtering, Phys. Rev. **B33**, 5054-5056.

Falcone G, Kelly R, Oliva A. (1987). Corrections to the collisional sputtering yield, Nucl. Instr. and Meth. **B18**, 399-401.

Falcone G, Sigmund P. (1981). Depth of origin of sputtered atoms, Appl. Phys. **25**, 307-310.

Farmery BW, Thompson MW. (1968). Energy spectra for copper, Philos. Mag. **18**, 415-424.

Foiles SM. (1985). Application of the embedded-atom method to liquid transition metals, Phys. Rev. **B32**, 3409-3415.

Fujimoto F. (1988) ed. Atomic Collisions in Solids, Nucl. Instr. and Meth. **B33**, 1-942.

Garrison BJ, Winograd N, Harrison DE. (1978). Atomic and molecular ejection from ion-bombarded reacted single-crystal surfaces. Oxygen on copper (100), Phys. Rev. **B18**, 6000-6010.

Gnaser H, Hofer WO. (1989). The emission of neutral clusters in sputtering, Appl. Phys. **A48**, 261-271.

Gnaser H, Hutcheon ID. (1988). Preferential emission of lighter isotopes in the initial stage of sputtering, Surface Sci. **195**, 499-512.

Gruen D, Krauss AR, Pellin MJ, Young CE. (1987) eds. Particle and Photon Interactions with Surfaces, Nucl. Instr. and Meth. **B27**, 1-248.

Gschneidner KA. (1964). Physical properties and interrelationships of metallic and semimetallic elements, in: Solid State Physics **16**, F. Seitz and D. Turnbull (eds), Academic, New York, 275-426.

Guinan MW, Kinney JH. (1981). Molecular dynamic calculations of energetic displacement cascades, J. Nucl. Mater. **103&104**, 1319-1324.

Guseva MI, Martynenko YV. (1976). Sputtering of materials by $H^+$, $D^+$, $T^+$ and $He^+$ ions, J. Nucl. Mater. **63**, 241-244.

Guttmann M, McLean D. (1979). Grain boundary segregation in multicomponent systems, in: Interfacial Segregation, W. C. Johnson and J. M. Blakely (eds), American Society for Metals, Metals Park, Ohio, 261-348.

Haff PK. (1977). A model for surface layer composition changes in sputtered alloys and compounds, Appl. Phys. Lett. **31**, 259-260.

Haff PK, Watson CC, Tombrello TA. (1981). Possible isotopic fractionation effects in material sputtered from minerals, J. Geophys. Res. **86**, 9553-9561.

Haring RA, Pedrys R, Oostra DJ, Haring A, de Vries AE. (1984). Reactive sputtering of simple condensed gases by keV ions III: Kinetic energy distributions, Nucl. Instr. and Meth. **B5**, 483-488.

Harrison DE. (1983). Sputtering models - A synoptic view, Rad. Effects **70**, 1-64.

Harrison DE, Avouris P, Walkup R. (1987). Classical trajectory study of atom and molecule ejection during low-energy bombardment of copper by oxygen, Nucl. Instr. and Meth. **B18**, 349-354.

Harrison DE, Delaplain CB. (1976). Computer simulation of the sputtering of clusters, J. Appl. Phys. **47**, 2252-2259.

Hautala M, Likonen J. (1988). The effect of near-surface structure on sputtering of Cu atoms by Ar ions, Nucl. Instr. and Meth. **B33**, 526-529.

Heinisch HL. (1981). Computer simulations of high energy recoils in FCC metals: cascade shapes and sizes, J. Nucl. Mater. **103&104**, 1325-1329.

Heinisch HL. (1983). Defect production in simulated cascades: cascade quenching and short-term annealing, J. Nucl. Mater. **117**, 46-54.

Ho PS. (1978). Effects of enhanced diffusion on preferred sputtering of homogeneous alloy surfaces, Surface Sci. **72**, 253-263.

Hofer WO. (1980). Emission of atoms and electrons from high-density collision cascades in metals, Nucl. Instr. and Meth. **170**, 275-279.

Hofer WO. (1986). Physical sputtering of elemental metals and semiconductors, in: Erosion and Growth of Solids Stimulated by Atom and Ion Beams, G. Kiriakidis, G. Carter and J. L. Whitton (eds), NATO ASI Series, No. 112, Martinus Nijhoff Publishers, Dordrecht, 1-24.

Hofer WO, Bay HL, Martin PJ. (1978). Sputter-erosion and impurity emission from titanium and vanadium at low-energy ion bombardment, J. Nucl. Mater. **76/77**, 156-162.

Hofer WO, Besocke K, Stritzker B. (1983). A search for a thermal spike effect in sputtering. II. Temperature dependence of the yield for heavy atomic and molecular ion bombardment, Appl. Phys. **A30**, 83-86.

Hofer WO, Gnaser H. (1987). Anisotropic emission of neutral clusters, Nucl. Instr. and Meth. **B18**, 605-608.

Hoff HA, Lam NQ. (1988). Surface and subsurface compositional modifications in Ni-Ge alloys measured by ion scattering spectroscopy, Surface Sci. **204**, 233-246.

Hofmann S. (1980a). Quantitative depth profiling in surface analysis: A review, Surf. Interface Anal. **2**, 148-160.

Hofmann S. (1980b). Surface segregation during sputtering at elevated temperatures, Mater. Sci. Eng. **42**, 55-58.

Hofmann S. (1985). Segregation to surfaces and interfaces, Scanning Electron Microsc. **1985**, III, 1071-1086.

Hondros ED, Seah MP. (1977). The theory of grain boundary segregation in terms of surface adsorption analogues, Met. Trans. **8A**, 1363-1371.

Honig RE. (1958). Sputtering of surfaces by positive ion beams of low energy, J. Appl. Phys. **29**, 549-555.

Hubbard KM, Weller RA, Weathers DL, Tombrello TA. (1989a). The angular distribution of atoms sputtered from a Ga-In eutectic alloy target, Nucl. Instr. and Meth. **B36**, 395-403.

Hubbard KM, Weller RA, Weathers DL, Tombrello TA. (1989b). Sputtering from a liquid Ga-In eutectic alloy, Nucl. Instr. and Meth. **B40/41**, 278-281.

Hucks P, Stöcklin G, Vietzke E, Vogelbruch K. (1978). Energy and angular distribution of gold and copper atoms sputtered with either 15- or 30-keV $H^+$, $He^+$, and $Ar^+$ ions, J. Nucl. Mater. **76&77**, 136-142.

Husinsky W, Betz G, Girgis I, Viehböck F, Bay HL. (1984). Velocity distributions and sputtering yields of

chromium atoms under argon, oxygen and carbon ion bombardment, J. Nucl. Mater. **128&129**, 577-582.

Husinsky W, Girgis I, Betz G. (1985). Doppler shift laser fluorescence spectroscopy of sputtered and evaporated atoms under $Ar^+$ bombardment, J. Vac. Sci. Technol. **B3**, 1543-1545.

Husinsky W, Wurz P, Strehl B, Betz G. (1987). Cr atoms sputtered from different matrices, Nucl. Instr. and Meth. **B18**, 452-457.

Ichimura S, Shimizu H, Murakami H, Ishida Y. (1984). Effect of surface segregation on angular distributions of atoms sputtered from binary alloys, J. Nucl. Mater. **128&129**, 601-604.

Ishitani T, Shimizu R. (1975). Computer simulation of atomic mixing during ion bombardment, Appl. Phys. **6**, 241-248.

Itoh N. (1987) Laser sputtering in the electronic excitation regime: comparison with electron and ion sputtering, Nucl. Instr. and Meth. **B27**, 155-166.

Itoh N, Morita K. (1984). Effect of segregation on preferred sputtering of alloys, Rad. Effects **80**, 163-182.

Jäger W, Merkle KL. (1988). Defect-cluster formation in high-energy-density cascades in gold, Philos. Mag. **A57**, 479-498.

Jarkas MM, Harrison DE. (1984). Influence of electronic energy losses on atom ejection processes, Phys. Rev. **B30**, 3573-3574.

Jarkas MM, Harrison DE. (1985). Dependence of atom ejection on electronic energy loss, Phys. Rev. **B32**, 2753-2760.

Johar SS, Thompson DA. (1979). Spike effects in heavy-ion sputtering of Ag, Au and Pt thin films, Surface Sci. **90**, 319-330.

Johnson RA, Lam NQ. (1976). Solute segregation in metals under irradiation, Phys. Rev. **B13**, 4364-4375.

Johnson RA, Lam NQ. (1977). Solute segregation to voids during irradiation, Phys. Rev. **B15**, 1794-1800.

Johnson RA, Lam NQ. (1978). Solute segregation under irradiation, J. Nucl. Mater. **69&70**, 424-433.

Johnson RE, Evatt R. (1980). Thermal spikes and sputtering yields, Rad. Effects **52**, 187-190.

Johnson WL, Cheng YT, VanRossum M, Nicolet MA. (1985). When is thermodynamics relevant to ion-induced atomic arrangements in metals? Nucl. Instr. and Meth. **B7/8**, 657-665.

Jung P. (1983). Atomic displacement functions of cubic metals, J. Nucl. Mater. **117**, 70-77.

Karashima S. (1982). Non-linear effects of molecular ion bombardment on sputtering yields, Jap. J. Appl. Phys. **21**, 434-439.

Kelly R. (1977). Theory of thermal sputtering, Rad. Effects **32**, 91-100.

Kelly R. (1978). An attempt to understand preferential sputtering, Nucl. Instr. and Meth. **149**, 553-558.

Kelly R. (1979). Thermal effects in sputtering, Surface Sci. **90**, 280-318.

Kelly R. (1980). On the problem of whether mass or chemical bonding is more important to bombardment-induced compositional changes in alloys and oxides, Surface Sci. **100**, 85-107.

Kelly R. (1981). Phase changes in insulators produced by particle bombardment, Nucl. Instr. and Meth. **182/183**, 351-378.

Kelly R. (1984a). The mechanisms of sputtering. Part I: Prompt and slow collisional sputtering, Rad. Effects **80**, 273-317.

Kelly R. (1984b). Implantation, recoil implantation, and sputtering, in: Ion Bombardment Modification of Surfaces: Fundamentals and Applications, O. Auciello and R. Kelly (eds), Elsevier, Amsterdam, 27-78.

Kelly R. (1984c). The varieties of surface alteration: structural, topographical, and compositional, in: Ion Bombardment Modification of Surfaces: Fundamentals and Applications, O. Auciello and R. Kelly (eds), Elsevier, Amsterdam, 79-126.

Kelly R. (1985). On the role of Gibbsian segregation in causing preferential sputtering, Surf. Interface Anal. **7**, 1-7.

Kelly R. (1987a). The sputtering of insulators, in: Ion Beam Modification of Insulators, P. Mazzoldi and G. W. Arnold (eds), Elsevier, Amsterdam, 57-113.

Kelly R. (1987b). The surface binding energy in slow collisional sputtering, Nucl. Instr. and Meth. **B18**, 388-398.

Kelly R. (1989). Bombardment-induced compositional change with alloys, oxides, oxysalts and halides III. The role of chemical driving forces, Mater. Sci. Eng. **A115**, 11-24.

Kelly R, Oliva A. (1986a). New estimates of the characteristic depth of sputtering and of the bombardment-induced segregation ratio, Nucl. Instr. and Meth. **B13**, 283-294.

Kelly R, Oliva A. (1986b). The theory of the preferential sputtering of alloys, including the role of Gibbsian segregation, in: Erosion and Growth of Solids Stimulated by Atom and Ion Beams, G. Kiriakidis, G. Carter and J. L. Whitton (eds), NATO ASI Series, No. 112, Martinus Nijhoff Publishers, Dordrecht, 41-69.

Kim SJ, Nicolet MA, Averback RS, Baldo P. (1985). Low-temperature ion beam mixing of Pt and Si markers in Ge, Appl. Phys. Lett. **46**, 154-156.

Kinchin GH, Pease RS. (1955). The displacement of atoms in solids by radiation, Repts. Progr. in Phys. **18**, 1-51.

King WE, Benedek R. (1983). Molecular dynamics simulation of low energy displacement cascades in Cu, J. Nucl. Mater. **117**, 26-35.

King WE, Merkle KL, Meshii M. (1983). Threshold energy surface and Frenkel pair resistivity for Cu, J. Nucl. Mater. **117**, 12-25.

Kiritani M. (1987). Point defect processes in the defect structure development from cascade damage, Mater. Sci. Forum **15-18**, 1023-1046.

Kirk MA, Blewitt TH. (1982). Ordered alloys reveal fundamental mechanisms of neutron damage production, J. Nucl. Mater. **108/109**, 124-136.

Können GP, Tip A, de Vries AE. (1974). On the energy distribution of sputtered dimers, Rad. Effects **21**, 269-274.

Können GP, Tip A, de Vries AE. (1975). On the energy distribution of sputtered clusters, Rad. Effects **26**, 23-29.

Koshikawa T, Goto K. (1987). Surface compositional changes by segregation in sputtered alloys, Nucl. Instr. and Meth. **B18**, 504-508.

Krauss AR, Gruen DM, DeWald AB. (1984). Modification of alloy surface composition by segregation processes as a means of impurity control in fusion devices, J. Nucl. Mater. **121**, 398-403.

Krohn VE. (1962). Emission of negative ions from metal surfaces bombarded by positive cesium ions, J. Appl. Phys. **33**, 3523-3525.

Lam NQ. (1988a). Ion bombardment effects on the near-surface composition during sputter profiling, Surf. Interface Anal. **12**, 65-77.

Lam NQ. (1988b). Mechanisms and kinetics of ion beam-induced compositional modifications, Mat. Res. Soc. Symp. Proc. **100**, 29-43.

Lam NQ, Hoff HA. (1988). Surface and subsurface composition changes in Ni-Si alloys during elevated-temperature sputtering, Surface Sci. **193**, 353-372.

Lam NQ, Hoff HA, Régnier PG. (1985a). Elevated temperature sputtering of Ni-Au alloys: surface and subsurface composition modifications measured by ion scattering spectroscopy, J. Vac. Sci. Technol. **A3**, 2152-2160.

Lam NQ, Hoff HA, Wiedersich H, Rehn LE. (1985b). Subsurface compositional modifications in Ni-Cu alloys during high-temperature ion sputtering, Surface Sci. **149**, 517-536.

Lam NQ, Leaf GK, Wiedersich H. (1979). Effects of radiation-induced segregation and preferential sputtering on the sputtering rate of alloys, J. Nucl. Mater. **85&86**, 1085-1089.

Lam NQ, Leaf GK, Wiedersich H. (1980). Sputter-induced surface composition changes in alloys, J. Nucl. Mater. **88**, 289-298.

Lam NQ, Okamoto PR. (1986). Damage-rate gradient effects on radiation-induced segregation and phase stability in irradiated alloys, in: Solute-Defect Interaction: Theory and Experiment, S. Saimoto, G. R. Purdy and G. V. Kidson (eds), Pergamon Press, Toronto, 307-316.

Lam NQ, Okamoto PR, Johnson RA. (1978). Solute segregation and precipitation under heavy-ion bombardment, J. Nucl. Mater. **78**, 408-418.

Lam NQ, Rothman SJ. (1976). Radiation-enhanced diffusion in metals and alloys, in: Radiation Damage in Metals, N. L. Peterson and S. D. Harkness (eds), American Society for Metals, Metals Park, Ohio, 125-156.

Lam NQ, Rothman SJ, Sizmann R. (1974). Steady-state point-defect diffusion profiles in solids during irradiation, Rad. Effects **23**, 53-59.

Lam NQ, Wiedersich H. (1981). Modifications of subsurface alloy composition during high-temperature sputtering, J. Nucl. Mater. **103&104**, 433-438.

Lam NQ, Wiedersich H. (1982a). Dynamical behavior of the subsurface region in alloys under ion bombardment at high temperatures, Mater. Res. Soc. Symp. Proc. **7**, 35-42.

Lam NQ, Wiedersich H. (1982b). Ion bombardment-induced subsurface composition modifications in alloys at elevated temperatures, Rad. Effects Lett. **67**, 107-112.

Lam NQ, Wiedersich H. (1987). Bombardment-induced segregation and redistribution, Nucl. Instr. and Meth. **B18**, 471-485.

Li RS. (1988). Temperature dependence of the surface composition changes under Ar ion bombardment of an $Au_{0.5}Cu_{0.5}$ alloy between 30°C and 700°C, Surface Sci. **193**, 373-386.

Li RS. (1989). A comparative study of the surface composition changes of a $Au_{0.5}Cu_{0.5}$ alloy under nitrogen and argon ion bombardment, Appl. Surface Sci. **35**, 409-422.

Li RS, Koshikawa T, Goto K. (1983). Quantitative Auger electron spectroscopy analysis with co-evaporated Au-Cu films, Surface Sci. **129**, 192-204.

Lindhard J, Nielsen V, Scharff M, Thomsen PV. (1963a). Integral equations governing radiation effects, Mat. Fys. Medd. Dan. Vid. Selsk. **33**, No. 10.

Lindhard J, Scharff M, Schiøtt HE. (1963b). Range concepts and heavy ion ranges, Mat. Fys. Medd. Dan. Vid. Selsk. **33**, No. 14.

Lindhard J. (1965). Influence of crystal lattice on motion of energetic charged particles, Mat. Fys. Medd. Dan. Vid. Selsk. **34**, No. 14.

Lindhard J, Nielsen V, Scharff M. (1968). Approximation method in classical scattering by screened Coulomb fields, Mat. Fys. Medd. Dan. Vid. Selsk. **36**, No. 10.

Littmark U. (1985). Aspects of the theoretical description of ballistic atomic mixing, Nucl. Instr. and Meth. **B7/8**, 684-693.

Littmark U, Fedder S. (1982). Primary recoil contribution to low energy light ion scattering, Nucl. Instr. and Meth. **194**, 607-610.

Littmark U, Hofer WO. (1980). Recoil mixing in solids by energetic ion beams, Nucl. Instr. and Meth. **168**, 329-342.

Littmark U, Hofer WO. (1984). The theory of recoil mixing in solids, in: Thin Film and Depth Profile Analysis (Top. Appl. Phys. **37**), H. Oechsner (ed), Springer-Verlag, Berlin, 159-200.

Loftager P, Besenbacher F, Jensen OS, Sørensen VS. (1979). Experimental study of effective interatomic potentials, Phys. Rev. **A20**, 1443-1447.

Mansfield JF, Rehn LE, Okamoto PR, Zaluzec NJ. (1987). Radiation effects on x-ray microanalysis of a light element alloy in a medium-voltage electron microscope, Ultramicroscopy **21**, 13-22.

Martin G, Cauvin R, Barbu A. (1983). Solid solution stability under irradiation, in: Phase Transformations during Irradiation, F. V. Nolfi, Jr. (ed), Applied Science Publishers, London, 47-74.

Matsunami N, Yamamura Y, Itikawa Y, Itoh N, Kazumata Y, Miyagawa S, Morita K, Shimizu R. (1980). A semiempirical formula for the energy dependence of the sputtering yield, Rad. Effects Lett. **57**, 15-21.

Matteson S, Nicolet MA. (1983). Ion mixing, Ann. Rev. Mater. Sci. **13**, 339-362.

Matteson S, Paine BM, Nicolet MA. (1981). Ion beam mixing in amorphous silicon II. Theoretical interpretation, Nucl. Instr. and Meth. **182/183**, 53-61.

Mayer JW, Lau SS. (1983). Ion beam mixing, in: Surface Modification and Alloying, J. M. Poate, G. Foti and D. C. Jacobson (eds), Plenum Press, New York, 241-259.

Merkle KL. (1977). TEM evidence for the ejection of matter by energetic displacement cascades, in: 35th Ann. Proc. Electron Microscopy Society of America, Boston, Massachusetts, G. W. Bailey (ed), 36-37.

Merkle KL, Jäger W. (1981). Direct observations of spike effects in heavy-ion sputtering, Philos. Mag. **A44**, 741-762.

Merkle KL, King WE, Baily AC, Haga K, Meshii M. (1983). Experimental determination of the energy dependence of defect production, J. Nucl. Mater. **117**, 4-11.

Merkle KL, Singer LR, Hart RK. (1963). Fission-fragment damage in gold films, J. Appl. Phys. **34**, 2800-2804.

Morita K, Tsuchiya T, Hayashibara M, Itoh N. (1983). Suppression of sputtering of nickel by coverage with self-sustaining thin segregated carbon layers, J. Nucl. Mater. **116**, 63-68.

Morita K, Ohno H, Hayashibara M, Itoh N. (1984). Studies of temperatures and flux dependences of sputtering yield of nickel from two-layered films of Ni-$Ni_3C$, Nucl. Instr. and Meth. **B2**, 596-600.

Nelson RS. (1965). An investigation of thermal spikes by studying the high energy sputtering of metals at elevated tempertatures, Philos. Mag. **11**, 291-302.

Oechsner H. (1975). Sputtering-A review of some recent experimental and theoretical aspects, Appl. Phys. **8**, 185-198.

Oechsner H. (1985). Formation of sputtered molecules, in: Physics of Ionized Gases, M. Popovic and P. Hrstic (eds), World Scientific, Singapore, Philadelphia, 571-598.

Oechsner H, Bartella J. (1981). Energy distributions of neutral atoms sputtered from pure Ni and W and from a Ni-W alloy, in Proc. 7th Intern. Conf. on Atomic Collisions in Solids, Moscow, September 19-23, 1977, I. U. Bulgakov and A. F. Tulinov (eds), Moscow State University Publishing House, USSR, 327-338.

Oechsner H, Gerhard W. (1974). Mass spectroscopy of sputtered neutrals and its application for surface analysis, Surface Sci. **44**, 480-488.

Okamoto PR, Rehn LE. (1979). Radiation-induced segregation in binary and ternary alloys, J. Nucl. Mater. **83**, 2-23.

Okutani T, Shikata M, Shimizu R. (1980). Investigation on surface compositions of Cu-Ni alloy under $Ar^+$ ion bombardment by ISS and in situ AES measurements, Surface Sci. **99**, L410-L418.

Oliva A, Kelly R, Falcone G. (1987). Comments on collisional sputtering theory, Nucl. Instr. and Meth. **B19**, 101-108.

Oliva-Florio AR, Alonso EV, Baragiola RA, Ferron J, Jakas MM. (1979). Energy dependence of the molecular effect in sputtering, Rad. Effects Lett. **50**, 3-7.

Onderdelinden D. (1966). The influence of channeling on Cu single-crystal sputtering, Appl. Phys. Lett. **8**, 189-190.

Onderdelinden D. (1968). Single-crystal sputtering including the channeling phenomenon, Can. J. Phys. **46**, 739-745.

Okano J, Ochiai T, Nishimura H. (1985). Ion-beam-induced isotope composition changes in metal surfaces and recoil implantation, Appl. Surface Sci. **22/23**, 72-81.

Patterson H, Tomlin DH. (1962). Experiments by radioactive tracer methods on sputtering by rare-gas ions, Proc. Roy. Soc. **265**, 474-488.

Patterson WL, Shirn GA. (1967). The sputtering of nickel-chromium alloys, J. Vac. Sci. Technol. **4**, 343-346.

Pedrys R, Haring RA, Haring A, Saris FW, de Vries AE. (1981). Sputtering of Van der Waals molecules, Phys. Lett. **82A**, 371-374.

Pellin MJ, Young CE, Gruen DM, Aratono Y, DeWald AB. (1985). Oxygen underlayer formation on titanium by "static mode" laser fluorescence and Auger spectroscopy, Surface Sci. **151**, 477-502.

Pickering HW. (1976). Ion sputtering of alloys, J. Vac. Sci. Technol. **13**, 618-621.

Poate JM, Foti G, Jacobson DC. (1983) eds. Surface Modification and Alloying by Laser, Ion and Electron Beams (NATO Advanced Study Institute, series VI), Plenum, New York.

Pramanik D, Seidman DN. (1983). The irradiation of tungsten with metallic diatomic molecular ions: Atomic resolution observations of depleted zones, Nucl. Instr. and Meth. **209/210**, 453-459.

Qu Zhe (1985). A general expression of the steady state composition for multicomponent systems during ion sputtering, Surface Sci. **161**, L549-L553.

Qu Zhe (1986). Determination of the steady state composition in a ternary system from the corresponding binary systems under ion sputtering, Surface Sci. **176**, L873-L878.

Rajan K. (1987) ed. Intermediate Voltage Microscopy and its Applications to Materials Science, Electron Optics Publishing Group, Philips Electronic Instruments INC., Mahwah, New Jersey.

Régnier PG, Lam NQ. (1983). Radiation-induced microstructural changes in Ni-C and Pt-C alloys, in:

Dimensional Stability and Mechanical Behavior of Irradiated Metals and Alloys, British Nuclear Energy Society, London, 51-54.

Régnier PG, Lam NQ. (1985). Microstructural changes in dilute Ni-Be alloys during HVEM sub-threshold irradiations, J. Nucl. Mater. **133&134**, 423-426.

Régnier PG, Lam NQ, Westmacott KH. (1982). Defect clustering induced by secondary collisions in Pt(C) alloys during high-voltage-electron-microscope irradiation, Scripta Metall. **16**, 643-648.

Régnier PG, Lam NQ, Westmacott KH. (1983). Microstructural transitions in Pt-C alloys during high-voltage-electron-microscope irradiation, J. Nucl. Mater. **115**, 286-296.

Rehn LE. (1982). Surface modification and radiation-induced segregation, Mat. Res. Soc. Symp. Proc. **7**, 17-33.

Rehn LE, Boccio VT, Wiedersich H. (1983). Sputter-induced compositional changes in a Ni-Si alloy, Surface Sci. **128**, 37-50.

Rehn LE, Danyluk S, Wiedersich H. (1979). Sputter-induced subsurface segregation in a Cu-Ni alloy, Phys. Rev. Lett. **43**, 1764-1767.

Rehn LE, Lam NQ. (1987). Surface segregation during irradiation, J. Mater. Eng. **9**, 205-215.

Rehn LE, Lam NQ, Wiedersich H. (1985). Radiation-induced segregation during sputtering, Nucl. Instr. and Meth. **B7/8**, 764-767.

Rehn LE, Okamoto PR. (1983). Non-equilibrium segregation in irradiated alloys, in: Phase Transformations during Irradiation, F. V. Nolfi, Jr. (ed), Applied Science Publishers, London, 247-290.

Rehn LE, Okamoto PR. (1987). Production of freely-migrating defects during irradiation, Mater. Sci. Forum **15-18**, 985-1002.

Rehn LE, Okamoto PR, Averback RS. (1984). Relative efficiencies of different ions for producing freely migrating defects, Phys. Rev. **B30**, 3073-3080.

Remillieux J, Poizat JC, Gaillard MJ. (1982) eds. Atomic Collisions in Solids, Nucl. Instr. and Meth. **194**.

Robertson IM, Kirk MA, King WE. (1984). Formation of dislocation loops in iron by self-ion irradiations at 40 K, Scripta Metall. **18**, 317-320.

Robinson MT. (1969). Sputtering experiments with 1-5 keV $Ar^+$ ions. Displacement of ejection pattern spots, J. Appl. Phys. **40**, 4982-4983.

Robinson MT. (1981). Theoretical aspects of monocrystal sputtering, in: Sputtering by Particle Bombardment I (Top. Appl. Phys. **47**), R. Behrisch (ed), Springer-Verlag, Heidelberg, 72-144.

Robinson MT. (1983). Computer simulation of the self-sputtering of uranium, J. Appl. Phys. **54**, 2650-2659.

Robinson MT, Torrens IM. (1974). Computer simulation of atomic-displacement cascades in solids in the binary-collision approximation, Phys. Rev. **B9**, 5008-5024.

Rödelsperger K, Scharmann A. (1976). Angular distribution measurements of sputtered atoms with characteristic x-ray emission, Nucl. Instr. and Meth. **132**, 355-362.

Roosendaal HE. (1981). Sputtering yields of single crystalline targets, in: Sputtering by Particle Bombardment I (Top. Appl. Phys. **47**), R. Behrisch (ed), Springer-Verlag, Heidelberg, 219-256.

Roosendaal HE, Haring RA, Sanders JB. (1982). Surface disruption as an observable factor in the energy distribution of sputtered particles, Nucl. Instr. and Meth. **194**, 579-581.

Rosen M, Mueller GP, Fraser WA. (1983). Computer study of self-sputtering of Cu and Ni at 90 keV, Nucl. Instr. and Meth. **209/210**, 63-66.

Roth J. (1980). Sputtering with light ions, in: Symposium on Sputtering, P.Varga, G. Betz, F. P. Viehböck (eds), Institut für Allgemeine Physik, Technische Universität Wien, Austria, 773-820.

Rothman SJ. (1983). Effects of irradiation on diffusion in metals and alloys, in: Phase Transformations during Irradiation, F. V. Nolfi, Jr. (ed), Applied Science Publishers, London, 189-211.

Rothman SJ, Lam NQ, Sizmann R, Bisswanger H. (1973). Buildup of point-defect diffusion profiles in a foil during irradiation, Rad. Effects **20**, 223-227.

Sanders JB. (1980). Time evolution of collision-induced hot spikes, Rad. Effects **51**, 43-48.

Schorn RP, Zaki Ewiss MA, Hintz E. (1988). Velocity distributions of copper and lithium atoms sputtered from a Cu/Li alloy measured with laser induced fluorescence, Appl. Phys. **A46**, 291-297.

Schou J. (1987). Sputtering of frozen gases, Nucl. Instr. and Meth. **B27**, 188-200.

Schou J. (1989). Ion energy dissipation and sputtering during bombardment of multicomponent materials, in: Structure-Property Relationships in Ion-Beam Surface-Modified Ceramics-Theory and Practice (Proc. NATO-ASI Meeting, Il Ciocco, Italy, August-September 1988) in press.

Schwartz SA. (1986). Measurements of the secondary ion mass spectroscopy isotope effect, J. Vac. Sci. Technol. **A5**, 308-312.

Seeger A. (1958). On the theory of radiation damage and radiation hardening, in: Proc. Second United Nations Intern. Conf. on Peaceful Uses of Atomic Energy, United Nations Publication, Geneva, vol. **6**, 250-273.

Seitz F, Koehler JS. (1956). Displacement of atoms during irradiation, in: Solid State Physics **2**, F. Seitz and D. Turnbull (eds), Academic, New York, 305-448.

Shapiro MH, Haff PK, Tombrello TA, Harrison DA, Webb RP. (1985). Computer-simulated energy and angular distributions of sputtered Cu atoms, Rad. Effects **89**, 234-255.

Shapiro MH, Tombrello TA. (1987). Computer simulation of sticking and penetration of copper atoms on copper substrates, Nucl. Instr. and Meth. **B18**, 355-359.

Shapiro MH, Tombrello TA, Harrison DE. (1988). Simulation of isotopic mass effects in sputtering, II, Nucl.

Instr. and Meth. **B30**, 152-158.

Shimizu H, Ono M, Nakayama K. (1973). Quantitative Auger analysis of copper-nickel alloy surfaces after argon ion bombardment, Surface Sci. **36**, 817-821.

Shimizu H, Ono M, Nakayama K. (1975). Effect of target temperature on surface composition changes of Cu-Ni alloys during Ar ion bombardment, J. Appl. Phys. **46**, 460-462.

Shimizu N, Hart SR. (1982). Isotope fractionation in secondary ion mass spectrometry, J. Appl. Phys. **53**, 1303-1311.

Shimizu R. (1987). Preferential sputtering, Nucl. Instr. and Meth. **B18**, 486-495.

Shulga VI. (1983). Computer simulation of single-crystal and polycrystal sputtering I, Rad. Effects **70**, 65-83.

Shulga VI. (1984). Computer simulation of single-crystal and polycrystal sputtering II, Rad. Effects **82**, 169-187.

Shulga VI. (1985). Computer simulation of single-crystal and polycrystal sputtering III, Rad. Effects **84**, 1-25.

Sigmund P. (1969a). Theory of sputtering I. Sputtering yield of amorphous and polycrystalline targets, Phys. Rev. **184**, 383-416; **187**, 768.

Sigmund P. (1969b). On the number of atoms displaced by implanted ions or energetic recoil atoms, Appl. Phys. Lett. **14**, 114-117.

Sigmund P. (1969c). A note on integral equations of the Kinchin-Pease type, Rad. Effects **1**, 15-18.

Sigmund P. (1974). Energy density and time constant of heavy-ion-induced elastic-collision spikes in solids, Appl. Phys. Lett. **25**, 169-171; **27**, 52.

Sigmund P. (1977). Sputtering processes: collision cascades and spikes, in: Inelastic Ion-Surface Collisions, N. H. Tolk, J. C. Tully, W. Heiland and C. W. White (eds), Academic Press, New York, 121-152.

Sigmund P. (1981). Sputtering by ion bombardment: theoretical concepts in: Sputtering by Particle Bombardment I (Top. Appl. Phys. **47**), R. Behrisch (ed), Springer-Verlag, Heidelberg, 9-71.

Sigmund P. (1987a). Mechanisms and theory of physical sputtering by particle impact, Nucl. Instr. and Meth. **B27**, 1-20.

Sigmund P. (1987b). Preferential sputtering from isotopic mixtures and alloys of near-neighbor elements, Nucl. Instr. and Meth. **B18**, 375-387.

Sigmund P. (1988). Preferential recoil implantation in polyatomic targets, Nucl. Instr. and Meth. **B34**, 15-21.

Sigmund P, Claussen C. (1981). Sputtering from elastic-collision spikes in heavy-ion-bombarded metals, J. Appl. Phys. **52**, 990-993.

Sigmund P, Gras-Marti A. (1981). Theoretical aspects of atomic mixing by ion beams, Nucl. Instr. and Meth. **182/183**, 25-41.

Sigmund P, Oliva A, Falcone G. (1982). Sputtering of multicomponent materials: Elements of a theory, Nucl. Instr. and Meth. **194**, 541-548.

Sigmund P, Robinson MT, Baskes MI, Hautala M, Cui FZ, Eckstein W, Yamamura Y, Hosaka S, Ishitani T, Shulga VI, Harrison DE, Chakarov IR, Karpuzov DS, Kawatoh E, Shimizu R, Valkealahti S, Nieminen RM, Betz G, Husinsky W, Shapiro MH, Vicanek M, Urbassek HM. (1989). Round robin computer simulation of ejection probability in sputtering, Nucl. Instr. and Meth. **B36**, 110-123.

Sigmund P, Sanders JB. (1967). Spatial distribution of energy deposited by ion bombardment, in: Proc. Int. Conf. on Application of Ion Beams to Semiconductor Technology, P. Glotin (ed), Editions Ophrys, 215-237.

Sigmund P, Szymonski M. (1984). Temperature-dependent sputtering of metals and insulators, Appl. Phys. **A33**, 141-152.

Sizmann R. (1978). The effect of radiation upon diffusion in metals, J. Nucl. Mater. **69&70**, 386-412.

Slodzian G. (1983). Remarks on some factors influencing the charge state of sputtered particles, Phys. Scripta **T6**, 54-66.

Smith DL. (1978). Physical sputtering model for fusion reactor first-wall materials, J. Nucl. Mater. **75**, 20-31.

Staudenmaier G. (1972). Clusters sputtered from tungsten, Rad. Effects **13**, 87-91.

Staudenmaier G. (1973). Angular dependence of cluters sputtered from a tungsten single crystal surface, Rad. Effects **18**, 181-184.

Swartzfager DG, Ziemecki SB, Kelley MJ. (1981). Differential sputtering and surface segregation: The role of enhanced diffusion, J. Vac. Sci. Technol. **19**, 185-191.

Szymonski M. (1980). Sputtering of Cu and Zn atoms from elemental and alloy targets, Appl. Phys. **23**, 89-92.

Szymonski M. (1982). Sputtering mechanisms of compound solids, Nucl. Instr. and Meth. **194**, 523-531.

Szymonski M. (1984). Elastic-collision spikes in sputtering of metals at normal and oblique incidence, Nucl. Instr. and Meth. **B2**, 583-586.

Szymonski M, de Vries AE. (1977). Spikes in low energy sputtering of silver and gold, Phys. Lett. **63A**, 359-360.

Taglauer E. (1982). Surface modifications due to preferential sputtering, Appl. Surface Sci. **13**, 80-93.

Taglauer E, Heiland W. (1978). Mass and energy dependence of the equilibrium surface composition of sputtered tantalum oxide, Appl. Phys. Lett. **33**, 950-952.

Tang S, Lam NQ. (1989). Near-surface compositional changes in Ni-Pd alloys during elevated-temperature sputtering, Surface Sci. **223**, 179-192.

Thomas JP, Cachard A. (1978) eds. Material Characterization using Ion Beams (NATO Advanced Study Institute, series 28), Plenum Press, London.

Thomas LE. (1985). Light-element analysis with electrons and x-rays in a high-resolution STEM, Ultramicroscopy **18**, 173-184.

Thompson DA. (1981). High density cascade effects,

Rad. Effects **56**, 105-150.

Thompson DA, Johar SS. (1981). Influence of the bombarding angle on the sputtering yield of heavy atomic and molecular ion bombardment of Ag and Au, Rad. Effects **55**, 91-98.

Thompson MW. (1968). The energy spectrum of ejected atoms during the high-energy sputtering of gold, Philos. Mag. **18**, 377-414.

Thompson MW, Nelson RS. (1962). Evidence for heated spikes in bombarded gold from the energy spectrum of atoms ejected by 43 keV $Ar^+$ and $Xe^+$ ions, Philos. Mag. **7**, 2015-2026.

Tombrello TA. (1987). Scratching the surface, Nucl. Instr. and Meth. **B27**, 221-225.

Townsend PD. (1983). Sputtering by electrons and protons, in: Sputtering by Particle Bombardment II (Top. Appl. Phys. **52**), R. Behrisch (ed), Springer-Verlag, Berlin, 147-178.

Urbassek HM. (1987). Sputtering of molecules, Nucl. Instr. and Meth. **B18**, 587-595.

Urbassek HM, Sigmund P. (1984). A note on evaporation from heated spikes, Appl. Phys. **A35**, 19-25.

Varga P, Betz G, Viehböck FP. (1980) eds. Symposium on Sputtering, Tech. Univ. Wien, Austria.

Varga P, Taglauer E. (1981). Preferential sputtering of compounds due to light ion bombardment, J. Nucl. Mater. **111/112**, 726-731.

Vicanek M, Jimenez-Rodriguez JJ, Sigmund P. (1989). Depth of origin and angular spectrum of sputtered atoms, Nucl. Instr. and Meth. **B36**, 124-136.

Vinyard GH. (1976). Thermal spikes and activated processes, Rad. Effects **29**, 245-248.

Wagner W, Rehn LE, Wiedersich H, Naundorf V. (1983). Radiation-induced segregation in Ni-Cu alloys, Phys. Rev. **B28**, 6780-6794.

Watson CC, Haff PK. (1980). Sputter-induced isotopic fractionation at solid surfaces, J. Appl. Phys. **51**, 691-699.

Webb R, Carter G, Collins R. (1978). The influence of preferential enhanced diffusion on composition changes in sputtered binary alloys, Rad. Effects **39**, 129-139.

Wehner GK. (1956). Controlled sputtering of metals by low-energy Hg ions, Phys. Rev. **102**, 690-704.

Wehner GK. (1975). The aspects of sputtering in surface analysis methods, in: Methods of Surface Analysis, A. W. Czanderna (ed), Elsevier, Amsterdam, 5-37.

Wehner GK, Rosenberg D. (1960). Angular distribution of sputtered material, J. Appl. Phys. **31**, 177-179.

Weissman R, Sigmund P. (1973). Sputtering and backscattering of keV light ions bombarding random targets, Rad. Effects **19**, 7-14.

Weller RA, Tombrello TA. (1978). Energy spectrum of sputtered uranium - a new technique, Rad. Effects **37**, 83-92.

Wiedersich H. (1972). On the theory of void formation during irradiation, Rad. Effects **12**, 111-125.

Wiedersich H. (1983). Sputtering and compositional changes, in: Surface Modification and Alloying (NATO Advanced Study Institute, series VI), J. M. Poate, G. Foti and D. C. Jacobson (eds), Plenum, New York, 261-285.

Wiedersich H. (1984). Ion-induced surface modification of alloys, Mat. Res. Soc. Symp. Proc. **27**, 13-24.

Wiedersich H. (1985). Kinetic processes during ion bombardment, Nucl. Instr. and Meth. **B7/8**, 1-10.

Wiedersich H. (1986). Phase stability and solute segregation during irradiation, in: Physics of Radiation Effects in Crystals, R. A. Johnson and A. N. Orlov (eds), Elsevier Science Publisher, London, 225-280.

Wiedersich H, Lam NQ. (1983). Theory of radiation-induced segregation, in: Phase Transformations during Irradiation, F. V. Nolfi, Jr. (ed), Applied Science Publishers, London, 1-46.

Wiedersich H, Okamoto PR, Lam NQ. (1979). A theory of radiation-induced segregation in concentrated alloys, J. Nucl. Mater. **83**, 98-108.

Williams JS, Poate JM. (1984) eds. Ion Implantation and Beam Processing, Academic Press, Sydney.

Wilson WD, Haggmark LG, Biersack JP. (1977). Calculations of nuclear stopping, ranges, and straggling in the low-energy region, Phys. Rev. **B15**, 2458-2468.

Winograd N, Garrison BJ, Fleisch T, Delgrass WN, Harrison DE. (1979). Particle ejection from ion-bombarded clean and reacted single-crystal surfaces, J. Vac. Sci. Technol. **16**, 629-634.

Winterbon KB, Sigmund P, Sanders JB. (1970). Spatial distribution of energy deposited by atomic particles in elastic collisions, Mat. Fys. Medd. Dan. Vid. Selsk. **37**, No. 14.

Wynblatt P, Ku RC. (1979). Surface segregation in alloys, in: Interfacial Segregation, W. C. Johnson and J. M. Blakeley (eds), American Society for Metals, Metals Park, Ohio, 115-136.

Yacout AM, Lam NQ, Stubbins JF. (1989). Near-surface compositional modifications of ternary alloys during sputtering at elevated temperatures, Nucl. Instr. and Meth. **B42**, 49-60.

Yamamura Y, Kitazoe Y. (1978). Computer simulation of cascade developments in amorphous targets, Rad. Effects **39**, 251-254.

Zaluzec NJ, Mansfield JF. (1987). Electron sputtering in the analytical electron microscope: calculations and experimental data, in: Intermediate Voltage Microscopy and Its Application to Materials Science, K. Rajan (ed), Electron Optics Publishing Group, Philips Electronic Instruments, Inc., New Jersey, 29-31.

Zaluzec NJ, Mansfield JF, Okamoto PR, Lam NQ. (1985). Medium voltage analytical electron microscopy: microanalysis versus radiation damage (EMAG-85). Inst. Phys. Conf. Ser. No. 78, 583-586.

Zee RH, Guinan MW, Kulcinski GL. (1983). Order-disorder transformation in CuPd under 14.8 MeV neutron and 1.8 MeV electron irradiations, J. Nuc. Mater. **114**, 190-198.

Ziegler JF, Biersack JP, Littmark U. (1985). The Stopping and Range of Ions in Solids, Pergamon, New York.

Editor's Note: All of the reviewer's concerns were appropriately addressed by text changes, hence there is no Discussion with Reviewers.